

PHOTOCATALYTIC AND PHOTOELECTROCHEMICAL WATER
SPLITTING OVER ORDERED TITANIA NANOTUBE ARRAYS

A THESIS SUBMITTED TO
THE GRADUATE SCHOOL OF NATURAL AND APPLIED SCIENCES
OF
MIDDLE EAST TECHNICAL UNIVERSITY

BY

OSMAN KARSLIOĞLU

IN PARTIAL FULFILLMENT OF THE REQUIREMENTS
FOR
THE DEGREE OF MASTER OF SCIENCE
IN
CHEMICAL ENGINEERING

JANUARY 2009

Approval of the thesis:

**PHOTOCATALYTIC AND PHOTOELECTROCHEMICAL WATER
SPLITTING OVER ORDERED TITANIA NANOTUBE ARRAYS**

submitted by **OSMAN KARSLIOĞLU** in partial fulfillment of the requirements for the degree of **Master of Science in Chemical Engineering Department, Middle East Technical University** by,

Prof. Dr. Canan Özgen
Dean, Graduate School of **Natural and Applied Sciences** _____

Prof. Dr. Gürkan Karakaş
Head of Department, **Chemical Engineering** _____

Prof. Dr. Deniz Üner
Supervisor, **Chemical Engineering Dept., METU** _____

Dr. Sadıg Guliyev
Co-supervisor, **Vestel Defence Industry** _____

Examining Committee Members:

Prof. Dr. İnci Erođlu
Chemical Engineering Dept., METU _____

Prof. Dr. Deniz Üner
Chemical Engineering Dept., METU _____

Prof. Dr. Gürkan Karakaş
Chemical Engineering Dept., METU _____

Assist Prof. Dr. Ayşen Yılmaz
Chemistry Dept., METU _____

Assist. Prof. Dr. Niyazi Alper Tapan
Chemical Engineering Dept., Gazi Üiversity _____

Date: _____

I hereby declare that all information in this document has been obtained and presented in accordance with academic rules and ethical conduct. I also declare that, as required by these rules and conduct, I have fully cited and referenced all material and results that are not original to this work.

Name, Last name : Osman Karslıođlu

Signature :

ABSTRACT

PHOTOCATALYTIC AND PHOTOELECTROCHEMICAL WATER SPLITTING OVER ORDERED TITANIA NANOTUBE ARRAYS

Karshiođlu, Osman

M.S., Department of Chemical Engineering

Supervisor: Prof. Dr. Deniz Üner

Co-Supervisor: Dr. Sadıđ Guliyev

January 2009, 94 pages

The objective of this study was to investigate photocatalytic water splitting over ordered TiO₂ nanotube arrays. Synthesis of ordered nanotube arrays of titania, as a micron thick film on a titanium foil was accomplished by electrochemical anodization methods defined in the literature. Effect of two types of electrolyte (aqueous and organic) on the micro-morphology was observed by scanning electron microscopy. Optimum anodization times for the TiO₂ nanotube electrodes, synthesized in ethylene glycol electrolyte, were different for acidic and basic electrolytes. Optimum times were determined as 2 hours in acidic and 4 hours in basic solutions. An H-type cell was constructed using a two side anodized titanium foil aiming the photocatalytic, stoichiometric and separate evolution of H₂/O₂ from the splitting of water. Gas evolution was observed at a rate of approximately 1 mL/h in the anode and 0.5 mL/h in the cathode, which implied the reverse of the desired stoichiometry. As the surface was corroded in that experimental conditions, electrochemical

properties of the synthesized films were investigated by cyclic voltammetry (CV) at milder conditions. CV showed the reduction of Ti^{4+} to Ti^{3+} , beginning at -0.2 V (vs. Ag/AgCl). Since the process is accompanied by proton intercalation to the oxide, non-annealed samples showed higher currents in that region. Non-annealed samples showed no photocurrent. Photocurrents obtained in this work, on the average 0.1-0.2 mA/cm², were one order of magnitude lower than the similar studies in the literature.

Keywords: titanium dioxide, nanotube, water splitting, photocatalysis, solar energy, hydrogen, photooxidation, photocorrosion, H-type cell, electrochemistry

ÖZ

DÜZENLİ TİTANYA NANOTÜPLER ÜZERİNDE FOTOKATALİTİK VE FOTOKİMYASAL SU PARÇALANMASI

Karşlıođlu, Osman

Yüksek Lisans, Kimya Mühendisliđi Bölümü

Tez Yöneticisi: Prof. Dr. Deniz Üner

Ortak Tez Yöneticisi: Dr. Sadıđ Guliyev

Ocak 2009, 94 sayfa

Bu alıřmanın amacı düzenli titanya nanotüpler üzerinde fotokatalitik su paralanmasını incelemektir. Düzenli titanya nanotüplerin mikron kalınlıđında tabaka olarak titanyum folyo üzerinde sentezlenmesi literatürde tanımlanmış elektrokimyasal anotlařtırma yöntemleriyle başarıldı. İki tip elektrolitin (sulu ve organik) mikro-morfolojiye etkisi taramalı elektron mikroskopisiyle incelendi. Etilen glikol elektrolitinde sentezlenen TiO₂ nanotüp elektrotlar için optimum anotlařtırma süresi asidik ve bazik ortamlarda farklıydı. H-tipi bir hücre, iki yüzü anotlařtırılmış bir titanyum folyo kullanılarak, suyun paralanmasıyla fotokatalitik, stokiyometrik ve ayrı H₂/O₂ üretimi amacıyla kuruldu. Beklenen stokiyometrinin tersine, anotta yaklaşık 1 mL/sa, katotta yaklaşık 0.5 mL/sa hızlarında gaz ıkıřı gözlemlendi. Deney kořullarında yüzey ařındıđından, sentezlenmiş tabakaların elektrokimyasal özellikleri daha yumuřak kořullarda devirsel voltametriyle (DV) incelendi. DV -0.2 V'den (Ag/AgCl'ye karřı) başlayarak Ti⁺⁴'ün Ti⁺³'e indirgenmesini gösterdi. Sürece,

oksidin arasına proton eklenmesi de eşlik ettiğinden, tavlammamış örnekler bu bölgede daha yüksek akım gösterdi. Tavlammamış örnekler hiç fotoakım göstermedi. Optimum süreler asidik elektrolitte 2 saat ve bazik elektrolitte 4 saat olarak belirlendi. Bu çalışmada elde edilen fotoakımlar, ortalama 0.1-0.2 mA/cm², literatürdeki benzer çalışmaların bir büyüklük mertebesi altındaydı.

Anahtar kelimeler: titanyum dioksit, nanotüp, su parçalanması, fotokataliz, güneş enerjisi, hidrojen, fotooksitleme, fotokorozyon, H-tipi hücre, elektrokimya

to my sunshine

ACKNOWLEDGEMENTS

My first acknowledgment goes to my family, Fatma, Ekrem and Ozan Karslıođlu: the soil I have grown in. Everything began with you, your support is invaluable.

I would like to thank my supervisor Prof. Dr. Deniz Üner not only for her valuable scientific contribution to my background but also for her support in every aspect of life. Your wisdom has given me a lot, none to be forgotten.

I feel lucky having worked with Dr. Sadıđ Guliyev, a great electrochemist and a great person. You have opened for me a different window on chemistry.

You are not just colleagues for me, you are real friends, you are the best I could ask for. Members of the Cactus Group, Bařar ađlar, Orun Ergün, Volkan Deđirmenci, Hilal Demir Kıvrak, Arzu Kanca, Mukaddes Can, Ebru Erunal, Mehmet Kaptan, Mert Oymak, Berk Giray and Özge Güner, these unique individuals deserve my deepest love and appreciation. Bahar, Ođuz, Saygın and Svetlana, the fresh members of our group; getting to know you was the bright side of the prolonging of my thesis period. Thanks a lot.

Friends from the Chemical Engineering Department, Murat Erdođan, Göke Avcıođlu, Canan Gücüyener, Fehmi Par Beki, Semih Kumluk, Fulya Akpınar, Egemen Ađı, Kenan Cem Tokay, Saltuk Pirgaliođlu, Barıř Erdođan, Canan Yeniova and Bilal Bayram; you have always supplied me with the necessary motivation. Thank you all.

Serdar Erkan is the one who deserve a special thanks. He was the one who came up with solutions to my technical problems throughout this thesis. Serdar, your support will not be forgotten.

Members of the Chemical Engineering Department workshop, İsa Çağlar, Nevzat Bekçi, Süleyman Arslan, Adil Demir and Ertuğrul Özdemir have always provided me with the technical assistance I needed, enduring my endless demands. Your works are kindly appreciated.

Bilkent University Chemistry Department, Asst. Prof. Dr. Emrah Özensoy and Seda Şentürk for supplying one set of the SEM measurements along with Asst. Prof. Dr. Ayşen Yılmaz and Mehmet Kayhan from METU Chemistry Department for supplying the XRD measurements, are kindly appreciated

I must thank Vestel Defence Industry and İbrahim Pamuk for financial and institutional support. Staff from Vestel; Yalçın Seven, Arif Mutlu and Deniz Kozlu are deeply appreciated for the warm environment and the valuable technical help.

I am grateful to TÜBİTAK-BİDEB for the graduate scholarship under program code 2228. Support from TÜBİTAK through project ÇAYDAG 106Y075 also contributed significantly to the progress of this thesis.

Last words are reserved for my darling, my sunshine and my dear wife Aydan Karşlıoğlu. I am sorry that my English (even my Turkish) is not enough to put my appreciation to you into words. It was impossible without you!

TABLE OF CONTENTS

ABSTRACT	iv
ÖZ.....	vi
ACKNOWLEDGEMENTS	ix
TABLE OF CONTENTS	xi
LIST OF TABLES	xiii
LIST OF FIGURES.....	xiv
LIST OF SYMBOLS.....	xix
CHAPTERS	
1. INTRODUCTION.....	1
1.1. TITANIUM DIOXIDE PHOTOCATALYSIS.....	3
1.1.1. Phases of TiO ₂	3
1.1.2. Band Structure of TiO ₂	4
1.1.3. Surfaces and Surface Defects of TiO ₂	6
1.2. OBJECTIVE OF STUDY.....	10
2. LITERATURE SURVEY	11
2.1. TiO ₂ NANOTUBES	11
2.1.1. Mechanism of TNT Formation	12
2.1.2. Synthesis of TNTs in Different Electrolytes.....	15
2.1.3. Effect of Experimental Parameters on Nanotube Properties	16
2.2. IMPROVEMENT OF ACTIVITY IN ORDERED TITANIA.....	17
2.3. WATER SPLITTING.....	18
2.3.1. Adsorption of Water on TiO ₂	18
2.3.2. Mechanism of Water Splitting	20
2.3.3. Alternative Water Splitting Catalysts	25
2.3.4. Selected Results	25

2.4. VOLTAMMOGRAMS OF TiO ₂ NANOTUBES	26
2.5. HYDROGEN PRODUCTION RATES	36
3. MATERIALS AND METHODS	39
3.1. PREPARATION OF MATERIALS	39
3.1.1. Catalytic Surfaces	39
3.2. CHARACTERIZATION	42
3.3. WATER SPLITTING CELL (H-TYPE CELL)	43
3.4. PHOTOELECTROCHEMICAL TESTS	45
4. RESULTS AND DISCUSSIONS	47
4.1. CHARACTERIZATION OF TiO ₂ NANOTUBES	47
4.1.1. SEM Images	47
4.1.2. X-Ray Diffractogram	50
4.2. GAS EVOLUTION IN H-TYPE CELL	51
4.3. CYCLIC VOLTAMMOGRAMS OF TiO ₂ NANOTUBES	61
4.3.1. Pure TiO ₂ Nanotubes	62
4.3.2. Platinized TiO ₂ Nanotubes	68
5. CONCLUSIONS	70
6. RECOMMENDATIONS	72
REFERENCES	73
APPENDICES	
A. PLATINUM LOADING ON TITANIUM/TITANIUM DIOXIDE BY DIFFERENT MEANS	83
B. INFORMATION ON PURE TITANIUM	87
C. CO OXIDATION IN THE GAS PHASE USING Pt/TNT	90

LIST OF TABLES

TABLES

Table 1-1. Main hydrogen production processes, their status of development in 1992 [2] and recent percentages in world production [1].	2
Table 1-2. Fundamental properties of the three phases of TiO ₂ .	4
Table 2-1. Methods for the synthesis of TiO ₂ nanotubes.	12
Table 2-2. Synthesis parameters for TNTs and their effects on tube dimensions.	17
Table 2-3. Rates of photocatalytic hydrogen production in the literature by water splitting reaction.	37
Table 3-1. Descriptions of different sample abbreviations used throughout the text.	39
Table 3-2. Experimental parameters for Pt loading and the calculated Pt loading densities (approximate)	42
Table 4-1. Spatial properties of pure TiO ₂ nanotubes as measured and calculated from their SEM images.	49

LIST OF FIGURES

FIGURES

Figure 1-1. Illustration of (a) terrace (b) step and (c) kink structures in an idealized surface [22].	6
Figure 1-2. Ball and stick model for the rutile(110) surface illustrating the bridging oxygen vacancy as the point defect [26].	8
Figure 1-3. Most common low index surfaces of rutile and anatase phases of TiO ₂ [19].	9
Figure 2-1. SEM image (top view) of titania nanotubes synthesized by the electrochemical anodization of a titanium foil in a fluoride containing electrolyte (inset; side view) [29].	11
Figure 2-2. Stages of nanotube growth [37]. Graph on the upper left side is a typical current transient recorded during anodization. In that current-time plot, nanotube growth process is divided into three sections. The state of the surface in each section is shown in the other three illustrations.	13
Figure 2-3. Examples to TNTs that are formed in aqueous (a) and organic (b) electrolytes [41].	16
Figure 2-4. A proposed mechanism to the photocatalytic O ₂ evolution on TiO ₂ [72].	23
Figure 2-5. Active complex formation as proposed by Nowotny <i>et al.</i> in the photocatalytic formation of O ₂ from water [78]. Active site here is the titanium vacancy.	23
Figure 2-6. Cyclic voltammograms of TNTs taken in 1M (NH ₄) ₂ SO ₄ , showing reduction of Ti ⁴⁺ and evolution of hydrogen. Left [98], right [37].	27
Figure 2-7. Cyclic voltammogram of (A) anodic compact TiO ₂ , (B) amorphous TNT, (C) anatase TNT [99]	27

Figure 2-8. Cyclic voltammograms of (a) TNT vs Pt (b) NiO deposited TNT vs Pt and (c) NiO deposited TNT vs graphite, all taken in 1 M NaOH with a SCE reference [100]..... 28

Figure 2-9. Photocurrent and dark current of TNT prepared in boric and nitric acid containing electrolyte (left) and of a thermally grown oxide layer with 250 nm thickness (right) [101]..... 29

Figure 2-10. Photocurrent plots of TNTs prepared in acetic acid, HF, water mixtures at various temperatures [43]. Experiments were carried out in 1 M KOH and under 320-400 nm UV irradiation..... 30

Figure 2-11. Linear sweep voltammogram under illumination for: (a) etched TiO₂ + 0.1 M formate; (b) etched TiO₂ + blank electrolyte; (c) unetched TiO₂ + blank electrolyte; (d) unetched TiO₂ + 0.1 M formate; (e) etched-TiO₂ in the dark [102]. Scan from -0.6 to +1.0 V at a rate 50 mV/s. The blank electrolyte is 0.5 M Na₂SO₄ (pH = 3) with the bubble of N₂ during the experiment. 31

Figure 2-12. Photocurrent-potential profiles under chopped irradiation (0.05 Hz) for TNTs prepared using pulse (a) and constant (b) anodization. TNTs were grown in 0.36 M NH₄F in water. Data taken in 0.5 M Na₂SO₄ [32]. 32

Figure 2-13. Linear-sweep photovoltammograms with 0.1 Hz chopped irradiation of a TNT obtained by anodization of Ti foil (20 V, 10 h) in 0.15 M NH₄F/glycerol in (a) 0.5 M Na₂SO₄ supporting electrolyte and (b) 0.5 M Na₂SO₄ + 0.1 M HCOONa. Photovoltammograms were obtained at 2 mV/s using the full output of a 150 W Xe lamp [103]..... 32

Figure 2-14. Potentiodynamic plot of TNT photoanode in 1 M KOH solution containing (a) without organic additives (b) 5% methanol, (c) 5% glycerol and (d) 5% ethylene glycol as organic additive. Anodization of foil was done in 0.5 M H₃PO₄ + 0.14 M NaF (pH 2.1) at 20 V for 45 min with ultrasonication [104]. 33

Figure 2-15. Photovoltammograms of C doped TiO₂ nanotubes as a visible responsive photoanode and Pt foil as cathode, recorded in 1 M KOH under

illumination of varying range of wavelengths. Light is filtered from artificial sunlight [105].	34
Figure 2-16. Photovoltammograms of TNTs prepared in an aqueous environment, recorded under simulated solar irradiation [106]. UAT: Ultrasonic agitation during anodization, SAT: Magnetic stirring during anodization, N ₂ /O ₂ : Annealing under nitrogen or oxygen environment.	35
Figure 2-17. Photocurrent characteristics of nanotube films with varying lengths, prepared in 1M NH ₄ H ₂ PO ₄ + 0.5 wt% NH ₄ F electrolyte (left) and of films of similar thickness with different morphologies: P-25 nanoparticle film, nanoporous film and nanotubular film (right) [51].	35
Figure 3-1. Scheme of the water splitting setup, utilizing the H-type cell.	44
Figure 3-2. Scheme of the first cell fabricated for the electrochemical test. This cell could not be utilized due to poor conductance.	46
Figure 4-1. SEM pictures of TNT-aq, with side view inset (left) and Pt/TNT-aq-1 (right).	47
Figure 4-2. SEM pictures of, from left to right, TNT-org-2h, TNT-org-4h and TNT-org-6h.	48
Figure 4-3. SEM picture of Pt/TNT-aq-PEC and EDX mapping of the same surface (a different spot).	50
Figure 4-4. X-Ray diffractogram of Pt/TNT-aq-1, showing peaks of metallic titanium (base), anatase (nanotube oxide layer) and deposited platinum (in metallic state).	51
Figure 4-5. Scheme of the processes taking place inside the H-type cell.	52
Figure 4-6. Evolution of gases in H-type cell under UV illumination. H ₂ and O ₂ don't necessarily indicate the composition of the evolved gases, but their evolution side. H ₂ represent the cathode side gas and O ₂ represent the anode side gas.	54
Figure 4-7. X-ray diffractograms of anode and cathode sides of Pt/TNT-aq-cell after ca. 3 hours of UV illuminated experiments in the H-type cell.	55

Figure 4-8. SEM images of the anode side of Pt/TNT-aq-cell, which experienced severe surface etching. (a) surface outside the o-ring, not wetted by the aqueous NaOH electrolyte (b) surface under the o-ring, partially wetted by the aqueous NaOH electrolyte and partially illuminated by UV light (c) surface that is totally wetted by the aqueous NaOH electrolyte and illuminated by UV light..... 56

Figure 4-9. Gas evolution in a UV illuminated H-type cell, in which a pure titanium foil is used instead of Pt/TNT-aq-cell. H₂ and O₂ don't necessarily indicate the composition of the evolved gases, but their evolution side. O₂ represent the illuminated side gas and H₂ represent the dark side gas..... 58

Figure 4-10. Evolution of gases in the control experiment of H-type cell using a Pt/Ti/TiO₂ electrode under UV illumination and DI water as electrolytes. H₂ and O₂ don't necessarily indicate the composition of the evolved gases, but their evolution side. H₂ represent the cathode side gas and O₂ represent the anode side gas. Illumination begins after 41 minutes of dark period..... 59

Figure 4-11. Evolution of gases in the control experiment of H-type cell using a Pt/Ti/TiO₂ electrode under visible light illumination and DI water as electrolytes. H₂ and O₂ don't necessarily indicate the composition of the evolved gases, but their evolution side. H₂ represent the cathode side gas and O₂ represent the anode side gas. Illumination begins after 5 minutes..... 60

Figure 4-12. Cyclic voltammograms of TNT-aq under UV illumination, taken in 0.1 N H₂SO₄ (top) and 0.1 N KOH (bottom). Dotted lines represent non-annealed, solid lines represent annealed samples..... 63

Figure 4-13. Cyclic voltammograms of TNTs synthesized for varying times (2, 4 and 6 hours) in organic electrolyte. CVs were taken under UV illumination in 0.1 N H₂SO₄ (top) and 0.1 N KOH (bottom) media..... 65

Figure 4-14. Cyclic voltammograms of TNTs (top: TNT-aq, bottom: TNT-org-4h) taken in acidic (0.1 N H₂SO₄, dotted lines) and basic media (0.1 N KOH, solid lines). 67

Figure 4-15. Cyclic voltammograms of Pt/TNT-aq-PEC electrode taken in 0.1 N H ₂ SO ₄ with 0.1V/s sweep rate in the dark (dotted line) and under UV illumination (solid line). Main graph is zoomed to the important features while inset shows the whole voltammogram.	68
Figure 4-16. Cyclic voltammograms of Pt/TNT-aq-PEC electrode taken in 0.1 N KOH with 0.1 V/s sweep rate in the dark (dashed line) and with 0.05 V/s sweep rate under UV illumination (solid line).	69
Figure A-1. CV of the Pt/Ti electrode, Pt deposited by high voltage DC source, taken in 1 N H ₂ SO ₄ , with a sweep rate of 0.05 V/s.....	84
Figure A-2. Current-voltage curve of the final cycle of 16 Pt deposition cycles by using a potentiostat.	85
Figure A-3. CV of the Pt/Ti electrode, Pt deposited by potentiostat, taken in 1 N H ₂ SO ₄ , with a sweep rate of 0.05 V/s.....	85
Figure A-4. SEM images of (a) Pt wet impregnated TNT film (b) Pt deposited on titanium metal via high voltage source (c) Pt deposited on titanium metal via potentiostat	86
Figure B-1. SEM image of the surface of a pure titanium foil.....	87
Figure B-2. CV of pure titanium foil (~1 cm ²) in 1 N H ₂ SO ₄ taken in the dark with 0.05 V/s sweep rate	88
Figure B-3. CV of pure titanium foil (~8 cm ²) in 0.1 N KOH taken in the dark (solid line) and under UV illumination (dotted line) with 0.05 V/s sweep rate	88
Figure B-4. X-ray diffractogram of pure titanium (foil)	89
Figure C-1. Schematic illustration of the setup that was used to study CO oxidation over titania nanotubes in batch and semi-flow through conditions..	90
Figure C-2. Photograph of the setup that was used to study CO oxidation over titania nanotubes in batch and semi-flow through conditions.	91
Figure C-3. IR spectra of gases during thermal CO oxidation test.	92
Figure C-4. IR spectra of gases during photocatalytic CO oxidation test.	93

LIST OF SYMBOLS

(lmn)	Surface of a crystal that is cut by the crystallographic plane denoted by l, m, n Miller indices
A	Anatase
AES	Auger electron spectroscopy
CB	Conduction band
CV	Cyclic voltammetry (or “cyclic voltammogram” depending on the place of use)
ELS	Energy loss spectroscopy
ID	Inner diameter
n-TiO ₂	n type doped TiO ₂
‘n’ c ‘x’	‘n’ fold coordinated ‘x’ atom
PEC	Photoelectrochemical cell
R	Rutile
TNT	TiO ₂ Nanotube
TPD	Temperature programmed desorption
UHV	Ultra-High vacuum
UPS	Ultraviolet photoelectron spectroscopy
VB	Valance band
XPS	X-ray photoelectron spectroscopy

CHAPTER 1

INTRODUCTION

In the recent years, hydrogen has become the center of attention in research due to its possible role as the energy carrier molecule of tomorrow's energy system. Its oxidation product being water is attractive for reducing urban air pollution. Fuel cell compatibility is important for increasing energy conversion efficiency, reducing moving parts thus noise and maintenance. What is unfortunate is that cheap and high purity production and efficient storage of hydrogen is still being sought.

Most of the hydrogen used in the world today is produced on site, by the reforming of fossil fuels. The other method, electrolysis, which produces by far the highest purity hydrogen (> 99.999%) accounts only for about 4% of the world production [1]. Current and possible future production processes of hydrogen and their status of development in 1992 are presented in Table 1-1.

Table 1-1. Main hydrogen production processes, their status of development in 1992 [2] and recent percentages in world production [1].

Production Process	Status	Percentage
Steam reforming of natural gas	Mature	~50%
Catalytic decomposition of natural gas	Mature	
Partial oxidation of heavy oil	Mature	~46%
Coal gasification	R & D - Mature	
Steam-iron coal gasification	R & D	NA
Water electrolysis	Mature	4%
Thermochemical cycles	R & D	NA
Photochemical processes	Early R & D	NA
Photoelectrochemical processes	Early R & D	NA
Photobiological processes	Early R & D	NA

Since fossil fuels (especially natural gas) are still the most feasible source for the production of hydrogen, processes that utilize these sources are mature and those that utilize alternative sources are in the process of development. Thermochemical cycles are attractive ways of producing hydrogen for systems that are capable of generating high temperatures like nuclear power plants, and for countries that possess these plants. Photoprocesses, on the other hand, require abundant sunlight, which can be plentiful in some regions but is not suited for every region or country.

Hydrogen production using photobacteria and different biodegradable sources have been studied in our department by Eroğlu Group for more than a decade [3-12]. In a series of papers, they have reported hydrogen production rates in the range of 8-28 mL H₂/(L·h). This method of hydrogen production, allowing the utilization of local resources, has potential for future applications.

1.1. TITANIUM DIOXIDE PHOTOCATALYSIS

Titanium dioxide (TiO_2) has been of great industrial importance as a pigment due to its unique optical properties (i.e. high refractive index), chemical inertness and non-toxicity. After the reporting of photolytic water oxidation on TiO_2 single crystal surface by Fujishima and Honda [13] photocatalytic applications of TiO_2 has been of utmost attention and since then it is recognized as a photocatalyst. Its photocatalytic applications are mainly decoloration of textile wastewater, purification of indoor air from organic contaminants and production of self cleaning surfaces (tiles, windows, etc.). O'Regan and Grätzel's [14] report of a dye-sensitized solar cell fabricated from relatively cheap nanocrystalline TiO_2 with nearly 10 % efficiency has made the material even more popular. In all these applications of TiO_2 , it is subject to challenging conditions like acidity/basicity, UV and/or visible light illumination, oxygen and water exposure and so on. Thus, the popularity of TiO_2 can be ascribed to its stability in all these conditions, where other materials may easily undergo irreversible changes.

There is a huge collection of data in the literature about the science and applications of TiO_2 . Among many publications that review titanium dioxide and its applications, Yates and Diebold groups have published the most detailed accounts [15-19].

1.1.1. Phases of TiO_2

Three phases of pure TiO_2 is of particular interest for research: rutile, anatase and brookite. Rutile is the thermodynamically favorable phase at high temperatures. Titania that is used as white pigment is composed of rutile crystals due to its strong scattering of light (which is a consequence of high refractive index). Anatase phase is stable at lower temperatures, not greater than ca. 500 °C. Although some ambiguity still exists, it is reported and widely accepted as the photocatalytically more active phase. Brookite, as is known to

us, has no significant application and it needs special recipe in order to be prepared from amorphous titania. Treatment of amorphous form in a variety of conditions lead to formation of anatase, rutile or a mixture of them. Information regarding these three phases is presented in Table 1-2.

Table 1-2. Fundamental properties of the three phases of TiO₂.

	Rutile	Anatase	Brookite
Crystal Structure	Tetragonal	Tetragonal	Orthorhombic
Space Group	D _{4h} ¹⁴ P4 ₂ /mmm	D _{4h} ¹⁹ I4 ₁ /amd	D _{2h} ¹⁵ Pbca
Molecule/Cell	2	4	8
Unit Cell (Å)			
a	4.584	3.733	5.436
b			9.166
c	2.953	9.37	5.135
Band Gap [20] (eV)			
Direct	3.37	3.53	3.56
Indirect	3.01	3.20	3.13
Density (g/cm³)	4.24	3.83	4.17

All data in this table are taken from reference [18] unless otherwise stated.

1.1.2. Band Structure of TiO₂

In solid state, electronic states of atoms combine to form a pseudo-continuum of states henceforth called *bands*. Positioning of bands relative to each other determine the electrical conductivity of the material, making it a conductor, semi-conductor or insulator. The highest energy band that is filled with electrons is called the *valance band* (VB) and the band after that which possesses empty states is called the *conduction band* (CB). Overlapping VB and CB makes a conductor, non-overlapping VB and CB make a semi-

conductor or insulator depending on the energy difference between the highest energy of the VB and the lowest energy of the CB. If this energy gap, so called the *band gap* (E_g), is greater than a certain value such that Fermi-Dirac distribution of electrons lead to a very small fraction of them to accommodate at the conduction band, then there are no free charge carriers and the material becomes an insulator. If the density of thermally excited electrons is more than a certain extent (i.e. band gap is low enough), then the material becomes a semi-conductor. There is no universally accepted value of threshold band gap for insulator/semi-conductor discrimination.

Band gap of TiO_2 is on the verge of making it an insulator or a semi-conductor. Since electrons in the valance band can be promoted to the conduction band if a photon of energy equal to or greater than the band gap energy is absorbed, non-conductors are transparent to light with photon energy smaller than E_g . If photon absorption (with $h\nu > E_g$) exists and a valance band electron is excited to the conduction band, electron-hole pair formation occurs. A *hole* is a positive center in the solid and regarded as a (+) charge carrier complementary to the electron (-). Equation (1-1) represents the formation of an electron-hole pair in TiO_2 .



Densities of electrons or holes in a material, besides from the band gap, is a strong function of impurities and/or defects. In titania, defects contribute significantly to the bulk and surface properties. Generally, TiO_2 is a material with oxygen deficiency and its formula may be expressed as TiO_{2-x} , x being in the range 10^{-4} - 10^{-2} [21]. This deficiency can be thought as doping with donor impurities and it makes TiO_2 an n-type semiconductor, which gives much higher conductivity to the material relative to stoichiometric TiO_2 .

Photo-processes that take place in/on titania all rely on the initiative event of photon absorption. In photocatalytic reactions, excited electron is utilized in a

reduction step and hole is utilized in an oxidation step. From the chemist's perspective, electron-hole pair formation is not a charge carrier generation like the physicist's perception but rather generation of reactive centers, which are able to trigger chemical reactions.

Wide band gap of TiO_2 and its position with respect to redox couples in water cause oxidation/reduction potentials of holes/electrons (especially holes) to become relatively greater which is another advantage in surface redox processes. Wide band gap on the other side, makes TiO_2 only excitable with photons having energies higher than the 3.0-3.2 eV band gap. This corresponds to the UV or short wavelength visible range of the electromagnetic spectrum ($\lambda < 415 \text{ nm}$) which comprises only about 5% of solar illumination on Earth's surface.

1.1.3. Surfaces and Surface Defects of TiO_2

A solid understanding of *the solid surface* is critical in the understanding of the surface reactions, thus heterogeneous catalysis. One of the simplest but useful pictures of the solid surface is depicted by the Terrace-Step-Kink model (TSK model, sometimes referred as Terrace-Ledge-Kink, TLK, model). A scheme of the surface as understood by TSK model is given in Figure 1-1.

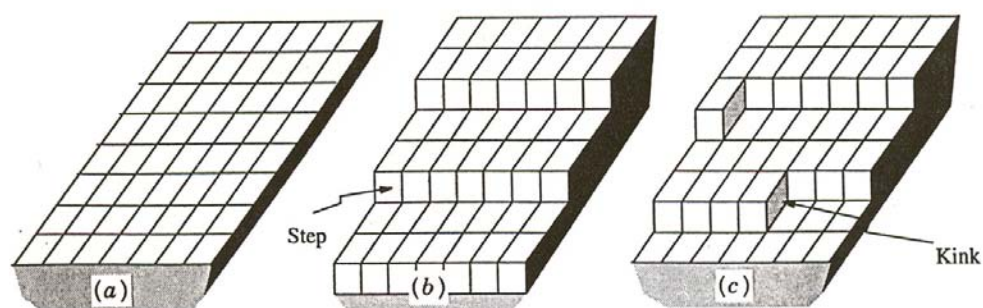


Figure 1-1. Illustration of (a) terrace (b) step and (c) kink structures in an idealized surface [22].

The most fundamental reason that TiO₂ is active in photocatalysis -or catalysis in general- is that it has an active surface which may survive catalytic cycles without being changed or consumed. Surface activity implies the existence of *active sites* on the surface on which adsorption or reaction steps of the overall reaction take place. In that respect, one must have the understanding of the most commonly encountered surfaces of TiO₂.

Rutile (110) is the most stable surface of titania and the dominant surface in its crystals. It is relatively flat. Most important feature on R(110) is the bridging oxygen atoms that bridge two titanium atoms. These atoms may be partially removed by heating in the absence of oxygen to form oxygen vacancies on the surface. Other than that, 5 fold coordinated titanium atom is significant, reported as a Lewis acid site. These two atoms have dangling bonds (i.e. coordination number is lower than the bulk counterparts), other surface Ti and O atoms are saturated (6 and 3 coordinated respectively) and generally regarded as inactive. Most single crystal studies of TiO₂ have been carried out on R(110) and there is an extensive collection of data in the literature.

Atoms on R(100) have coordination similar to R(110). A 5cTi, a 6cTi, a 2cO and a 3cO. It is the second most common surface of rutile crystals. R(001) on the other hand, has all its Ti atoms 4 fold and all its O atoms 2 fold coordinated, which leads to reconstruction of the surface and high surface energy. Due to high surface energy (001) surfaces are scarce in rutile crystals.

The most commonly reported active site that is responsible for the activity of TiO₂ is the oxygen vacancy. Surface (bridging) oxygen vacancy is an active site for the adsorption of water and oxygen (O₂) with consequent formation of ions and/or radicals [15,23-25]. This defect is illustrated in Figure 1-2.

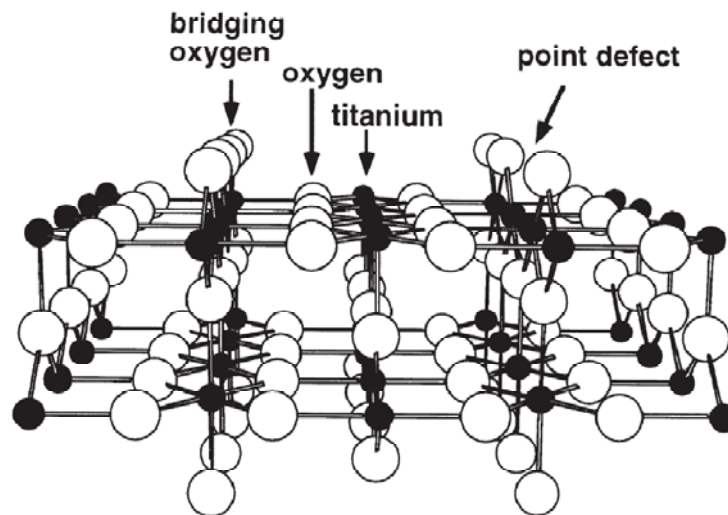
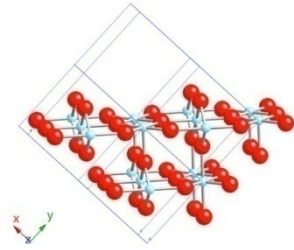


Figure 1-2. Ball and stick model for the rutile(110) surface illustrating the bridging oxygen vacancy as the point defect [26].

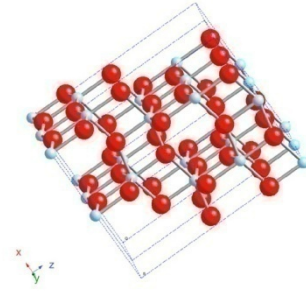
A reaction where oxygen vacancies on TiO_2 play a role is the CO oxidation. Linsebigler *et al.* [27] have shown that photocatalytic CO oxidation on R(110) is very site specific and these sites are not excited thermally. Annealing the surface at high temperatures ($400 \text{ K} < T < 900 \text{ K}$) creates the necessary oxygen vacancies on the surface, while sputtering with Ar^+ does not give the same effect (i.e. same sites are not created). Isotopic labeling experiments exclude a dissociative pathway for CO oxidation; C-O bond is not broken. Only photon energy greater than the band gap energy initiates the reaction. O_2 photodesorption and CO_2 photoreaction-desorption processes have very similar time constants. Two types of molecularly adsorbed O_2 are reported and denoted as $\alpha\text{-O}_2$ and $\beta\text{-O}_2$. It is claimed that $\alpha\text{-O}_2$ is the active species for the photooxidation of CO. $\alpha\text{-O}_2$ is thought to be a structure close to O_2^- or O_2^{2-} . In Lu and co-workers' paper [28], creation of oxygen vacancies is observed at temperatures higher than 500 K.

The surfaces mentioned in this section are illustrated in Figure 1-3.

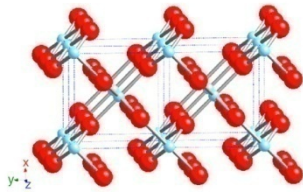
RUTILE (110)



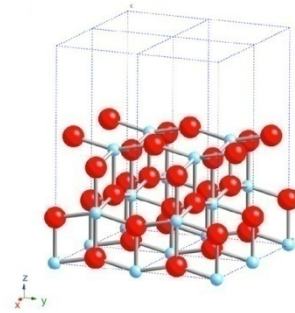
ANATASE (101)



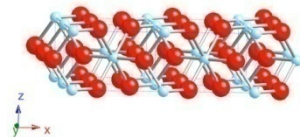
RUTILE (100)



ANATASE (100)



RUTILE (001)



ANATASE (001)

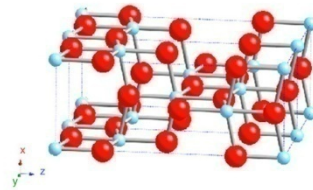


Figure 1-3. Most common low index surfaces of rutile and anatase phases of TiO_2 [19].

1.2. OBJECTIVE OF STUDY

The objective of this thesis is to study photocatalytic water splitting reaction over ordered titania nanotube arrays. As ordered structures of titania were reported to have improved charge transfer in photocatalysis, and phenomenon like photon trapping is known to take place in similar structured photonic materials, higher efficiencies were expected in the photocatalytic water splitting as well.

CHAPTER 2

LITERATURE SURVEY

2.1. TiO₂ NANOTUBES

After the widespread use of electron microscopy in scientific research, many different forms of known materials have been identified. Nanotubular forms of TiO₂ is an example to such materials. Figure 2-1 illustrates TiO₂ nanotubes synthesized by electrochemical anodization of titanium metal.

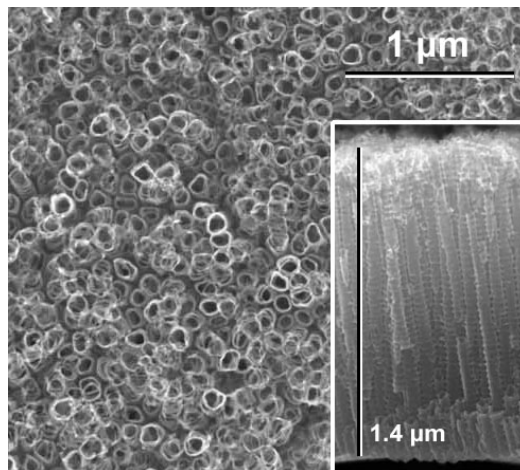


Figure 2-1. SEM image (top view) of titania nanotubes synthesized by the electrochemical anodization of a titanium foil in a fluoride containing electrolyte (inset; side view) [29].

There are basically three methods reported in the literature for the synthesis of titania nanotubes; these are electrochemical anodization, hydrothermal synthesis and soft chemical synthesis. The relevant literature regarding the

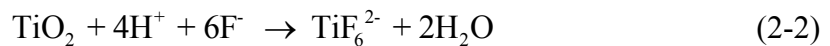
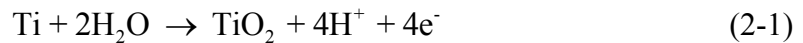
techniques are summarized in Table 2-1. Electrochemical anodization is by far the most commonly used method owing to its simple preparation procedure. Different from the other two methods, nanotubes prepared with this method are self-organized tubes, which are parallel to each other in an infinite bundle form.

Table 2-1. Methods for the synthesis of TiO₂ nanotubes.

Method	Description	References
Electrochemical anodization	Titanium foil is made anode material at high potentials in an electrolysis cell that contains fluoride anions in its electrolyte solution.	Zwillig <i>et al.</i> 1999 [30] Gong <i>et al.</i> 2001 [31] Chanmanee <i>et al.</i> 2007 [32]
Hydrothermal synthesis	Material is crystallized at high temperatures and pressures in an aqueous solution. Liquid precursors are used.	Kasuga <i>et al.</i> 1998 [33] Xu <i>et al.</i> 2007 [34] Li <i>et al.</i> 2008 [35]
Soft chemical synthesis	TiO ₂ powder is treated in an alkali medium at mild conditions to form nanotubular structure.	Wang <i>et al.</i> 2004 [36]

2.1.1. Mechanism of TNT Formation

The formation of the self-organized nanotubes of titania follows a scheme in which titanium is oxidized, forming an amorphous oxide layer, and the oxide is dissolved by the fluoride ions. The governing reactions are as follows:



Considering these two reactions, we must be aware that dissolution of the oxide uncovers more metallic titanium to be oxidized. The instant oxidation

(Reaction (2-1)) creates more H^+ ions thus the dissolution process becomes autocatalytic.

Schmuki group proposed three stages during the formation of nanotube morphologies [37]. These steps are correlated with the typical current-time behavior during anodization as well. First step is the formation of a compact oxide layer. Random pores begin to form after some time and finally these pores self-organize to an ordered structure. Typical current-time behavior together with the 3 steps of nanotube formation is illustrated in Figure 2-2.

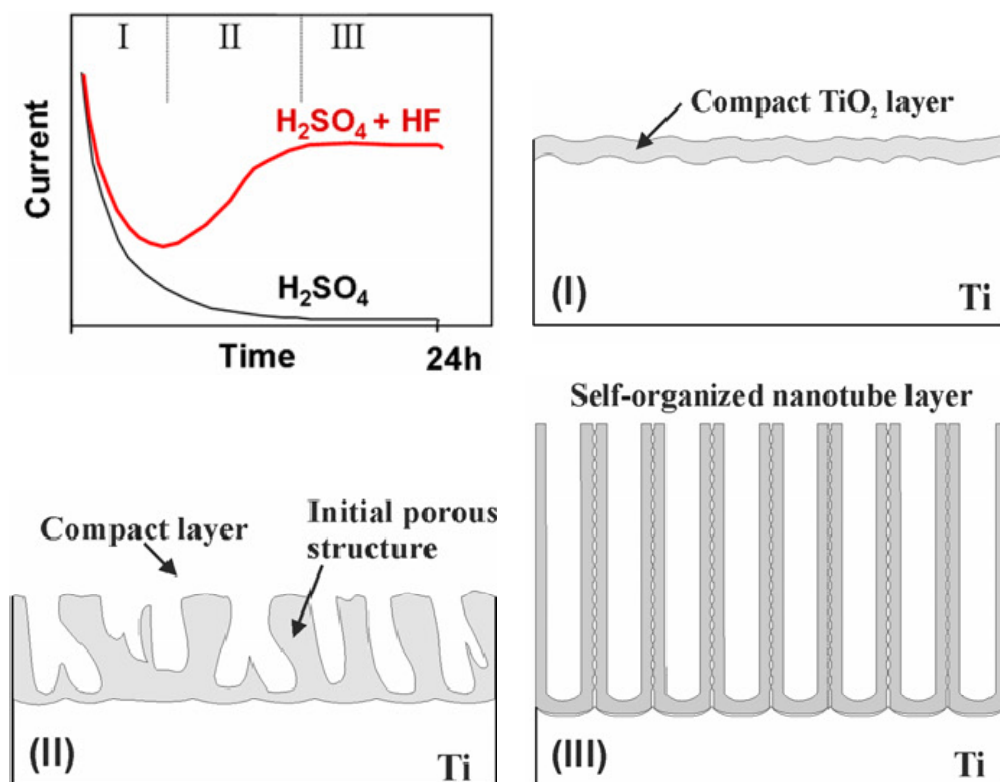


Figure 2-2. Stages of nanotube growth [37]. Graph on the upper left side is a typical current transient recorded during anodization. In that current-time plot, nanotube growth process is divided into three sections. The state of the surface in each section is shown in the other three illustrations.

Mechanism of the self-organized pore formation is described by Yasuda *et al.* [38]. Small and shallow pores, randomly created on the surface tend to go deeper due to local acidification of the etched volume (Reactions (2-1) and (2-2)). Neighboring pores compete for oxidation of the underlying metal. At this stage, deeper pores bear an advantage against shallow ones due to their larger volume of impact. Holes become subject to a natural selection mechanism on this basis and self-organization occurs.

Preparation of highly ordered TiO₂ nanotube arrays was shown and explained in detail by Shin and Lee [39]. For the formation of not just ordered but highly ordered and having a narrow pore size distribution TNTs, they claim that (i) electropolishing and (ii) two step anodization are requisites. Electropolishing creates a smooth surface, removing the roughness. This, in turn, results in homogeneous distribution of the electric field and the pores formed have a narrower diameter distribution, besides the top surface of the tubes become flat rather than rough. Two step anodization that they mention include a first anodization, removing of the formed nanotube layer by an adhesion tape and a second anodization. The remained morphology of the removed layer acts as a template for the formation of the second layer and hence, a highly ordered structure is formed.

In a recent study by Yang *et al.*, synthesis of anatase crystals with a high percentage of reactive (001) facets have been accomplished by introducing fluoride ions into the synthesis medium [40]. Termination of the surface with fluoride atoms decreased the surface energy of (001) facet, thus increasing its abundance. A similar effect may be present to some extent in the synthesis of TiO₂ nanotubes since fluoride ions are present in those synthesis media as well.

Unsurprisingly, TNTs synthesized by the electrochemical anodization method are almost always amorphous. Annealing at high temperatures is required to convert this amorphous oxide to a crystalline form (anatase or rutile), and it is

generally the case since amorphous form is inactive in catalytic and sensing applications.

2.1.2. Synthesis of TNTs in Different Electrolytes

Two major types of electrolytes are reported in the literature as the synthesis environments for TNTs; aqueous and organic. By definition, the electrolyte is a conductive medium, which bears charge carriers (i.e. ions) that migrate to corresponding electrodes to generate current. Most ions are highly soluble in water but generally not in organic liquids. This problem is generally solved by adding some water to the organic, which is enough to solvate the ions. Obviously, organic liquid and water must be miscible to some extent. Water, besides dissolving the ions, has an oxidation role in the oxide formation mechanism (Reaction (2-1)). Similarly, ion solubility is not a matter of conductivity only. Fluoride and titaniumhexafluoride ions, which are elements of the oxide dissolution in the self-organization mechanism (Reaction (2-2)), must also be soluble in the solvent.

Aqueous electrolytes may contain various types of base groups like sulfate, ammonium or phosphate. As we mentioned before, organic solvents must be either miscible with water or must be able to solvate ions. Most suitable organic molecules for this task are the ones that contain hydroxyl groups like ethylene glycol or glycerol.

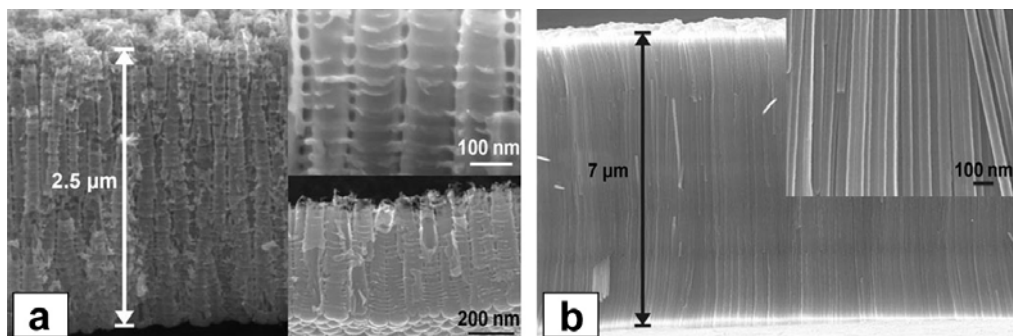


Figure 2-3. Examples to TNTs that are formed in aqueous (a) and organic (b) electrolytes [41].

The most dramatic effect of the choice of solvent is seen in the morphology of the nanotubes. Aqueous electrolytes result in the formation of tubes with ripples on the walls and non-uniform tube cross-section. On the other hand, organic electrolytes (which have higher viscosity compared to water) form tubes with smooth walls and more uniform tube cross section. Other than the morphology, organic electrolytes generally allow the production of much longer tubes compared to aqueous electrolytes. The effect of organic .vs. aqueous electrolytes on the morphology of tubes is illustrated in Figure 2-3.

2.1.3. Effect of Experimental Parameters on Nanotube Properties

Spatial properties of the TNTs like tube diameter, wall thickness and tube length can be controlled by manipulating the synthesis parameters. These are summarized in Table 2-2.

Table 2-2. Synthesis parameters for TNTs and their effects on tube dimensions.

Parameter	Effect
Anodization Voltage	Increasing potential difference results in a linear increase in the tube diameter and tube length [42]. Although 20 V is a commonly used potential for many reported syntheses, self-organization can be obtained in a very broad range of potentials by changing other parameters.
Temperature	Increasing temperature result in a decrease in the tube length and wall thickness. Tubes synthesized at lower temperatures show higher photocatalytic activity [43].
Anodization Time	Increasing anodization time results in longer tubes. However, length approaches a limiting value when etching rate of tubes at the top and oxidation rate of metal at the bottom become equal [37].
Fluoride Concentration	Fluoride concentration, which is a determinative factor of etching rate, has upper and lower limits for the formation of self-organized pores. Etching should be neither too slow nor too fast [42].
pH	H ⁺ concentration determines the rate of oxide dissolution. Hence lower pH results in shorter tubes by etching the top of the tubes. Buffering of the solution helps preventing the local acidification, producing longer tubes [44].

2.2. IMPROVEMENT OF ACTIVITY IN ORDERED TITANIA

The improvement of activity when using ordered titania, whether be photocatalytic efficiency in photocatalytic reactions, or be any kind of cell efficiency in solar cells, has been put forward in many studies. Therefore many groups are working on implementing these ordered materials to known systems like dye-sensitized solar cells [45-49].

Aprile *et al.* have reviewed the concept of improved activity of TiO₂ only caused by spatial modification (i.e. particle size and shape control) [50]. Encapsulation of titania particles inside well defined zeolite pores, formation of periodic mesoporous materials, self-ordered nanotubes, photonic crystals with inverse opal structures and photonic sponges are mentioned. Titania particles encapsulated inside zeolite pores tend to show increased or decreased

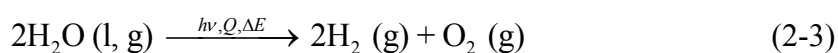
activity depending on the reaction, especially depending on the substrate size (pore size selectivity of zeolites). Photonic crystals, by slowing down the visible light photons inside the material, increase the effective optical path and this leads to increased light absorption near the absorption onset. This is a desired property for titania to carry out visible light photocatalysis.

For the case of titania nanotubes, Aprile *et al.* emphasize the increased diffusion length of charge carriers, which in turn favors the photocatalytic activity [50]. Park *et al.* compare the water splitting performance of TiO₂ nanotubes with Degussa P-25 and with nanoporous (formed by anodization) films of similar thickness [51]. Nanotubes give 20 times higher photocurrent than P-25 film and about twice that of nanoporous film.

If control on spatial tailoring of titania nanotubes can be achieved at the utmost level, then it may be possible to synthesize nanotubes with photonic crystal structure and increase their light absorption on the visible region.

2.3. WATER SPLITTING

Water splitting reaction is the reaction where hydrogen and oxygen is formed from water.



2.3.1. Adsorption of Water on TiO₂

General Aspects

The necessity of any heterogeneously catalyzed reaction is the adsorption of reactants to the catalyst surface. In that respect, the most comprehensive review of interaction of water with several surfaces (including TiO₂) has been given by Henderson [52].

Adsorption of water on TiO₂ surfaces has been studied extensively in the literature [53-62]. The most critical question is whether H₂O adsorbs molecularly or dissociatively. Since the main concern in most TiO₂ related research is its photocatalytic activity, behavior of the surface species upon illumination shall also be known.

Sato and White, in 1981 [63], described the water adsorption as happening together with hole trapping and with the release of a proton -Equation (2-4)- (in a basic solution, trapping by hydroxide is more probable -Equation (2-5)-). Shapovalov *et al.*, in a more recent computational study [61] confirmed that, under illumination, water may dissociate by hole trapping on a R(110) surface just as Sato and White depicted.



It is customary to mention here, a similar, commonly accepted process: trapping of photogenerated holes by surface hydroxyls -Equation (2-6)-.



This process has reports in the literature, dating back to 1977 [64,65]. It is also the most commonly cited mechanism for the initiation of water oxidation to form oxygen.

Studies on Specific Surfaces

Due to the stability of rutile single crystals, surface science studies on rutile are far more abundant, especially on R(110). 5 fold coordinated Ti sites and bridging oxygen vacancies are cited as the adsorption centers for H₂O. Although there is still discrepancy on the adsorption mode of water on R(110), molecular adsorption on terraces and dissociative adsorption on oxygen vacancies seem to be the most widely accepted view.

Both molecular and dissociative adsorption states of water were reported by Henderson on the R(100) surface, monitored by TPD [66]. On the other hand, water was found to adsorb only dissociatively on R(001) surface under UHV conditions, deduced from UPS, ELS and AES experiments [67].

Surface science studies on anatase surfaces are mainly theoretical due to the lack of stability of crystals, but still, experimental studies (generally utilizing natural anatase crystals) exist. Theoretical studies show that for non-illuminated surfaces, water adsorbs molecularly on the more abundant A(101) facet, however on the more reactive (but less abundant) A(001) surface, adsorption is dissociative under 1 monolayer [54,56,57]. Experimental studies confirm these observations as well. Blomquist *et al.*, using synchrotron-excited core level spectroscopy, showed that water dissociated into hydroxyls on A(001) (4x1) reconstructed surface [59]. Herman *et al.*, from a single crystal UHV study employing TPD and XPS, interpreted their findings such that water adsorbed molecularly on A(101) [68].

2.3.2. Mechanism of Water Splitting

Several attempts have been put forward using different methods in search for the mechanism of water splitting. Most critical questions that arise in this challenge are ‘which intermediates?’ and ‘which sites?’. Some answers are now present even though there is no consensus on them.

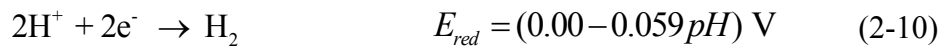
Water splitting is a combination of water oxidation (2-7) and water reduction (2-8).



In a photoelectrochemical cell, these two reactions occur at different electrodes, hence the sites for oxygen and hydrogen evolution is spatially

separated. One phenomenon that assists this drive of electrons and holes to their corresponding electrodes is the formation of an electric field (band bending) near the TiO₂/solution interface [69]. When electron-hole pairs are formed in this layer (having 5-200 nm thickness) holes are drifted to the surface and electrons to the bulk, suppressing the recombination.

Potentials of half reactions have pH dependency according to Nerst Equation.



Values reported in these equations represent the equilibrium potentials. In the actual experimental setup, additional resistances hinder the reaction such as oxygen evolution overpotential. Nozik reported ~1.0 V overpotential for oxygen evolution on a TiO₂ electrode [70].

Photocatalytic reduction of water (or H⁺/H₃O⁺) to generate hydrogen using pure titania powder photocatalysts was reported in the literature but rates have always been too low. Acceptable rates are possible only with a proper metal loading such as platinum. Pt loaded TiO₂ powder can be thought as a short circuited electrochemical cell.

Hydrogen evolution with platinum is understandable since it supplies, as always, the necessary active sites for hydrogen desorption and act as an electron pool for the reduction. Tsai *et al.* studied photoassisted water gas shift reaction (WGS) using Pt loaded TiO₂ single crystals and depicted a mechanism which involve the removal of oxygen atoms at the periphery of the Pt islands [71]. Hydrogen atoms removed from water is transferred directly to Pt and desorb as H₂. Their WGS activity with the number of peripheral Pt sites shows a reasonable correlation. While hydrogen reduction on Pt follows a simple mechanism, same reaction on pure TiO₂ cannot be treated the same way due to

very different electronic properties and surface structure. In the literature, an explicit mechanism for hydrogen evolution on pure TiO₂ could not be found.

Oxidation of water, on the other hand, has been extensively studied by many groups since 1970s. Since the value of TiO₂ stems from its resistance to corrosion under illumination when it is the photoanode in a photoelectrochemical cell (PEC), water oxidation reaction is the main concern in studies regarding water splitting using TiO₂.

Nakato and co-workers have studied the mechanism of water oxidation (O₂ evolution) on R(110) and R(100) thoroughly and published their findings in a series of papers [72-77]. The mechanism they propose involve the nucleophilic attack of a water molecule to a surface trapped hole and formation of a bridging peroxy species. This mechanism is illustrated in Figure 2-4.

First, a hole is trapped at a surface O site. It either diffuses on the surface or recombines with a conduction band electron yielding a photoluminescent photon. At a proper site, diffused hole is subjected to a nucleophilic attack by a water molecule to give vicinal $\cdot\text{O}$ and OH . These vicinal oxygen species couple to yield a peroxy bridge between two surface titanium atoms. Once the O–O bond is formed, consecutive nucleophilic water addition and electron transfer reactions end up in releasing O₂ and restoring the surface structure.

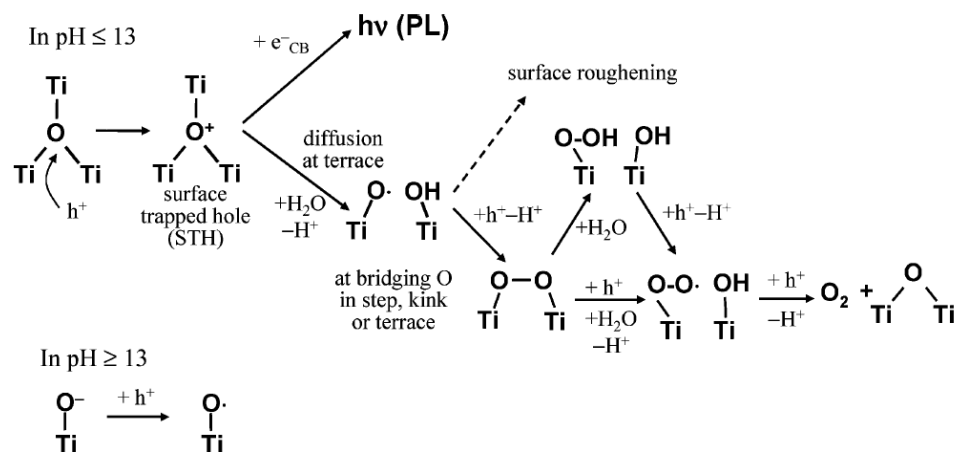


Figure 2-4. A proposed mechanism to the photocatalytic O_2 evolution on TiO_2 [72].

Nowotny *et al.*, combining their extensive knowledge on TiO_2 defect structure with the water oxidation phenomenon, propose a model which involves titanium vacancies as the active sites for the evolution of oxygen [78]. The formation of an active complex is illustrated in Figure 2-5.

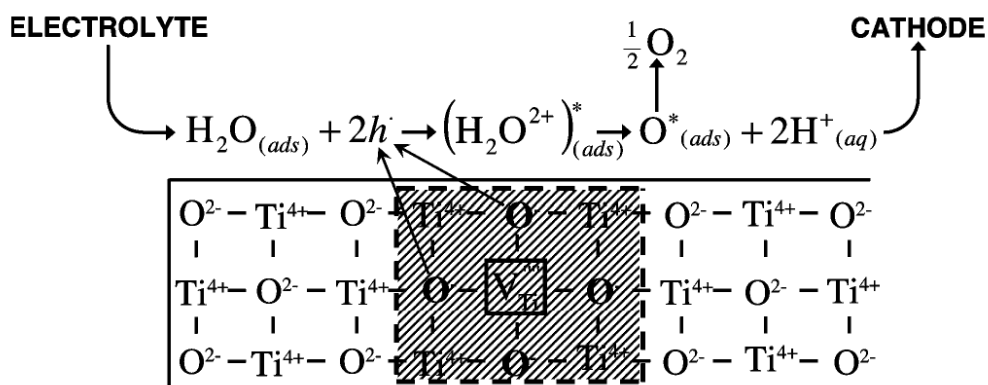


Figure 2-5. Active complex formation as proposed by Nowotny *et al.* in the photocatalytic formation of O_2 from water [78]. Active site here is the titanium vacancy.

Since titanium vacancy is a recently reported defect in TiO₂, their proposal is unique in that sense. It is argued that both oxygen vacancies and titanium interstitials, which are well known defects in TiO₂ for decades [79,80], are donor type defects and the oxidation of water requires acceptor type defects in order for electron transfer from water to TiO₂ to occur. For the production of one oxygen molecule, four electrons must be transferred and two water molecules must be involved to have two oxygen atoms. Since titanium ion is in +4 oxidation state in TiO₂, one titanium vacancy has 4 electron deficiency, which is enough to transfer all electrons at once. Although 4 electrons can be transferred at once, it is not a necessity since regeneration of the vacancy may occur in between the process through the transfer of photogenerated holes from the bulk to the vacancy.

Titanium vacancy is a novel type of defect, introduced to TiO₂ chemistry, and to our knowledge, it does not exist on the surface, but in the bulk. Nowotny's argument is meaningful only assuming the Ti vacancy that is responsible for water oxidation is near the surface site where oxygen evolution takes place, and this site is not explicitly stated by them.

Titanium vacancies are created at high temperatures and in the presence of oxygen, furthermore formation equilibria of this defect strongly depends on the oxygen activity [81-84]. Even though titanium vacancy is a reversible type defect (in theory), it is reported to be very immobile at low temperatures (i.e. such as in typical water splitting experiments) and considered as an acceptor type impurity [85].

Oxidation and photooxidation of water on R(110) was studied by Norskov and co-workers [86] using density functional theory calculations. They have shown that there is a necessary 0.78 V overpotential (at pH=0) for water oxidation, which can be compensated by UV illumination. Their calculations suggest that the rate limiting step of the photooxidation process which occurs in the coordinatively unsaturated sites (5cTi) is the splitting of water to give an

adsorbed OH radical (i.e. $\text{H}_2\text{O} + * \rightarrow \text{HO}^* + \text{H}^+ + \text{e}^-$). Another finding is that the relevant surface termination for photooxidation is the fully O covered surface.

2.3.3. Alternative Water Splitting Catalysts

Alternative water splitting catalysts to TiO_2 cover a wide spectrum from oxides to nitrides, phosphides and sulfides, all of which combine with metals of main group, transition and rare earth. Two recent reviews by Osterloh [87] and Kudo and Miseki [88] summarize the literature on the rate of photocatalytic water splitting reaction by solid catalysts. Kudo [89], Domen [90,91] and Meier [92] groups hold the current records in terms of quantum efficiencies. Kudo and Meier groups report very close production rates for hydrogen, around $20,000 \mu\text{mol H}_2 \cdot \text{h}^{-1} \cdot \text{g}^{-1}$, obtained under UV irradiation. Domen group, on the other hand, reported $3,000 \mu\text{mol H}_2 \cdot \text{h}^{-1} \cdot \text{g}^{-1}$ production rate under visible light irradiation.

2.3.4. Selected Results

Splitting of water with a single crystal TiO_2 -R(110)- photoanode coupled with a platinum black cathode was demonstrated in the famous work of Fujishima and Honda in 1972 [13]. Since TiO_2 -Pt pair does not generate enough potential to split water at a reasonable rate, external bias (additional driving force) is necessary [93]. This bias can be electrical (external electrical potential, like a battery), chemical (difference of pH between the anolyte and catholyte) or both. Chemical bias for water splitting reaction on n- TiO_2 anode can be created by keeping the anolyte basic and catholyte acidic, as dictated by equations (2-9) and (2-10).

A very popular study on water splitting is by Khan and co-workers published in Science [94]. In that study, they employ an oxide covered Ti foil to stoichiometrically split water under artificial visible light irradiation. Oxidation

of titanium surface is done in an optimized (for maximum photocurrent) natural gas/O₂ flame, therefore forming a heavily C doped TiO₂ layer. Although an external bias has been applied, this layer being visible light responsive and probably conductive, achieves an extraordinary rate of hydrogen production (~90 μmol H₂/(cm² h)). It should be mentioned that this result could not be reproduced and reported in the literature by any other group.

Park *et al.* [51] has published the first example of water splitting that utilizes visible light responsive carbon doped TNTs as the photoanode of a photoelectrochemical cell (PEC). Further details of this work is presented in the next section.

In a series of papers, Anpo and co-workers studied the stoichiometric and separate production of H₂/O₂ by the splitting of water, in a stand-alone H-type cell, utilizing concentrated sunlight as the sole energy source [95-97]. These works are significant in the sense that an H-type cell was used for the same purpose in this thesis as well.

2.4. VOLTAMMOGRAMS OF TiO₂ NANOTUBES

Among the many studies in the literature on TiO₂ nanotubes, several attempts have been put forward to characterize their photoelectrochemical behavior. Voltammograms, whether cyclic or linear sweep, have been obtained under illuminated or dark conditions. This section presents a collection of these voltammograms.

In two different publications, Macak *et al.* [37,98] report the cyclic voltammogram of a TNT electrode taken in 1 M (NH₄)₂SO₄. These are given together in Figure 2-6. CV on the left belong to an electrode which has been anodized in 1M H₂SO₄ + 0.13 wt% HF and has 500 nm of tube length. In that experiment, a potential scan between -2.0 and 0 V (Ag/AgCl reference) reveals the oxidation-reduction peaks for Ti⁴⁺ and the onset of H₂ evolution. The

voltammogram on the right show a similar result along with the CV of amorphous (as formed) nanotubes.

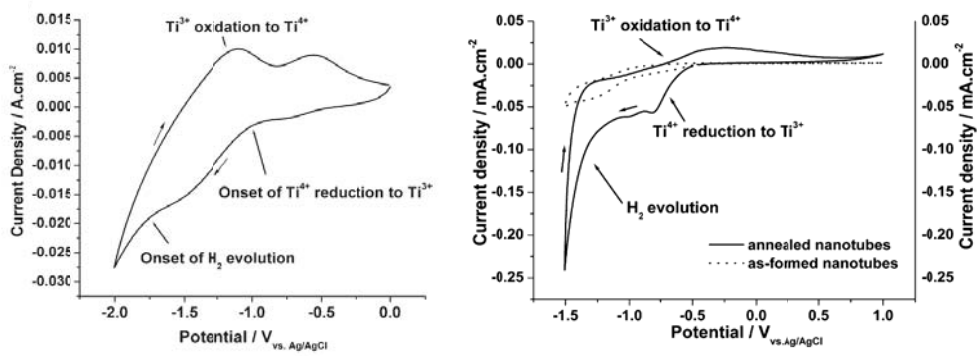


Figure 2-6. Cyclic voltammograms of TNTs taken in 1M $(\text{NH}_4)_2\text{SO}_4$, showing reduction of Ti^{4+} and evolution of hydrogen. Left [98], right [37].

In Figure 2-7 cyclic voltammograms of a compact anodic titanium oxide layer, an amorphous TNT layer and an anatase TNT layer are given together from the work of Ghicov *et al.* [99].

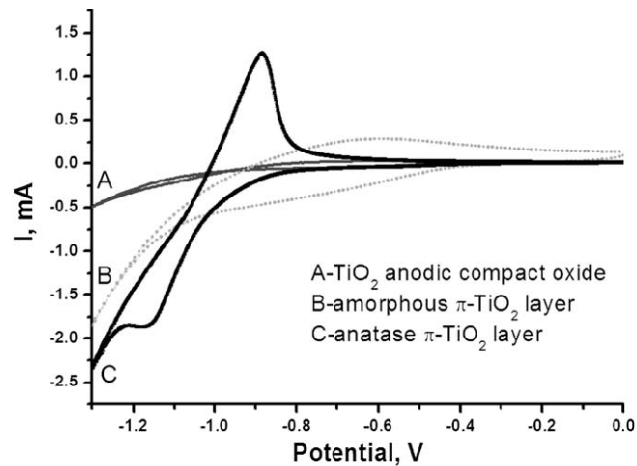


Figure 2-7. Cyclic voltammogram of (A) anodic compact TiO_2 , (B) amorphous TNT, (C) anatase TNT [99]

In a recent study, Xie *et al.* report the electrochemical properties of nickel oxide deposited TNT [100]. Curve (a) in Figure 2-8 shows the cyclic voltammogram of bare TNT taken in 1.0 M NaOH with 5 mV/s scan rate. Curves (b) and (c) belong to NiO deposited TNTs and show 3 orders of magnitude enhancement in the photoresponse.

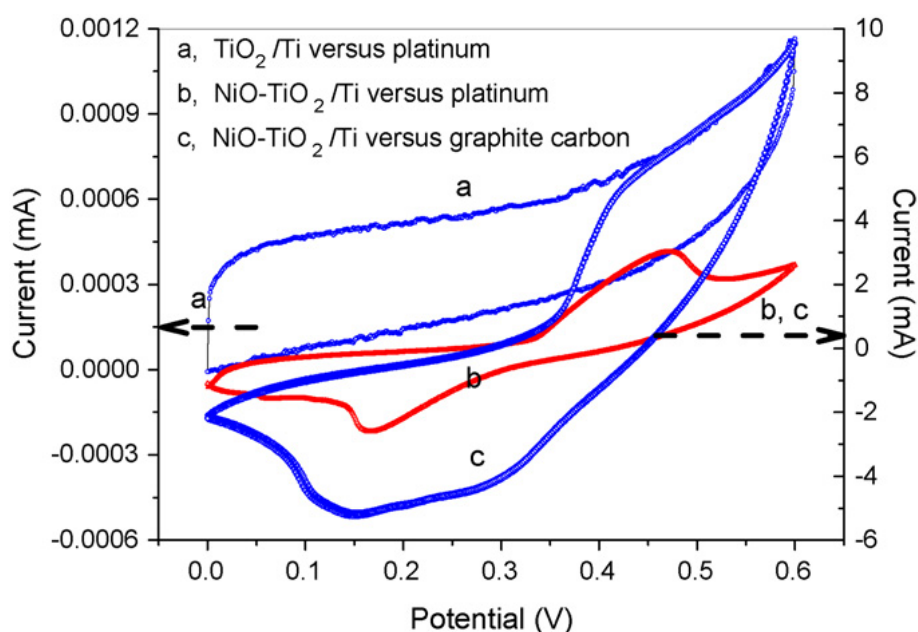


Figure 2-8. Cyclic voltammograms of (a) TNT vs Pt (b) NiO deposited TNT vs Pt and (c) NiO deposited TNT vs graphite, all taken in 1 M NaOH with a SCE reference [100].

Voltammograms that will be presented from this point on are linear sweep voltammograms, mostly showing dark current and photocurrent curves together.

Ruan *et al.* studied the anodization of titanium in boric acid containing electrolytes [101]. Their photocurrent measurements carried out in 1 M KOH and under 320-400 nm UV irradiation (98 mW/cm^2) are given in Figure 2-9 (left). For comparison, photocurrent of a similarly annealed, but not anodized,

titanium foil is given in the second graph (right). This film generates no considerable photocurrent compared to the nanotube layer.

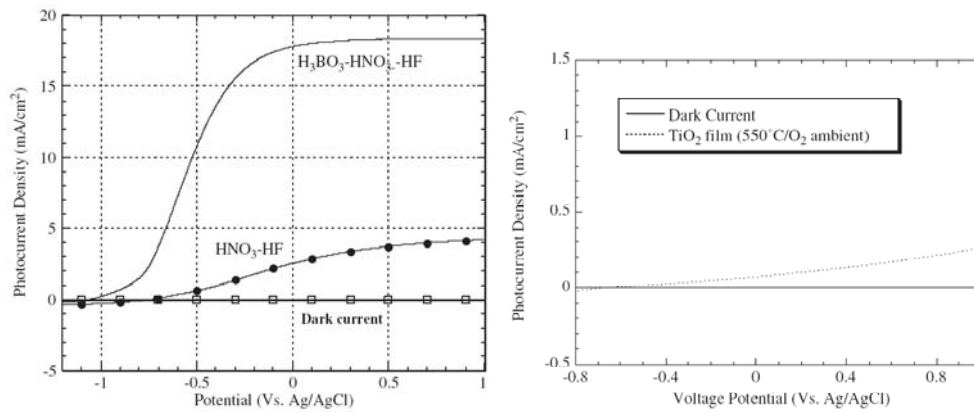


Figure 2-9. Photocurrent and dark current of TNT prepared in boric and nitric acid containing electrolyte (left) and of a thermally grown oxide layer with 250 nm thickness (right) [101].

Mor *et al.* studied the effect of anodization temperature on nanotube properties, reporting their photocurrents as well [43]. Lower anodization temperature lead to the formation of longer tubes with thicker walls. This morphology is seen to enhance the photoresponse of the film. Their results are presented in Figure 2-10.

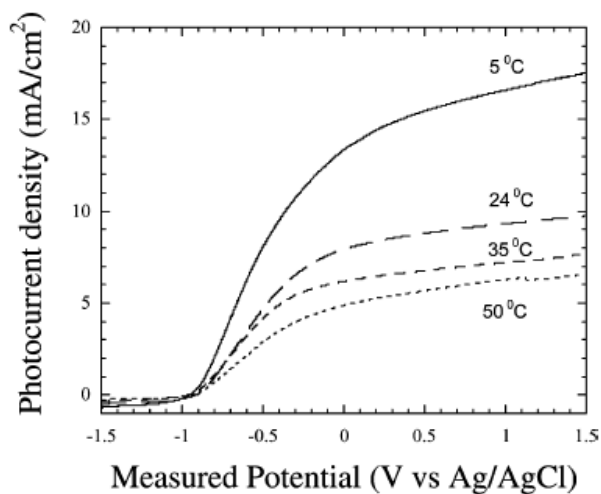


Figure 2-10. Photocurrent plots of TNTs prepared in acetic acid, HF, water mixtures at various temperatures [43]. Experiments were carried out in 1 M KOH and under 320-400 nm UV irradiation.

Figure 2-11 shows the photocurrent curve of not nanotubular but rather high surface area, etched and fluorinated TiO₂ surface [102]. UV illumination intensity is about 3 mW/cm² and there is a wavelength cutoff at 300 nm. This information is presented to demonstrate that photocurrents are strongly influenced by the morphology.

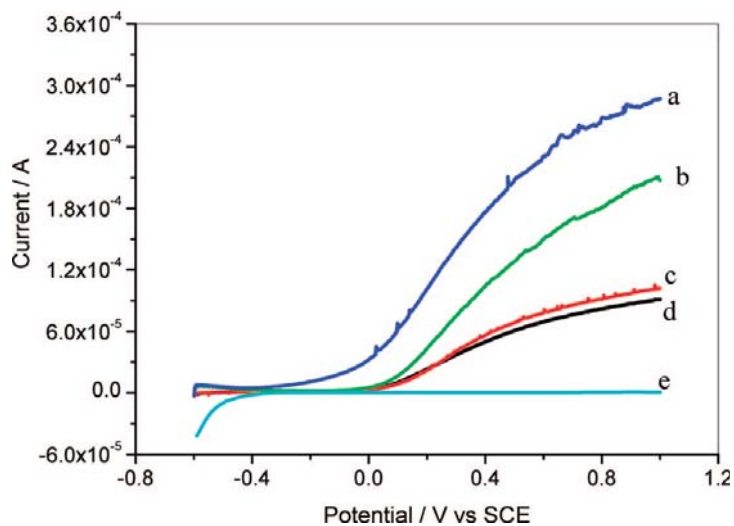


Figure 2-11. Linear sweep voltammogram under illumination for: (a) etched TiO_2 + 0.1 M formate; (b) etched TiO_2 + blank electrolyte; (c) unetched TiO_2 + blank electrolyte; (d) unetched TiO_2 + 0.1 M formate; (e) etched- TiO_2 in the dark [102]. Scan from -0.6 to +1.0 V at a rate 50 mV/s. The blank electrolyte is 0.5 M Na_2SO_4 (pH = 3) with the bubble of N_2 during the experiment.

Chanmanee *et al.* studied the photoelectrical response of a TNT, prepared under a pulse regime [32]. As given in Figure 2-12, pulse anodized nanotubes give higher photocurrent under the same conditions. Oscillatory behavior of the photocurrent is due to the chopping of incident light, proving that current is generated by the light.

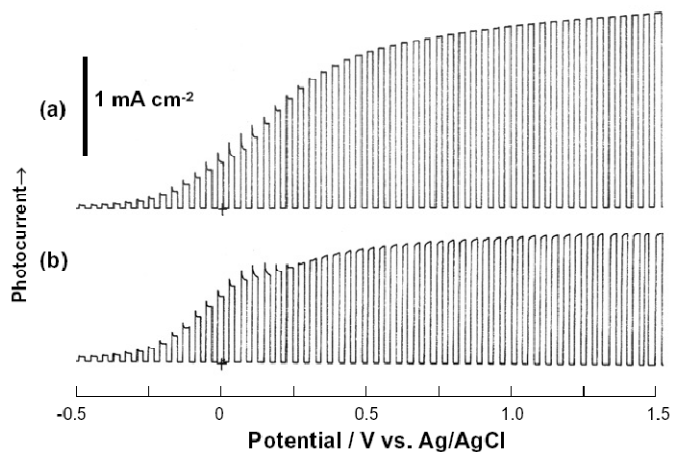


Figure 2-12. Photocurrent-potential profiles under chopped irradiation (0.05 Hz) for TNTs prepared using pulse (a) and constant (b) anodization. TNTs were grown in 0.36 M NH_4F in water. Data taken in 0.5 M Na_2SO_4 [32].

A similar study, by the same group, was carried out in order to observe the effect of formate addition to the PEC electrolyte [103]. Data in Figure 2-13 illustrates the enhancement of photocurrent with the addition of sodium formate.

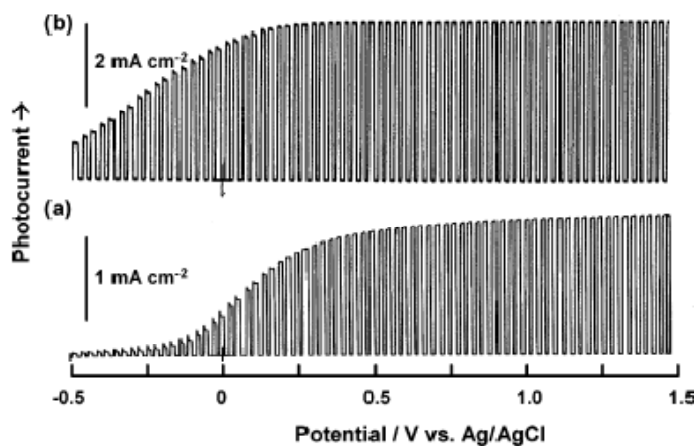


Figure 2-13. Linear-sweep photovoltammograms with 0.1 Hz chopped irradiation of a TNT obtained by anodization of Ti foil (20 V, 10 h) in 0.15 M NH_4F /glycerol in (a) 0.5 M Na_2SO_4 supporting electrolyte and (b) 0.5 M Na_2SO_4 + 0.1 M HCOONa . Photovoltammograms were obtained at 2 mV/s using the full output of a 150 W Xe lamp [103].

Another study investigating the effect of organic matter addition to the PEC electrolyte as a sacrificial reagent was carried out by Mohapatra *et al.* [104]. Figure 2-14 shows that among methanol, glycerol and ethylene glycol, glycerol makes the best improvement on photocurrent.

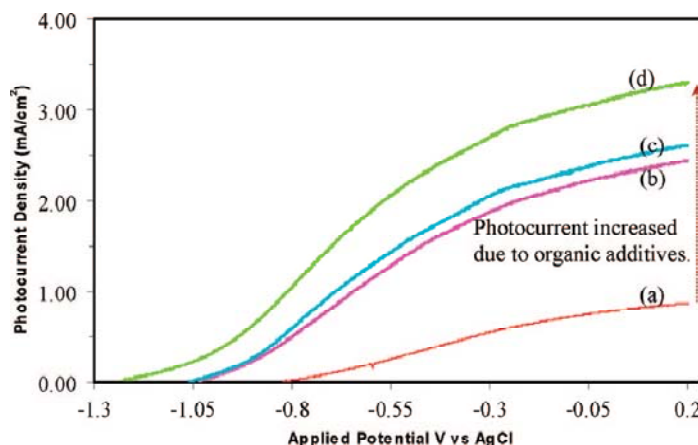


Figure 2-14. Potentiodynamic plot of TNT photoanode in 1 M KOH solution containing (a) without organic additives (b) 5% methanol, (c) 5% glycerol and (d) 5% ethylene glycol as organic additive. Anodization of foil was done in 0.5 M H_3PO_4 + 0.14 M NaF (pH 2.1) at 20 V for 45 min with ultrasonication [104].

Mohapatra *et al.* demonstrate a C doped TNT which is photoactive under visible light irradiation [105]. Nanotubes are synthesized in NH_4F , water, ethylene glycol mixture under ultrasonic agitation. Illustrative data are presented in Figure 2-15, which shows the photoresponses of nanotubes under UV, visible and complete solar spectrum. Care must be taken as the authors do not mention any normalization with respect to the incident photon flux.

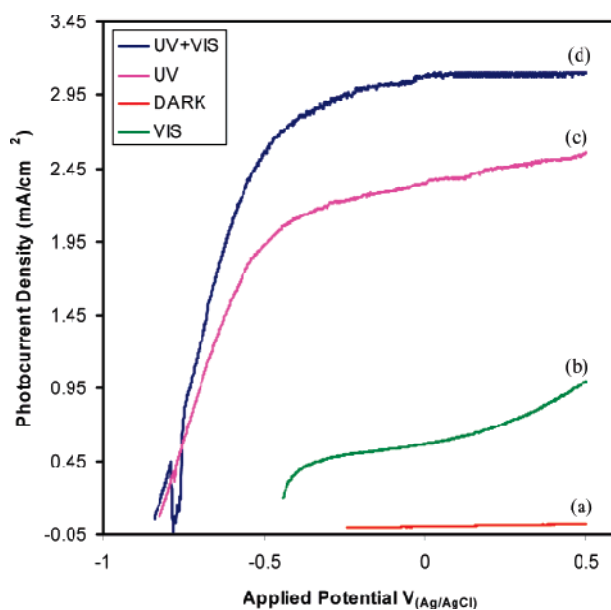


Figure 2-15. Photovoltammograms of C doped TiO₂ nanotubes as a visible responsive photoanode and Pt foil as cathode, recorded in 1 M KOH under illumination of varying range of wavelengths. Light is filtered from artificial sunlight [105].

Figure 2-16, which is taken from a study by Mohapatra *et al.* illustrates the effect of ultrasonic agitation (during anodization) and annealing atmosphere on the photocurrent [106]. It is indicated that annealing in N₂ atmosphere (rather than O₂) and ultrasonic agitation during anodization improves the photocurrent density of TNTs.

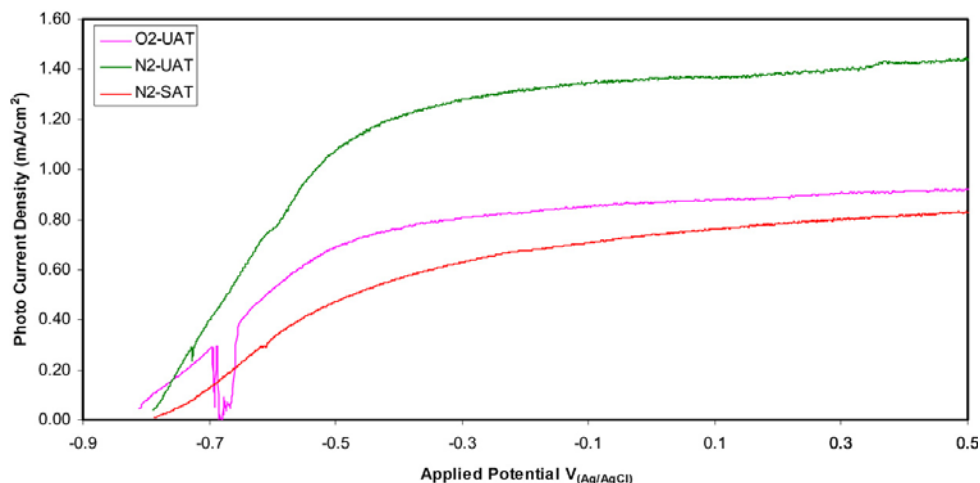


Figure 2-16. Photovoltammograms of TNTs prepared in an aqueous environment, recorded under simulated solar irradiation [106]. UAT: Ultrasonic agitation during anodization, SAT: Magnetic stirring during anodization, N₂/O₂: Annealing under nitrogen or oxygen environment.

Park *et al.* systematically investigated the effect of nanotube length (Figure 2-17 - left) and type of TiO₂ layer (Figure 2-17 - right) on the photocurrent [51]. Increasing film thickness up to 3.3 μm was seen to enhance photocurrent. Comparing Degussa P-25, nanoporous and nanotube films on titanium substrate, nanotube layer gave the higher photocurrent density.

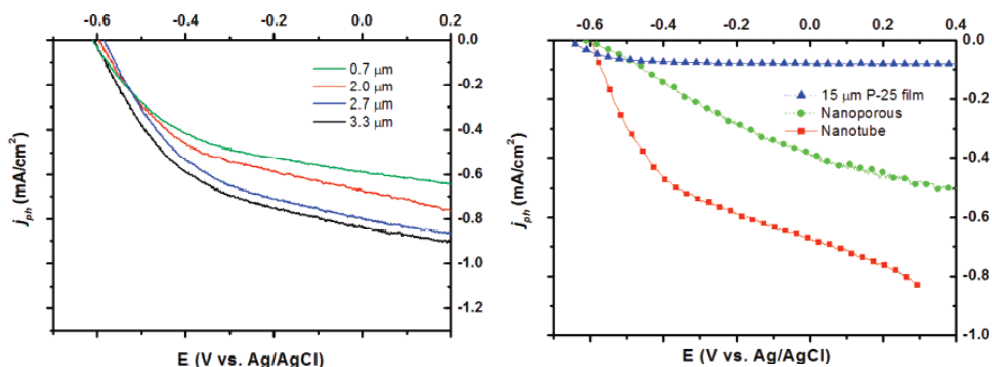


Figure 2-17. Photocurrent characteristics of nanotube films with varying lengths, prepared in 1M NH₄H₂PO₄ + 0.5 wt% NH₄F electrolyte (left) and of films of similar thickness with different morphologies: P-25 nanoparticle film, nanoporous film and nanotubular film (right) [51].

2.5. HYDROGEN PRODUCTION RATES

Photocatalytic hydrogen production rates of titania and titanate based catalysts (or photoelectrochemical systems, in which a photoanode is the key component) by water splitting reaction are reviewed and collected in Table 2-3. In commercial electrolyzers, hydrogen production rates are orders of magnitude higher than those reported in here. Alkali electrolyzers work at a typical 100-400 mA/cm² current density while PEM electrolyzers work at about 1600 mA/cm² current density [1]. These correspond to rates of 1900-7500 μmol H₂ h⁻¹ cm⁻² and 30,000 μmol H₂ h⁻¹ cm⁻² respectively.

Table 2-3. Rates of photocatalytic hydrogen production in the literature by water splitting reaction.

Work	Catalyst and System	Light	Solution	O ₂ /H ₂	Rate (μmol H ₂ /h·cm ²)	Rate (μmol H ₂ /h·g cat.)	Other
Fujishima <i>et al.</i> 1975 [107]	PEC, TiO ₂ film on Ti plate .vs. Pt black, no external bias	Natural sunlight	Anode: 1 N NaOH, Cathode: 1 N H ₂ SO ₄ ,		2.5		
Schrauzer and Guth 1977 [108]	TiO ₂ powder, chemisorbed H ₂ O, under Ar	UV, 360 W Hg Lamp		~1/2		5.8	
Sato and White 1980 [109]	Pt/TiO ₂ powder, gas phase	UV, 200W Hg Lamp		1/2		0.4	
Wagner and Somorjai 1980 [110]	SrTiO ₃ , single crystal, many variations	UV	Varying NaOH solutions	~1/2	~3 (max.)		
Smotkin <i>et al.</i> 1986 [93]	Anodized / Platinized bipolar electrodes in series to supply required potential	Xe lamp	KOH	1/2.4	3.5		Efficiency definition: $Eff = \frac{ff \cdot V_{oc} \cdot i_{sc}}{P \cdot A \cdot n}$ ff: fill factor, P: energy flux, A: panel area, n: number of panels
Abe <i>et al.</i> 2000 [111]	EosinY/TiO ₂	λ>460 nm	H ₂ PtCl ₆ (0.1% w/w) TEOA*	0		140	
Arakawa and Sayama 2000 [112]	NiO _x /TiO ₂ (%3 w/w)	AM-1.5	2.2 M Na ₂ CO ₃	~1/2	0.29		
	RuO ₂ /TiO ₂ (%3 w/w)	AM-1.5	2.2 M Na ₂ CO ₃	~1/2	0.11		
	Pt/TiO ₂ (%0.1 w/w)	AM-1.5	DI water 2.2 M Na ₂ CO ₃	0 ~0	0.014 0.031		
Yoshida <i>et al.</i> 2000 [113]	Suspension, Pt/TiO ₂ (0.1% w/w)	UV	DI water	~1/2		200	
Zou <i>et al.</i> 2001 [114]	NiO _x /In _{0.90} Ni _{0.10} TaO ₄	λ>420 nm	DI water	1/2		33	
	RuO ₂ /In _{0.90} Ni _{0.10} TaO ₄	λ>420 nm	DI water	1/2		17	
Abe <i>et al.</i> 2001 [115]	Pt/TiO ₂ (anatase) + TiO ₂ (rutile)	λ>300 nm	0.1 M NaI pH = 11	1/2		360	

* TEOA: triethanolamine

Table 2-3. Rates of photocatalytic hydrogen production in the literature by water splitting reaction. (cont'd)

Work	Catalyst and System	Light	Solution	O ₂ /H ₂	Rate (μmol H ₂ /h·cm ²)	Rate (μmol H ₂ /h·g cat.)	Other
Khan <i>et al.</i> 2002 [94]	PEC, TiO ₂ film on Ti plate .vs. Pt foil, external potential applied	Xe arc lamp	5 M KOH	1/2	~75*		Photoconversion efficiency: $\epsilon_{eff} = \frac{j_p (E_{rev}^0 - E_{app})}{I_0}$ j _p : photocurrent density, I ₀ : incident light intensity, E _{rev} ⁰ : 1.23 V, E _{app} : absolute value of applied potential = (E _{app} - E _{aoc}) = (measured electrode potential - open circuit electrode potential)
Kato <i>et al.</i> 2003 [89]	NiO (0.2wt %) / NaTaO ₃ :La (2%)	Hg lamp - UV	1 mM NaOH	~1/2		20,000	Presents a mechanism and identifies H ₂ and O ₂ evolution sites.
Abe <i>et al.</i> 2003 [116]	Pt/TiO ₂ (anatase)	UV, cut-off λ>300 nm	1 mM NaI	1/2		240	
Gondal <i>et al.</i> 2004 [117]	TiO ₂	UV laser, 335 nm	DI water			5,000	NiO, WO ₃ and Fe ₂ O ₃ are also studied.
Lee <i>et al.</i> 2004 [118]	Pt/TiO ₂	UV	0.01 M NaOH, 1 mM KI	No O ₂ report		~200-400	
Luo <i>et al.</i> 2004 [119]	Cl ⁻ & Br ⁻ co-doped Pt/TiO ₂ (70% anatase 30% rutile)	Hg lamp - UV	2.2 M Na ₂ CO ₃	~1/2		450	TiO ₂ is specially synthesized
Iwase <i>et al.</i> 2006 [120]	Au/ NaTaO ₃ :La	Hg lamp - UV	DI water	≤1/2		4,000	
Kitano <i>et al.</i> (2006-2007) [95-97]	TiO ₂ /Ti/Pt foil electrode, H type cell	λ>420 nm	pH = 0 and 14	~1/2	0.02		
		Collected sunlight	pH = 0 and 14	~1/2	0.3		

* At the point of highest photoconversion efficiency

CHAPTER 3

MATERIALS AND METHODS

3.1. PREPARATION OF MATERIALS

3.1.1. Catalytic Surfaces

Preparation procedure for the TNT surfaces is described below. Information on each different sample is summarized in Table 3-1.

Table 3-1. Descriptions of different sample abbreviations used throughout the text.

ABBREVIATION	DESCRIPTION
TNT-aq	Synthesized in aqueous electrolyte, annealed at 450 °C in air, 0.5x2.5 cm ² anodized area on each side
Pt/TNT-aq-cell (Used in H-type cell)	Synthesized in aqueous electrolyte, one side Pt loaded with 0.003 M Pt solution, annealed at 450 °C in air, 4x4 cm ² anodized area on each side
Pt/TNT-aq-1	Synthesized in aqueous electrolyte, two sides Pt loaded with 0.03 M Pt solution, annealed at 450 °C in air, 3x3 cm ² anodized area on each side
Pt/TNT-aq-PEC	Synthesized in aqueous electrolyte, dried at 120 °C before Pt loading, two sides Pt loaded with 3.8 wt% Pt solution, annealed at 450 °C in air, 2x2 cm ² anodized area on each side
TNT-org-2h	Synthesized in organic electrolyte for 2 hours, annealed at 500 °C in 10% H ₂ in Ar, 2.2x0.5 cm ² anodized area on each side
TNT-org-4h	Synthesized in organic electrolyte for 4 hours, annealed at 500 °C in 10% H ₂ in Ar, 2.6x0.5 cm ² anodized area on each side
TNT-org-6h	Synthesized in organic electrolyte for 6 hours, annealed at 500 °C in 10% H ₂ in Ar, 2.2x0.5 cm ² anodized area on each side

Pre-treatment

Before anodic oxidation, titanium foils (Ti -Aldrich 99.7%-) were cleaned in acetone and ethanol baths consecutively and finally rinsed thoroughly with DI water. Anodization was carried out immediately after cleaning. For the cleaning of platinum electrode, same procedure was applied from time to time, when the electrode was thought to be greased.

Anodic Oxidation

Since the concentration of fluoride in the anodization solution is critical, solid NH_4F (powder NH_4F -Merck *for analysis* 98.0%-) was dried in a heated mortar under the hood (with continuous grinding) for several minutes to remove moisture. Heating rate was controlled carefully to prevent excessive sublimation of NH_4F .

Anodization of the catalytic surfaces was established in a water-jacketed Pyrex cell. A relatively high voltage (up to ~ 100 V), DC power supply was used as the current source. In every anodization process, 20 V potential difference was applied.

Connected to the positive (+) terminal, titanium foils of varying sizes became anode. Every time, cathode was a platinum foil with 3×5.5 cm² dimensions point welded to a 3 cm platinum wire. Platinum wire was point welded to a long copper wire. To isolate the copper wire from the electrolyte, the wire part of the cathode assembly, beginning from the platinum wire, was taken inside a glass tube. Tip of the glass was melted and the melted glass covered the platinum wire, making the necessary isolation. Anode material was cut from the purchased plate using scissors, leaving a narrow tail that extends out of the solution to allow for electrical contact. This way, contamination from anode contacts was also prevented.

TNT-aq

The electrolyte was prepared as described by Ghicov [29]. 1 M $\text{NH}_4\text{H}_2\text{PO}_4$ was prepared from the solid (powder $\text{NH}_4\text{H}_2\text{PO}_4$ -Merck *for analysis* 99.0%-) and DI water, and then required amount of solid NH_4F was added in order to make the solution 0.5 wt% NH_4F . Anodization was carried out for 400 minutes. While selection of this electrolyte as anodization medium had no profound reasoning behind, application of the same conditions by Park *et al.* [51] was thought to be useful for comparison.

TNT-org

Electrolyte was prepared as described by Mohapatra *et al.* [105]. Solution consisted of 10 wt% DI water, 0.5 wt% NH_4F and balance ethylene glycol (liquid ethylene glycol -Merck *extra pure* 99.0%-). Three samples were anodized for three different times: 2 hours, 4 hours and 6 hours. These samples were identified as TNT-org-2h, TNT-org-4h and TNT-org-6h respectively. Electrolyte selection was based on the visible light active nature of the films produced in the referred study.

Post-treatment

Pt Loading

Pt loading was achieved by wetting the desired surface of foil with minimum amount of $\text{Pt}(\text{NH}_3)_4\text{Cl}_2$ solution (prepared using $\text{Pt}(\text{NH}_3)_4\text{Cl}_2 \cdot \text{H}_2\text{O}$ salt -56.4 wt% Pt Alfa-Aesar- and) and then subsequent annealing. Since the rate of heating was slow, a drying step was thought to be unnecessary. Table 3-1 contains the information on the concentration of these Pt solutions.

Amount of loaded platinum could not be controlled very precisely but considering the approximate volume that wets the surfaces, we can make a rough estimate. Approximate Pt loading densities are presented in Table 3-2.

Table 3-2. Experimental parameters for Pt loading and the calculated Pt loading densities (approximate)

Sample	Pt Solution	Approximate Volume of Pt Solution Used	Pt Loaded Area	Approximate Pt Loading Density
Pt/TNT-aq-1	0.03 M	0.5 mL	9 cm ²	0.3 mg/cm ²
Pt/TNT-aq-cell	0.003 M	1 mL	16 cm ²	0.04 mg/cm ²
Pt/TNT-aq-PEC	3.8 wt%	0.3 mL	4 cm ²	3 mg/cm ²

Annealing

Annealing of the samples synthesized in aqueous electrolytes was done in a tubular furnace under air flow. They were heated to 450 °C with a heating rate of 2 °C/min, kept there for 3 hours and then let cool naturally.

Samples synthesized in organic electrolytes were annealed also in a tubular furnace but under flow of 10% H₂ in Ar. They were heated to 500 °C with a heating rate of 2 °C/min kept there for 2 hours and let cool naturally.

3.2. CHARACTERIZATION

A Rigaku X-ray diffractometer with Cu target (30 kV, 15 mA) was used for the XRD measurements with a scan rate of 2 degrees/min.

For SEM analysis, two different instruments were employed at different times. The one with higher resolution was a QUANTA 400F Field Emission SEM supplied by the Central Laboratory of METU. Due to a technical failure in that device at the time of other measurements, namely the characterization of TNTs synthesized in organic electrolyte and sample “Pt/TNT-aq-PEC”, another instrument at the Chemistry Department of Bilkent University was employed.

This instrument was a Zeiss EVO40 environmental SEM equipped with a Bruker AXS XFlash 4010 detector for EDX.

3.3. WATER SPLITTING CELL (H-TYPE CELL)

A cell was fabricated from quartz, made up of two identical halves. Quartz was selected because of its UV transparency. In between these two halves of the cell, an electrode/membrane(Nafion) assembly was squeezed (o-rings were used to prevent leakage). Electrode/membrane assembly is kind of a sandwich of electrode and membrane between two 10 mm thick Plexiglas plates, fastened by four bolts. Plates are previously drilled, such that electrode and membrane contact both sides of the assembly. Scheme of the cell is shown in Figure 3-1. As can be deduced from this scheme, measurement of the evolved gases is done via the displacement of water in 1 mL burettes.

Electrode is designated as “Pt/TNT-aq-cell” throughout the text. It is an anodized foil, one side loaded with platinum as described in “Pt Loading” section.

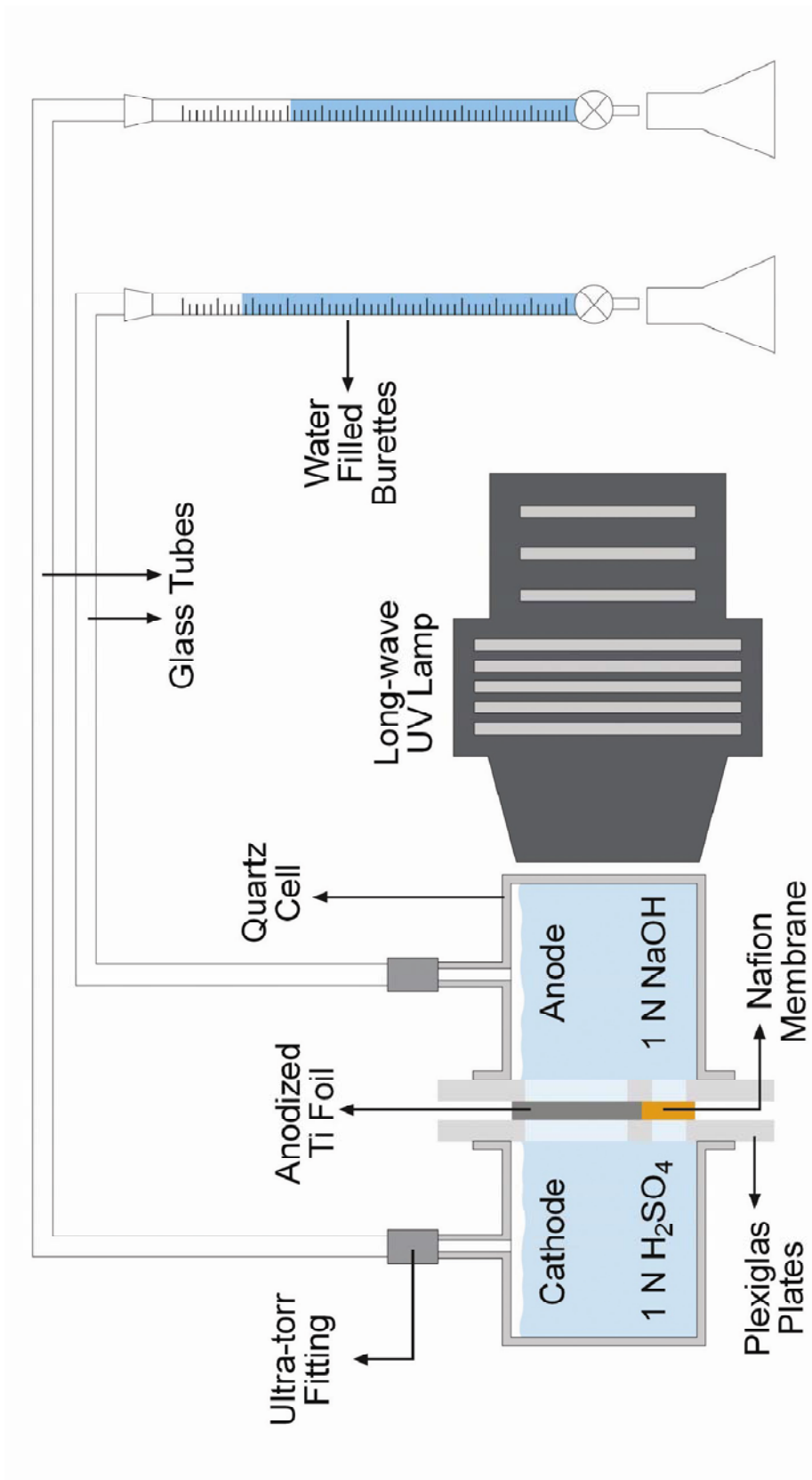


Figure 3-1. Scheme of the water splitting setup, utilizing the H-type cell

Anode side of the cell was filled with 1N NaOH and cathode side with 1N H₂SO₄ (prepared from H₂SO₄ -95-98% Merck *extra pure*-, pellet NaOH - 98% Merck *extra pure*- and DI water).

Nafion was kept in a series of baths at 80 °C containing DI water - 3% H₂O₂ - H₂SO₄ - DI water (3 consecutive), each for one hour for cleaning and restoration of ionic conductivity.

The cell was illuminated with a UVP B-100AP model 365 nm long-wave UV lamp equipped with a beam directing funnel. Light intensity is specified as 21.7 mW/cm² at 2 inches away the source. No filter was used to remove the infrared portion of illumination.

It is expected that the temperature of the cell may increase due to the exothermic recombination of photogenerated charge carriers and due to the infrared radiation generated by the light source, however temperature of the cell was not monitored nor controlled, thus assumed to be at room temperature.

3.4. PHOTOELECTROCHEMICAL TESTS

Photoelectrochemical tests were carried out using an IviumStat potentiostat/galvanostat connected to a BASi C3 cell stand. A BASi Ag/AgCl electrode filled with 3M NaCl was used as reference electrode.

As the electrochemical cell, first, a two compartment Pyrex cell separated with a porous glass frit was fabricated (Figure 3-2). TNT-org-4h (with 2x2 cm² area) was the working, Pt/TNT-aq-PEC was the counter electrode. Due to extensive resistance caused by the frit and the wide electrode spacing, no current could be measured. In order to eliminate this resistance, a one compartment cell was used. The cell was a cylinder with an open top, having 5.3 cm ID and 6.5 cm height. It had a 2.5x2.5 cm² flat quartz window on the side glued with silicone rubber and a Plexiglas top lid with 3 bores (6 mm ID)

for letting the electrodes in. This cell can be visualized as the right half of the previous cell, illustrated in Figure 3-2. The counter electrode in the one compartment cell was a Pt wire.

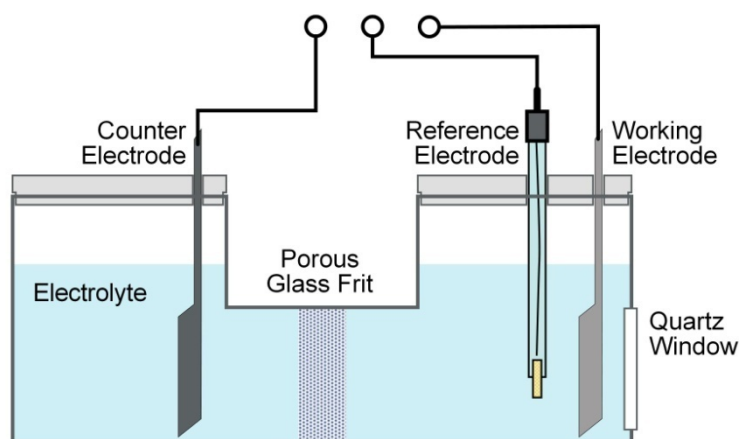


Figure 3-2. Scheme of the first cell fabricated for the electrochemical test. This cell could not be utilized due to poor conductance.

Cyclic voltammograms of the samples were taken with a scan rate of 0.05 V/s in 0.1N H₂SO₄ and 0.1N KOH solutions (prepared from H₂SO₄ -95-98% Merck *extra pure*-, pellet KOH -85% Merck *for analysis*- and DI water). Same experiments were conducted with non-annealed and annealed samples, under illumination and in the dark. All voltammograms were taken at room temperature.

CHAPTER 4

RESULTS AND DISCUSSIONS

4.1. CHARACTERIZATION OF TiO₂ NANOTUBES

4.1.1. SEM Images

SEM analysis was performed on each synthesized TNT surface. Figure 4-1 shows the morphology of surface obtained by anodization of Ti foil in aqueous NH₄H₂PO₄ electrolyte. Image on the right shows the platinum deposited surface, size of platinum particles being on the order of 50 nm. Underlying morphology of the nanotubes can clearly be seen.

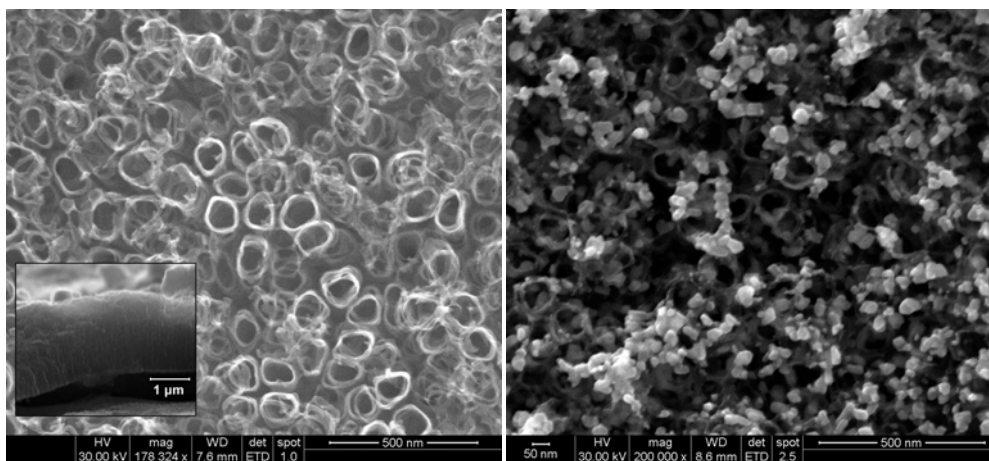


Figure 4-1. SEM pictures of TNT-aq, with side view inset (left) and Pt/TNT-aq-1 (right).

TNTs synthesized in organic electrolyte (ethylene glycol-water) have the morphology shown in Figure 4-2. Figure shows, from left to right, images of

nanotubes synthesized for 2, 4 and 6 hours. From top and side view (not shown here) images of these samples, we can conclude that self organization of nanotubes is almost complete in two hours of anodization.

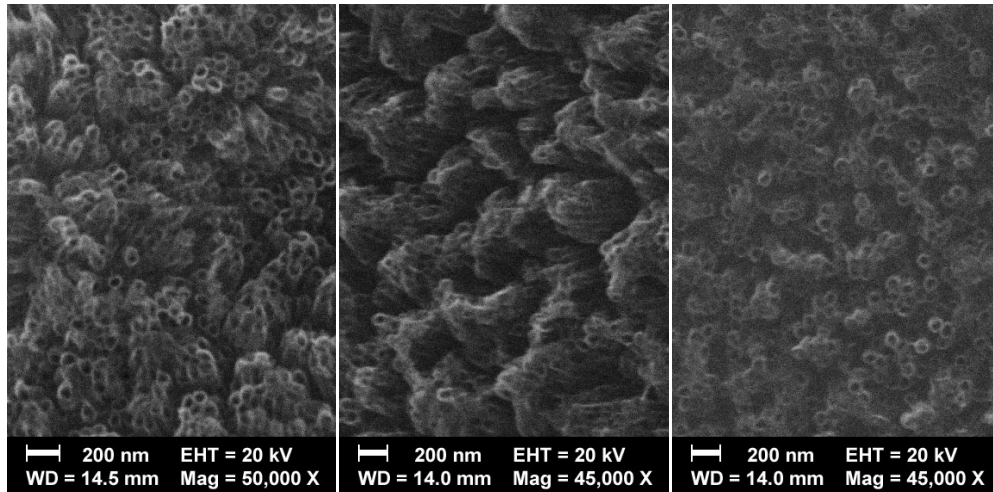


Figure 4-2. SEM pictures of, from left to right, TNT-org-2h, TNT-org-4h and TNT-org-6h.

The growth directions of nanotubes synthesized in organic electrolytes are irregular as deduced from the SEM images. This type of growth is seen to form mountain like morphology with valleys in between. This growth irregularity is not that pronounced in TNT-aq. One reason may be the non-homogeneous distribution of the electric field on the surface if untreated surface itself has an irregular morphology (Shin and Lee use electropolishing to obtain smooth surfaces prior to anodization [39]). This may be the situation in our case because titanium foils used in the synthesis with organic electrolytes were smaller in size (Table 3-1) and were subject to more mechanical forces to get them straightened.

Surface areas of the nanotubes were calculated by using a simple geometrical calculation. Average diameters and average lengths of the tubes were measured

and number of tubes in a given area is counted from the SEM images. Each tube was assumed to be cylindrical. Only the lateral surfaces of the tubes were considered and the area of one tube was taken as “ $\pi \times (\text{inner tube diameter}) \times (\text{tube length})$ ”. Most of the error in this calculation stems from the measurement of the tube lengths. Images of the tubes were not taken at a right angle so there is an error related to the image perspective. Still though, these errors shall be similar in each sample and we can still compare the areas relative to each other. Besides, the order of magnitude of the calculated numbers give an idea about the extent of real surface area.

Average inner diameters, average lengths, number densities of the tubes and the surface area per flat electrode area are presented in Table 4-1.

Table 4-1. Spatial properties of pure TiO₂ nanotubes as measured and calculated from their SEM images.

Sample	Average Inner Tube Diameter (nm)	Average Tube Length (μm)	Number Density of Tubes (tubes/cm²)	Surface Area* (cm²/cm²)
TNT-aq	75	1.9	4.6×10^9	21
TNT-org-2h	49	2.7	5.1×10^9	22
TNT-org-4h	47	3.1	3.2×10^9	15
TNT-org-6h	52	1.7	5.7×10^9	16

* Surface area is the calculated area of the tubes per flat area of the underlying titanium substrate

In the reported parameters of Table 4-1, the tube length of TNT-org-6h has the highest uncertainty because the perspective of the SEM image was tilted more than other images' perspectives. Besides, longer tubes are expected with

increasing anodization time. Therefore surface area of this sample shall be on the order of $30 \text{ cm}^2/\text{cm}^2$.

In the aim of producing a Pt equivalent cathode for the PEC by impregnating Pt to TNT-aq surface, we used a Pt solution of different concentration and dried the material before impregnation at $120 \text{ }^\circ\text{C}$. This procedure resulted in well dispersed Pt particles, which is shown in Figure 4-3 (Pt/TNT-aq-PEC). Unlike the images shown in Figure 4-1, collected on Quanta 400F SEM instrument, on Zeiss EVO40 SEM instrument, individual Pt particles could not be resolved. However EDX mapping was performed to verify the dispersion of Pt. Green dots in the right hand side image are signals from platinum particles, while red are from titanium. This indicates that loading procedure results in fine particles.

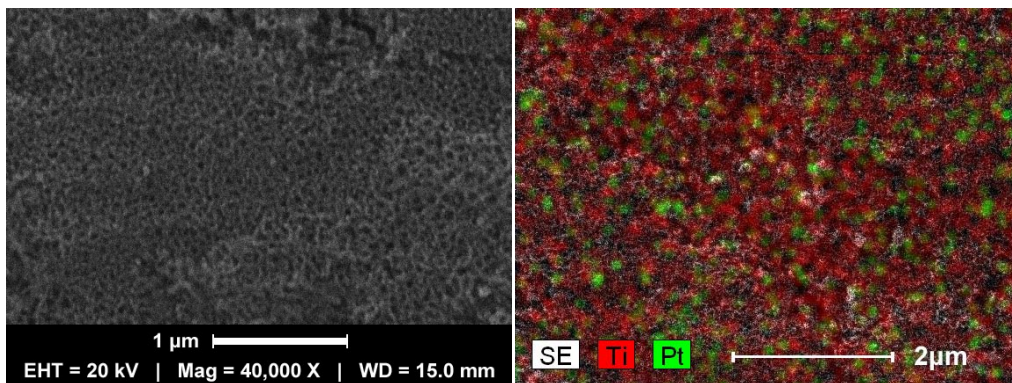


Figure 4-3. SEM picture of Pt/TNT-aq-PEC and EDX mapping of the same surface (a different spot).

4.1.2. X-Ray Diffractogram

X-ray diffractogram of Pt/TNT-aq-1 is given in Figure 4-4. Titanium base gives the most intense peaks. These peaks were verified by the X-ray diffractogram of pure titanium foil (given in Appendix B). Rest of the peaks fit

either to anatase or platinum (metallic), as identified from ICDD Powder Diffraction Database.

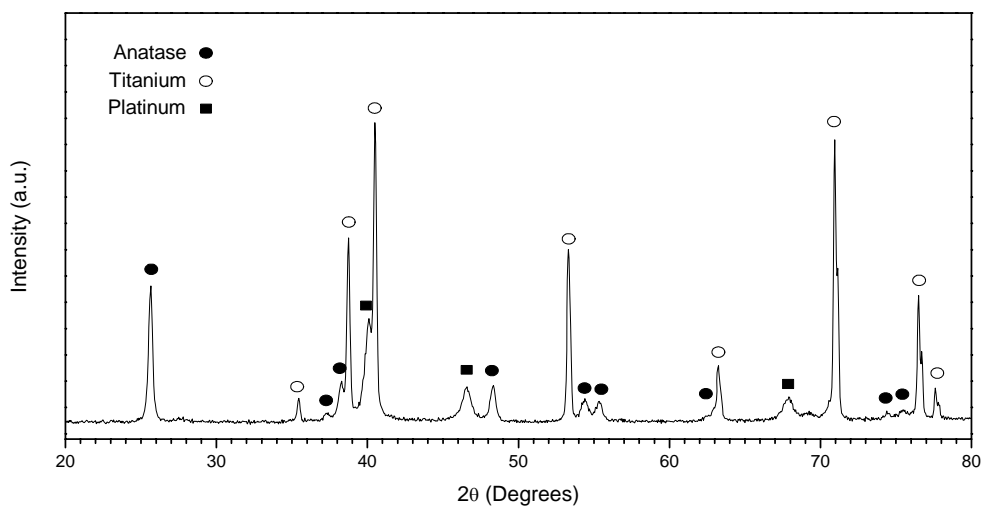


Figure 4-4. X-Ray diffractogram of Pt/TNT-aq-1, showing peaks of metallic titanium (base), anatase (nanotube oxide layer) and deposited platinum (in metallic state).

Band gap is a characteristic property of titania photocatalysts and is generally reported in related studies. Unfortunately, methods in the literature for the band gap determination of ordered titania nanotube films were not practical enough and could not be conducted due to technical incapability.

4.2. GAS EVOLUTION IN H-TYPE CELL

H-type cell is a device which, in principle, allows the separate evolution of photochemical half-reaction products, in our case H_2 and O_2 . Two compartments of the cell contains different electrolytes and these are separated by (i) a bipolar photoelectrode (ii) ion conducting material (Nafion in our case). What happens inside the H-type cell is schematically illustrated in Figure 4-5.

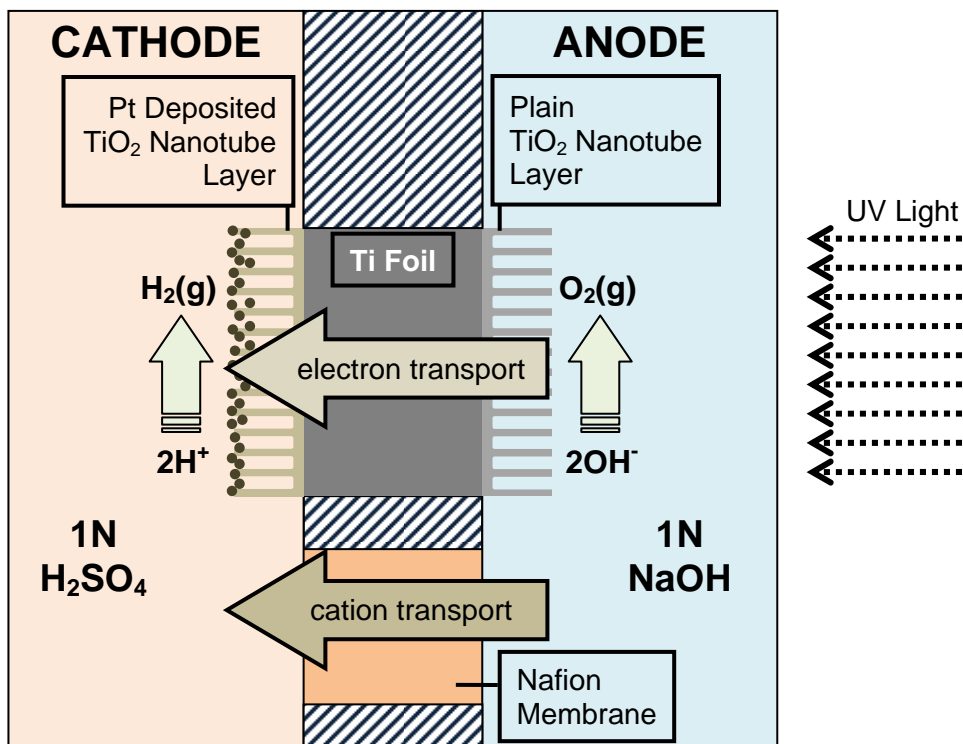


Figure 4-5. Scheme of the processes taking place inside the H-type cell.

Selection of the anode side electrolyte as 1N H₂SO₄ and cathode side electrolyte as 1N NaOH was for keeping the experimental parameters as close to the original work on H-type cell [95-97] (by Anpo group) as possible, to allow comparison.

As explained previously, evolution of hydrogen gas in PECs with minimum bias requires the presence of a catalytic material like platinum. Depending on this well accepted fact, loading of Pt was considered compulsory to observe the full activity of TNTs in photocatalytic water oxidation. Since cathode side of the foil was subjected to anodization as well in order to keep the synthesis

procedure as simple as possible, platinum loading was established on this oxide layer.

In order to test whether the produced films possessed any photocatalytic activity, they were tested for CO photooxidation reaction in a home built set up. The experimental details and the results are presented in Appendix C. Observing CO₂ formation on these structures confirmed the catalytic activity.

Accumulation rate of anode and cathode gases under UV illumination in our H-type cell is given in Figure 4-6. The two graphs show the first two runs for the water splitting experiment. Although it is assumed that the cell is at room temperature, exothermic recombination of charge carriers generated by UV and infrared radiation from the lamp may cause heating of electrolytes and increased vapor pressure may contribute to the observed gas evolution.

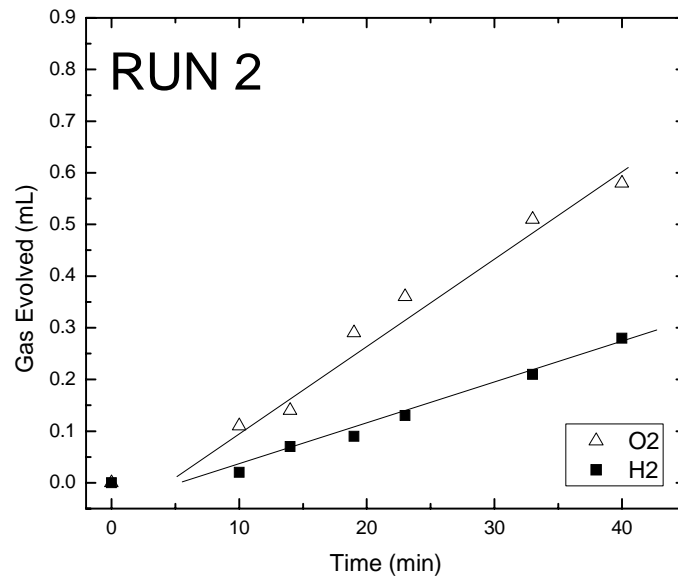
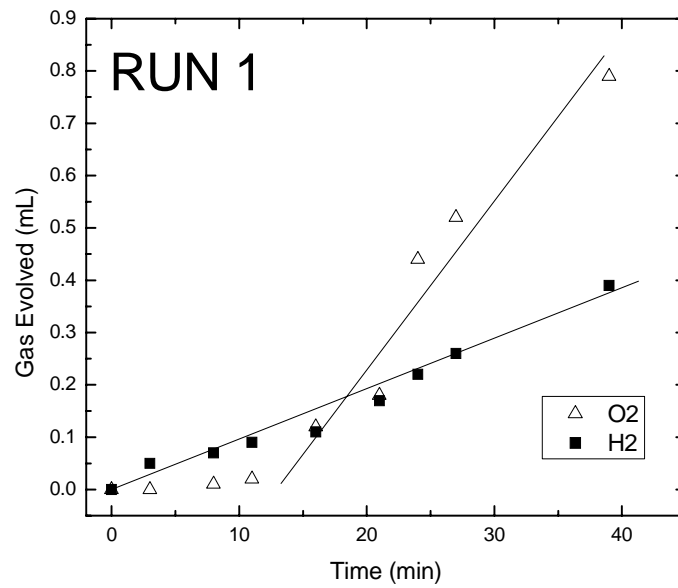


Figure 4-6. Evolution of gases in H-type cell under UV illumination. H₂ and O₂ don't necessarily indicate the composition of the evolved gases, but their evolution side. H₂ represent the cathode side gas and O₂ represent the anode side gas.

In a stoichiometric water splitting process, anode side gas (O₂) must be half the volume of the cathode side gas (H₂). In our case, this situation is reversed. Anode side gas evolves almost two times faster than the cathode side gas. Not surprisingly, the oxide layer on the anode side is seen to be etched after

experiments which involve ca. 3 hours of illumination. X-ray diffractogram of the anode side (Figure 4-7) verify the complete etching of the oxide layer here. Cathode side oxide and deposited platinum is seen to be etched from XRD as well, however oxide removal in here is not complete, as understood from one weak anatase peak at 2θ value of 26 degrees.

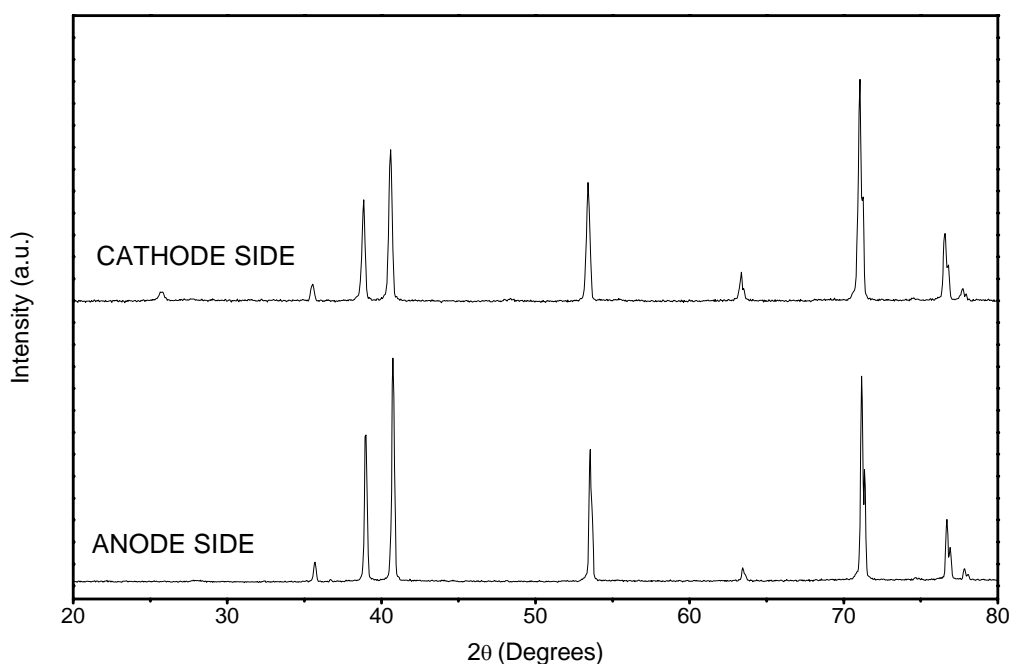


Figure 4-7. X-ray diffractograms of anode and cathode sides of Pt/TNT-aq-cell after ca. 3 hours of UV illuminated experiments in the H-type cell.

SEM images of the anode side surface were taken after the reaction. These images clearly demonstrate the etching of the oxide layer. Three images in Figure 4-8 show the surface not wetted by NaOH solution, the surface under the o-ring so partially wetted and the surface completely wetted by NaOH solution. The gradual destruction of the surface structure can be observed from these three images. Surface under the o-ring is not only partially wetted but also partially illuminated.

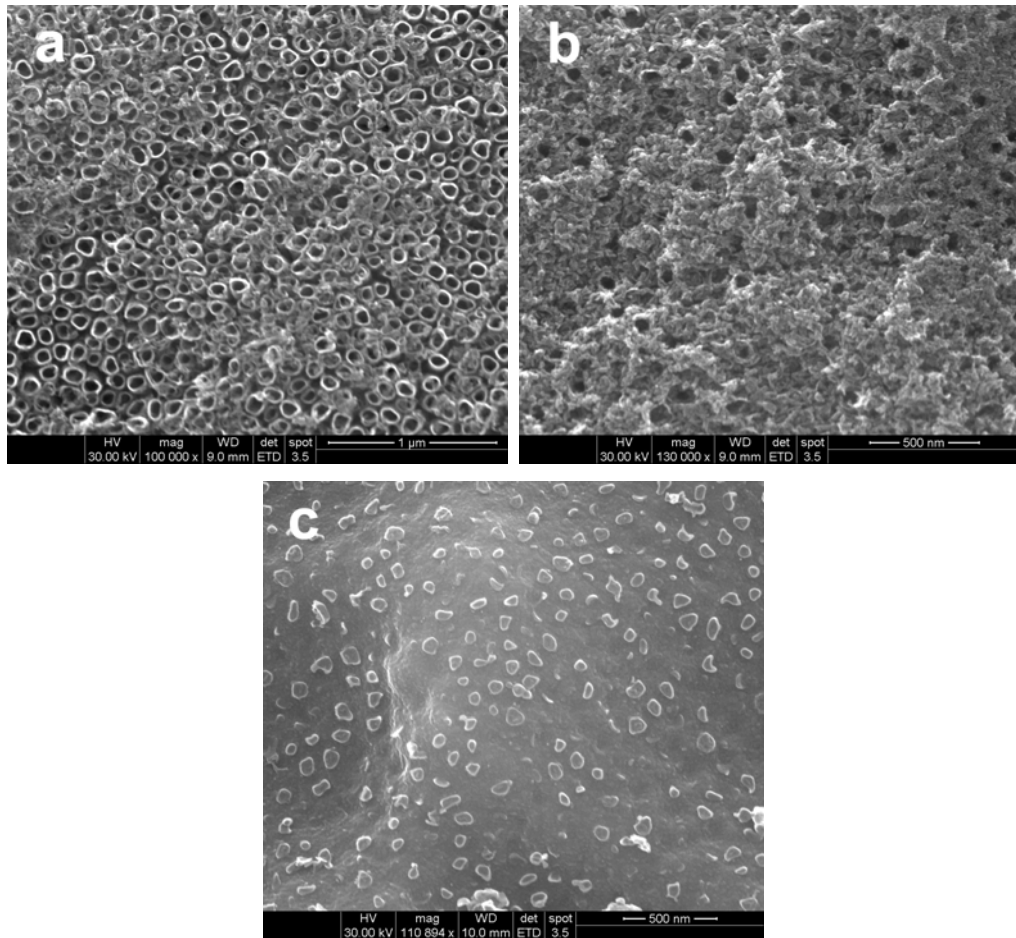


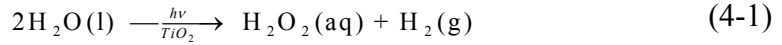
Figure 4-8. SEM images of the anode side of Pt/TNT-aq-cell, which experienced severe surface etching. (a) surface outside the o-ring, not wetted by the aqueous NaOH electrolyte (b) surface under the o-ring, partially wetted by the aqueous NaOH electrolyte and partially illuminated by UV light (c) surface that is totally wetted by the aqueous NaOH electrolyte and illuminated by UV light.

The destruction of the oxide layer may have at least four reasons. First is the highly basic/acidic environment, base being more corrosive. Second is the UV illumination. Such harsh chemical environment may not be that corrosive against a passive TiO_2 film without the ionizing effect of UV light. Third, formation of peroxide species cannot be excluded. Fourth reason is the high porosity of the surface, thus the enhanced rate of corrosion.

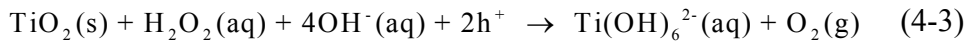
One parameter to be considered further is the area of the ion exchange membrane. If the resistance in the membrane is high, due to insufficient area, such that it limits the rate of photocatalytic reaction, then other reactions may come into play. This remains as an open question for further studies.

The 2/1 ratio of anode/cathode gas ratio may be explained by a reaction model involving hydrogen peroxide formation, as proposed below. However, one must bear in mind that this scheme is purely speculative and must be proved by further evidence.

ANODE SIDE



and/or



CATHODE SIDE



Illuminated, anode, side of the cell is subject to hydrogen peroxide formation with simultaneous formation of hydrogen gas. Hydrogen peroxide, on the titania surface, is oxidized to oxygen gas by the photogenerated holes. Reaction (4-2) can be combined with the dissolution of titania to yield Reaction (4-3). Electrons transferred to the cathode side reduces protons to release hydrogen gas.

Some control experiments were performed to get a further understanding of the observed phenomena. As the first control experiment, a pure titanium foil was put instead of the anodized foil in the H-type cell. Gas evolution plot is given in Figure 4-9. Note that while the y-axis scale is the same with the plot in Figure 4-6, time scale is about 5 times greater. This means that the gas evolution is about 5 times slower. While it is certain that the event is far from being photocatalytic, it gives an idea about the rate of gas evolution after the removal of a thick oxide layer.

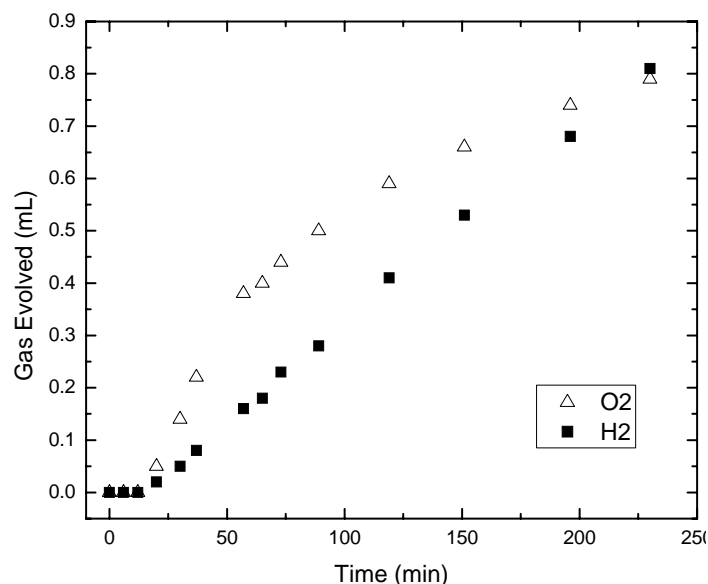


Figure 4-9. Gas evolution in a UV illuminated H-type cell, in which a pure titanium foil is used instead of Pt/TNT-aq-cell. H₂ and O₂ don't necessarily indicate the composition of the evolved gases, but their evolution side. O₂ represent the illuminated side gas and H₂ represent the dark side gas.

Other control experiments were conducted with a one side anodized titanium foil of 0.127 mm thickness due to unavailability of the 0.25 mm thick foil. Anodization was carried out in 1M NH₄H₂PO₄ + 0.5 wt% NH₄F solution under 20 V potential difference. Back side of the foil was masked with epoxy resin to

prevent oxidation. Resin was removed after anodization and calcination was carried out at 450 °C for 3 hours in air. Platinum was loaded using a 0.003 M $\text{Pt}(\text{NH}_3)_4\text{Cl}_2$ solution (solvent was 1/9, water/ethylene glycol). Pt solution was dropped on the surface and each drop was burned with a small butane torch leaving deposits of metallic platinum. This way, oxide's resistance to electron transfer on the Pt side was eliminated. Cathode and anode side electrolytes, 1N H_2SO_4 and 1N NaOH, were substituted with DI water to eliminate corrosion. One experiment was carried out under UV and one under visible light irradiation. A 100 W tungsten filament lamp was used as the visible light source. DI water on both sides were deaerated with bubbling Ar for 45 minutes prior to reaction. The results of UV irradiated experiment is given in Figure 4-10.

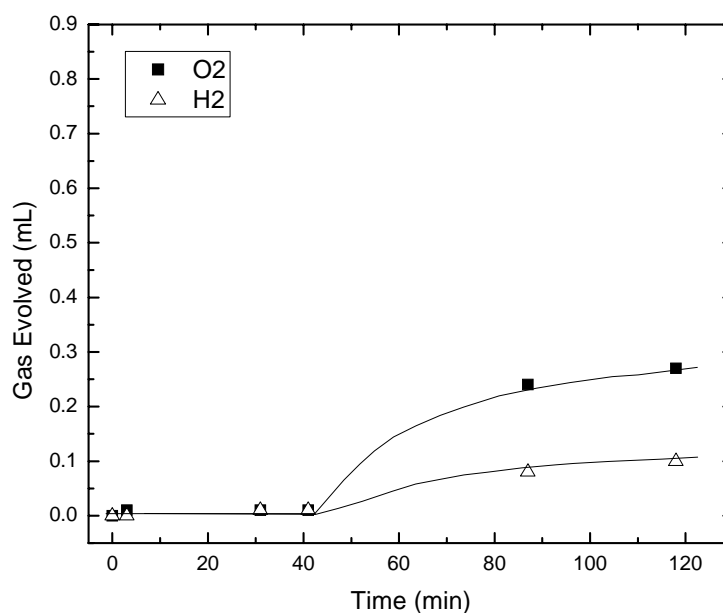


Figure 4-10. Evolution of gases in the control experiment of H-type cell using a Pt/Ti/TiO₂ electrode under UV illumination and DI water as electrolytes. H₂ and O₂ don't necessarily indicate the composition of the evolved gases, but their evolution side. H₂ represent the cathode side gas and O₂ represent the anode side gas. Illumination begins after 41 minutes of dark period.

Decaying behavior of the gas evolution suggests that the increase in the gas pressure is due to the heating of water and the corresponding increase in vapor pressure. Higher amount of evolved gas observation in the anode side, which is closer to the light source, confirms this hypothesis as well.

The results of visible light irradiated experiment are presented in Figure 4-11.

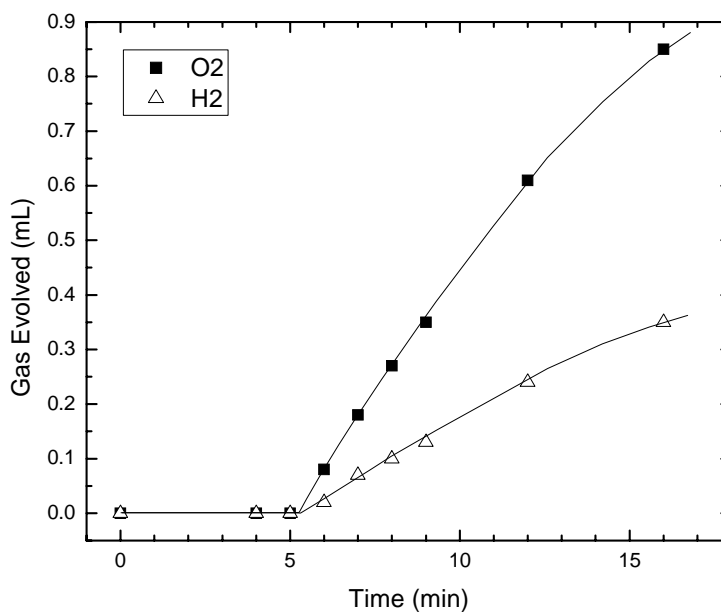


Figure 4-11. Evolution of gases in the control experiment of H-type cell using a Pt/Ti/TiO₂ electrode under visible light illumination and DI water as electrolytes. H₂ and O₂ don't necessarily indicate the composition of the evolved gases, but their evolution side. H₂ represent the cathode side gas and O₂ represent the anode side gas. Illumination begins after 5 minutes.

Similar behavior with the UV illuminated control experiment is observed in the visible illuminated control experiment as well. Since infrared radiation of the tungsten lamp is significantly higher than the UV lamp, heating effect is much more predominant here and thus the observed gas evolution is faster. Besides the gas evolution, no corrosion on either surface was observed with naked eye.

From the control experiments, it can be concluded that (i) heating is an important factor determining the observed gas evolution and should be separated from actual steady gas evolution (ii) without the bias created by the pH difference between the two poles of the electrode, splitting of water cannot be established using a Pt/Ti/TiO₂ type of bipolar electrode (iii) UV light and water is not a corrosive combination for TiO₂. Quantitative chemical analysis of the gas phase products is necessary for confirmation or dispute of these hypotheses.

4.3. CYCLIC VOLTAMMOGRAMS OF TiO₂ NANOTUBES

Since the water splitting performance evaluation of the synthesized TNTs using an H-type cell failed, cyclic voltammetry was used to see their photocatalytic oxygen evolution performance. In order to prevent a similar corrosion problem, electrolytes were kept 10 times more dilute than in the H-type cell.

The critical parameters when comparing the I-V characteristics of the prepared photoelectrodes is the minimum potential of steady photocurrent and the magnitude of the photocurrent. It is advantageous to see the highest possible photocurrent (higher rate) at a relatively more negative potential (smaller input energy).

The comparison of the obtained data with the literature is easy since CV is a commonly employed method for the electrochemical characterization of TNTs and similar electrodes. One of the earliest work in the literature, which report the photocleavage of water by utilizing TNTs as photoanode, is from Mor *et al.*, also mentioned in the literature survey chapter [43]. In this work, they report one of the -still- highest photocurrent results. By using a 320-400 nm UV light of 100 mW/cm² incident intensity, they obtain on the order of 10-15 mA/cm² steady photocurrent.

Calcination atmosphere (10% H₂/Ar) and temperature (500 °C) for TNT-org samples were the same as used by Mohapatra *et al.* [105], to allow comparison. These are different from the parameters used for TNT-aq samples (450 °C, air), selected on the basis of common usage in the literature.

4.3.1. Pure TiO₂ Nanotubes

The first solid finding of cyclic voltammograms was that no photocurrent could be obtained without annealing of the electrode (i.e. crystalline TiO₂ is required). Every annealed electrode on the other hand, showed photo-response under UV illumination regardless of the type of anodization or CV electrolyte.

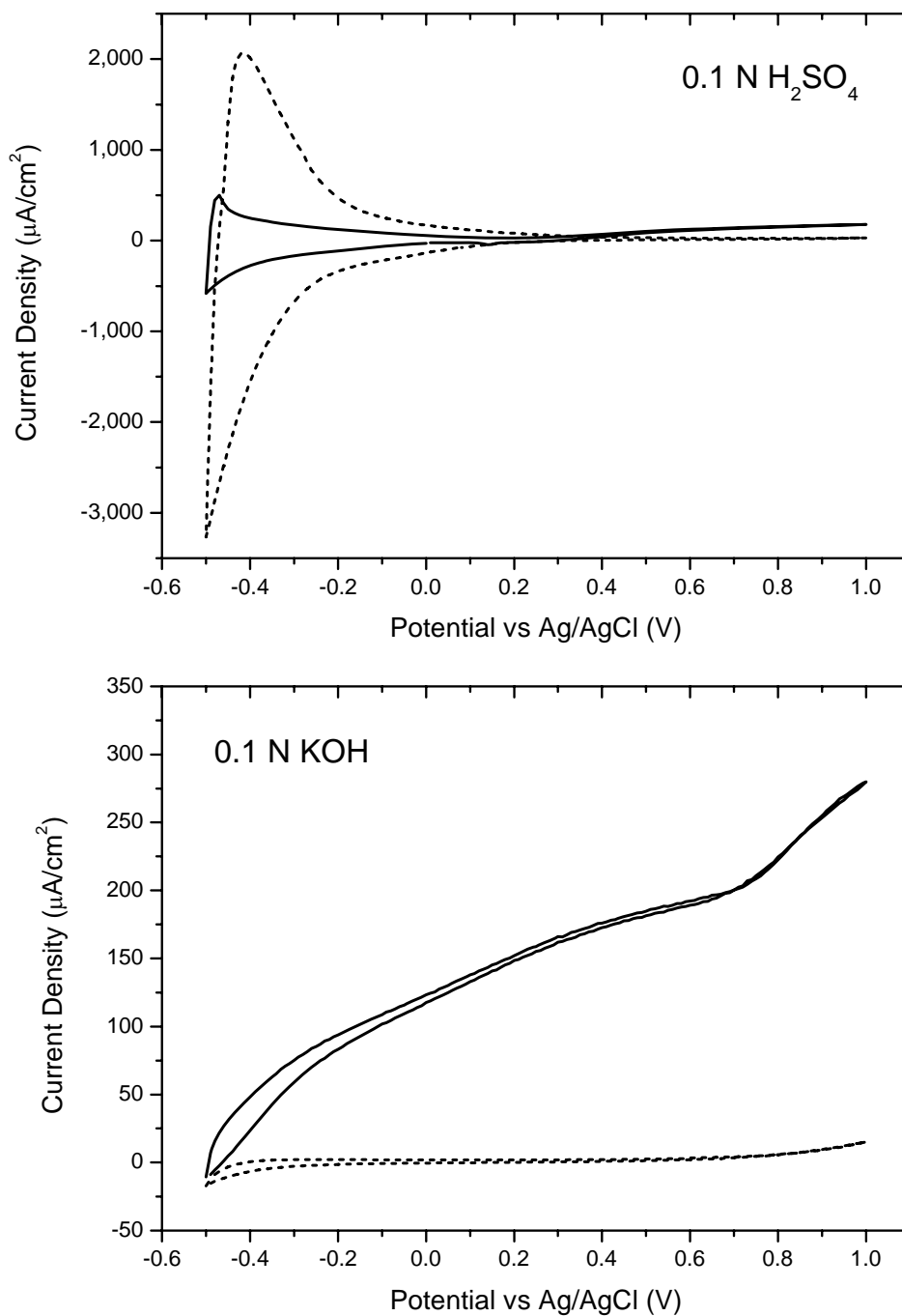


Figure 4-12. Cyclic voltammograms of TNT-aq under UV illumination, taken in 0.1 N H₂SO₄ (top) and 0.1 N KOH (bottom). Dotted lines represent non-annealed, solid lines represent annealed samples.

CV of the non-annealed sample on the top of Figure 4-12 show that very high currents can be obtained due to the reduction of Ti^{4+} at negative potentials. This is made possible by the intercalation of abundant H^+ in the acidic solution [99,121]. CV of the non-annealed sample on the right hand side does not show this behavior since solution is basic. As annealing increases the diffusion resistance of H^+ in TiO_2 , annealed samples show smaller current in acidic solution.

CVs of annealed samples given in Figure 4-12 show the generation of photocurrent under UV illumination. Photocurrent is a result of oxygen evolution and begins at more negative potentials for more basic solutions. In our case, onset of photocurrent shifts about 0.8 V to negative, upon changing the solution from 0.1 N H_2SO_4 to 0.1 N KOH.

Cyclic voltammograms of TNTs synthesized in organic electrolytes for different anodization times are compared in Figure 4-13. Ti^{4+} reduction currents of electrodes (in acidic medium) are proportional to their anodization times, which are (for short anodization times) proportional to their length [37]. On the other hand, photocurrents do not show the same proportional behavior. They are relatively close in acidic medium, but in the basic medium, TNT-org-4h show a significantly higher performance, indicating an optimum tube length for this case. The existence of an optimum tube length with respect to photocurrent maximization has also been reported in the literature [37]. The maximum value for the photocurrent is obtained by optimizing the increasing light absorption and increasing recombination losses as the film thickness increases. The problem in our data is that the optimum film thickness is not consistent in the acidic and basic CV. The performances of the three films are just in the reverse order in two extreme pH values.

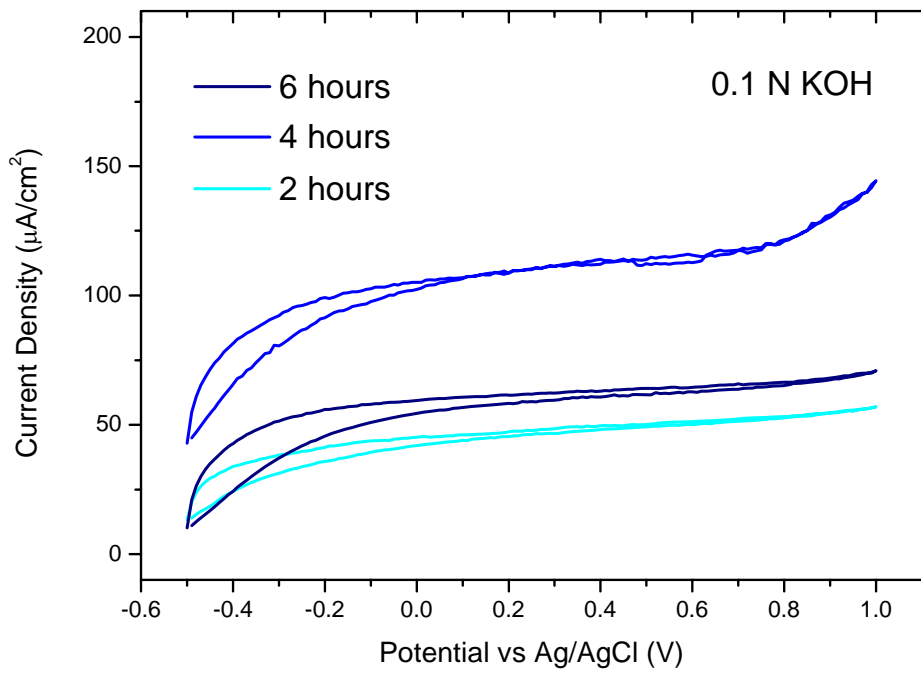
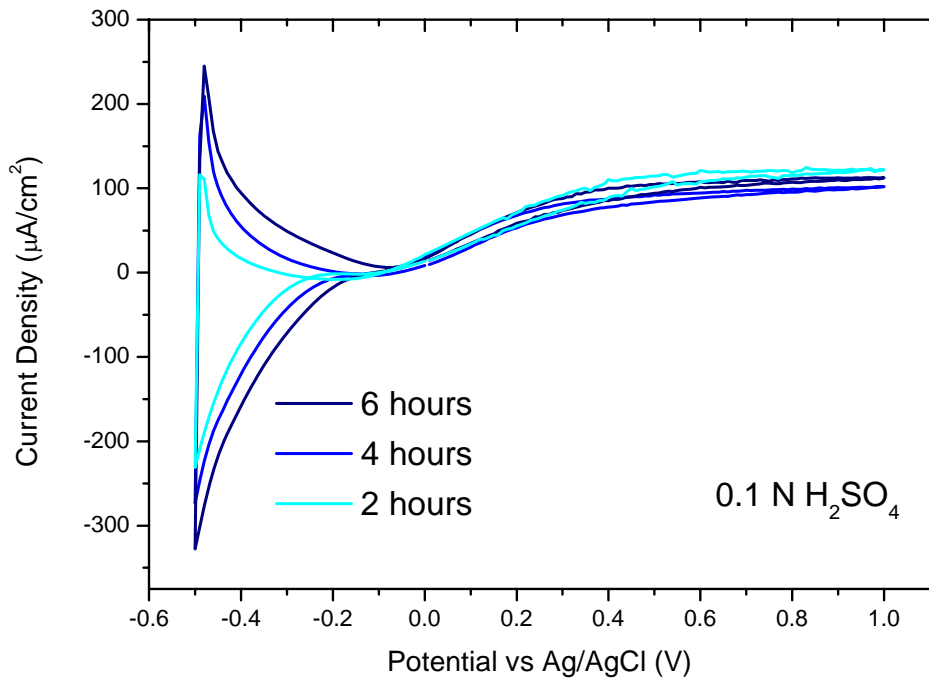


Figure 4-13. Cyclic voltammograms of TNTs synthesized for varying times (2, 4 and 6 hours) in organic electrolyte. CVs were taken under UV illumination in 0.1 N H₂SO₄ (top) and 0.1 N KOH (bottom) media.

We can refer to Figure 4-14 for the comparison of photocurrents in acidic and basic media. As mentioned earlier, in basic conditions, oxidation of water is accomplished at more negative potentials. One significant feature of the CVs taken in basic media is that two different oxidation currents superimpose beginning at ~ 0.85 V. The second current (indicating a second process) is not caused by the UV irradiation as it is also present in the CVs taken in the dark. This process is the feature observed in the CV of pure titanium (given in Appendix B) and close to the theoretical water oxidation potential (1.23 V vs SHE, ~ 1.0 V vs Ag/AgCl).

CVs of the TNTs synthesized in this work are in qualitative agreement with the literature. There is however, on the average, an order of magnitude difference in photocurrents as compared to studies summarized in the literature survey chapter. This may partly be due to the weaker UV intensity used in this study.

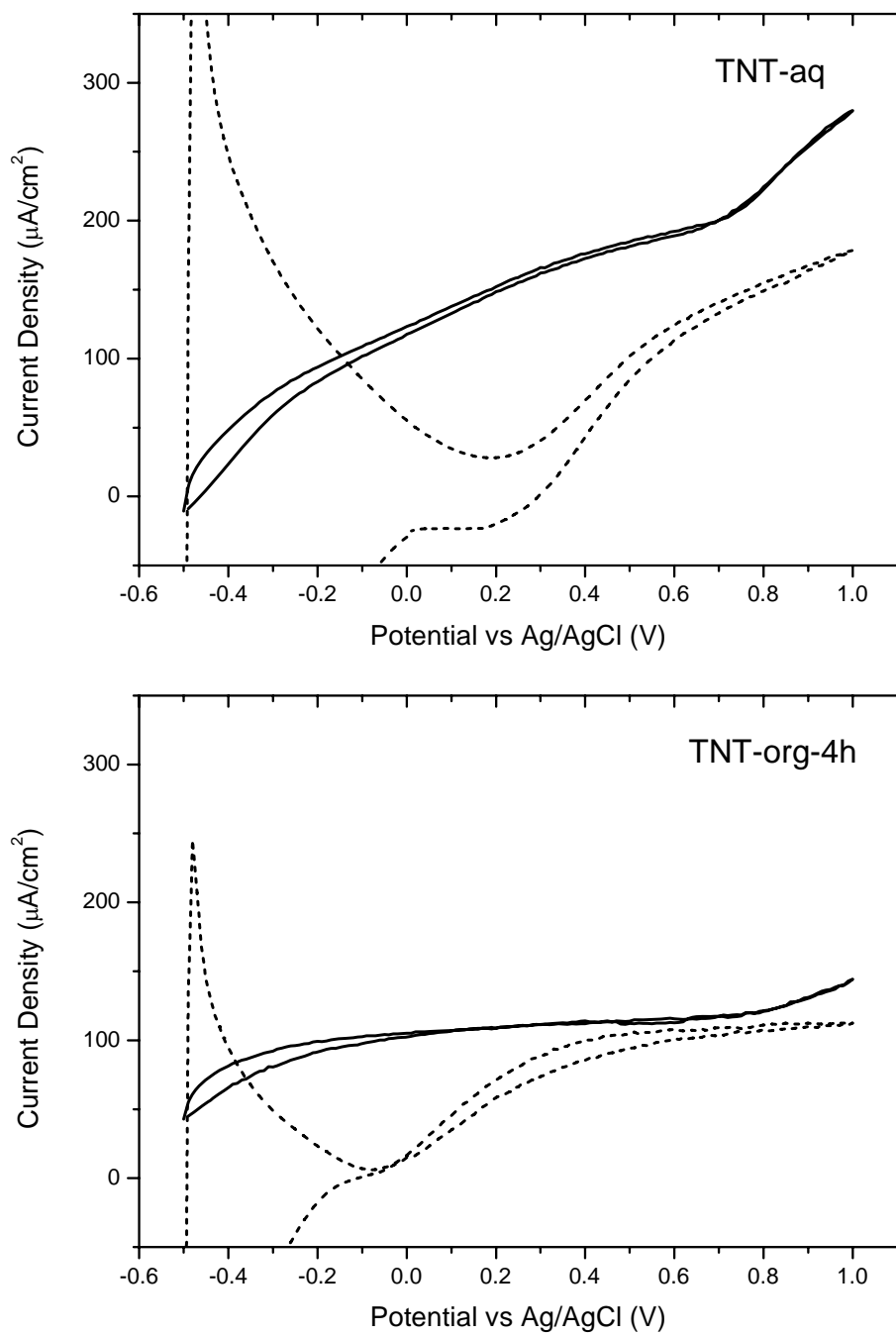


Figure 4-14. Cyclic voltammograms of TNTs (top: TNT-aq, bottom: TNT-org-4h) taken in acidic (0.1 N H_2SO_4 , dotted lines) and basic media (0.1 N KOH, solid lines).

4.3.2. Platinized TiO₂ Nanotubes

Figure 4-15 shows the cyclic voltammogram of Pt/TNT-aq-PEC electrode in 0.1 N H₂SO₄ in the dark and under UV illumination. Peaks at -0.26 and -0.14 V are similar to the peaks of hydrogen reduction on pure Pt.

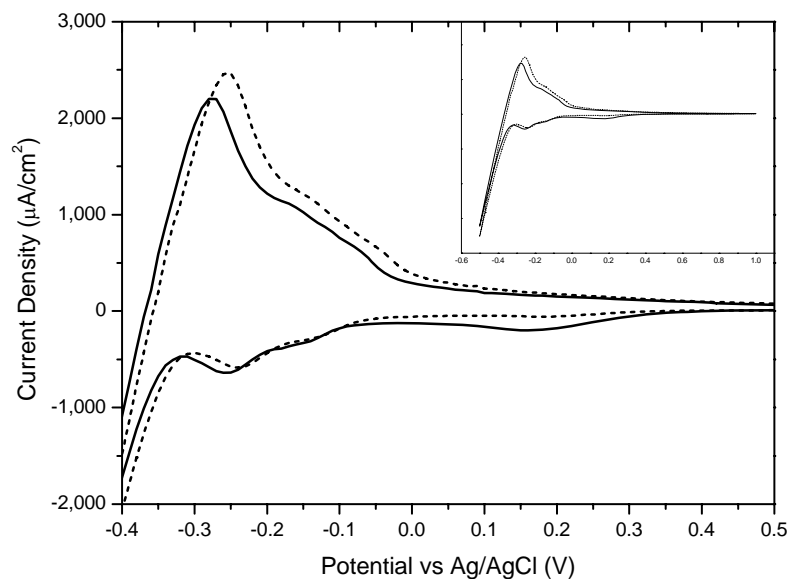


Figure 4-15. Cyclic voltammograms of Pt/TNT-aq-PEC electrode taken in 0.1 N H₂SO₄ with 0.1V/s sweep rate in the dark (dotted line) and under UV illumination (solid line). Main graph is zoomed to the important features while inset shows the whole voltammogram.

Cyclic voltammogram of Pt/TNT-aq-PEC electrode in 0.1 N KOH in the dark and under UV illumination is given in Figure 4-16. In all CVs of platinized samples, photocurrent is significantly reduced (KOH solution) or diminished (H₂SO₄ solution) as compared to non-platinized samples which yielded on the order of 200 µA/cm² photocurrent density. High density of Pt particles may block the penetration of UV light to the TiO₂ centers in the pores. Both situations suggest that sizes of Pt particles formed on the nanotubes' surface are bigger than it should be for functioning as a Pt/TiO₂ type photocatalyst. This is confirmed by the fact that, electrochemical behavior of this surface is

close to pure Pt, besides from the increased electrical resistance stemming from the oxide layer.

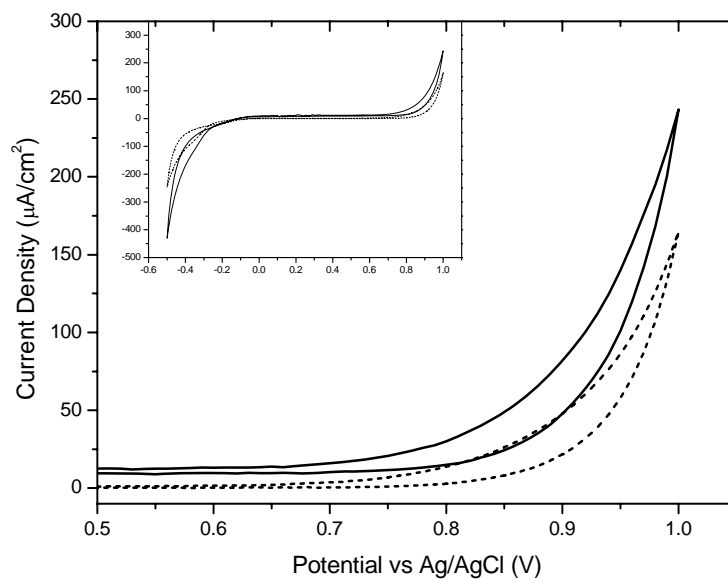


Figure 4-16. Cyclic voltammograms of Pt/TNT-aq-PEC electrode taken in 0.1 N KOH with 0.1 V/s sweep rate in the dark (dashed line) and with 0.05 V/s sweep rate under UV illumination (solid line).

CHAPTER 5

CONCLUSIONS

Ordered arrays of TiO₂ nanotubes (TNT) were synthesized via an electrochemical anodization procedure. Two types of electrolytes, an aqueous NH₄H₂PO₄ solution and an ethylene glycol solution with 10% water, both having 0.5 wt% NH₄F were utilized to prepare two different types of samples. Anodization time of nanotubes synthesized in organic electrolyte was varied to see the effect on material properties. Materials were characterized to see their water splitting performance.

An H-type cell was constructed with a bipolar electrode of type Pt/TNT/Ti/TNT and used for the splitting of water under UV illumination. The anode and cathode sides showed 1.0 mL/h and 0.5 mL/h gas evolution respectively, however this corresponded to the reverse of the desired stoichiometry. The SEM image and X-ray diffractogram of the illuminated surface showed that the nanotube oxide layer was completely etched after the experiment. To test the electrochemical properties under more benign conditions, a two compartment electrochemical cell separated by a glass frit was constructed with a TNT working, a Pt/TNT counter and a Ag/AgCl reference electrode. Extensive resistance caused by the frit and wide electrode spacing did not allow the passage of any current. Finally, tests were carried out in a simple one compartment cell having a quartz window for UV illumination. Cyclic voltammograms of annealed and non-annealed samples were taken in 0.1 N H₂SO₄ and 0.1 N KOH electrolytes in the dark and under UV illumination. CVs identified the reduction of Ti⁴⁺ to Ti³⁺ after -0.3 V. The intensities of the reduction peaks were qualitatively proportional to the anodization times of TNTs. Non-annealed samples were more prone to Ti⁴⁺

reduction but no photocurrent was observed in the non-annealed samples. Steady photocurrents observed in all pure titania samples were on the order of 0.2 mA/cm^2 , which is considerably low compared to the values reported in the literature. Platinized TiO_2 nanotubes exhibited an electrochemical behavior similar to pure Pt, showing the adsorption/desorption peaks of H^+ and the evolution of hydrogen gas. Photocurrent was hindered by a dense layer of Pt.

CHAPTER 6

RECOMMENDATIONS

For a complete understanding of the observed phenomena in the H-type cell, some recommendations shall be made for future studies.

First of all, the size and thickness of the Nafion membrane is a matter of question since the rate of reaction may be limited by the mass transfer through the membrane. A membrane with greater area and (if possible) less thickness should be implemented into the system. It should be noted that increase of the membrane area may require machining of the Plexiglas support.

Secondly, an experiment using a Pt/Ti/TiO₂ electrode and acid/base electrolyte in the cathode/anode shall be conducted in the H-type cell. This would be the closest case to the experiment reported by Anpo group.

Increasing the calcination temperature to 550-650 °C will most likely induce the formation of a anatase/rutile mixture film. Since mixtures of anatase and rutile are known to be better photocatalysts, a long term suggestion may be the maximization of performance by optimizing the calcination temperature and time.

During the course of this thesis, several studies have been published regarding the synthesis of ordered titania nanotube arrays. Our understanding of its synthesis has increased. In the future studies, methods of synthesis which result in better ordered structure shall be preferred, such as the method used by Shin and Lee [39]. This way, results will be a better representative of the ideal nanotubular structure.

REFERENCES

- [1] Harrison, K.; Levene, J. I. In *Solar Hydrogen Generation, Toward a Renewable Energy Future*; Rajeshwar, K., McConnell, R., Licht, S., Eds.; Springer: New York, 2008.
- [2] Rosen, M. A.; Scott, D. S. Ninth World Hydrogen Energy Conference, Paris, France, 1992; p 457.
- [3] Kars, G.; Gunduz, U.; Rakhely, G.; Yucel, M.; Eroglu, I.; Kovacs, K. L. *International Journal of Hydrogen Energy* **2008**, *33*, 3056-3060.
- [4] Eroglu, I.; Tabanoglu, A.; Gunduz, U.; Eroglu, E.; Yucel, M. *International Journal of Hydrogen Energy* **2008**, *33*, 531-541.
- [5] Eroglu, E.; Eroglu, I.; Gunduz, U.; Yucel, M. *Bioresource Technology* **2008**, *99*, 6799-6808.
- [6] Uyar, B.; Eroglu, I.; Yucel, M.; Gunduz, U.; Turker, L. *International Journal of Hydrogen Energy* **2007**, *32*, 4670-4677.
- [7] Zabut, B.; EI-Kahlout, K.; Yucel, M.; Gunduz, U.; Turker, L.; Eroglu, I. *International Journal of Hydrogen Energy* **2006**, *31*, 1553-1562.
- [8] Ozturk, Y.; Yucel, M.; Daldal, F.; Mandaci, S.; Gunduz, U.; Turker, L.; Eroglu, I. *International Journal of Hydrogen Energy* **2006**, *31*, 1545-1552.
- [9] Eroglu, E.; Eroglu, I.; Gunduz, U.; Turker, L.; Yucel, M. *International Journal of Hydrogen Energy* **2006**, *31*, 1527-1535.
- [10] Eroglu, E.; Gunduz, U.; Yucel, M.; Turker, L.; Eroglu, I. *International Journal of Hydrogen Energy* **2004**, *29*, 163-171.

- [11] Koku, H.; Eroglu, I.; Gunduz, U.; Yucel, M.; Turker, L. *International Journal of Hydrogen Energy* **2003**, *28*, 381-388.
- [12] Eroglu, I.; Aslan, K.; Gunduz, U.; Yucel, M.; Turker, L. *Journal of Biotechnology* **1999**, *70*, 103-113.
- [13] Fujishima, A.; Honda, K. *Nature* **1972**, *238*, 37-38.
- [14] Oregan, B.; Gratzel, M. *Nature* **1991**, *353*, 737-740.
- [15] Linsebigler, A. L.; Lu, G. Q.; Yates, J. T. *Chemical Reviews* **1995**, *95*, 735-758.
- [16] Thompson, T. L.; Yates, J. T. *Topics in Catalysis* **2005**, *35*, 197-210.
- [17] Thompson, T. L.; Yates, J. T. *Chemical Reviews* **2006**, *106*, 4428-4453.
- [18] Diebold, U. *Surface Science Reports* **2003**, *48*, 53-229.
- [19] Fujishima, A.; Zhang, X.; Tryk, D. A. *Surface Science Reports* **2008**, *63*, 515-582.
- [20] Reyes-Coronado, D.; Rodriguez-Gattorno, G.; Espinosa-Pesqueira, M. E.; Cab, C.; de Coss, R.; Oskam, G. *Nanotechnology* **2008**, *19*.
- [21] Nowotny, M. K.; Bak, T.; Nowotny, J. *Journal of Physical Chemistry B* **2006**, *110*, 16292-16301.
- [22] Masel, R. I. *Principles of Adsorption and Reaction on Solid Surfaces*; Wiley: New York, 1996.
- [23] Epling, W. S.; Peden, C. H. F.; Henderson, M. A.; Diebold, U. *Surface Science* **1998**, *413*, 333-343.
- [24] Gopel, W.; Rucker, G.; Feierabend, R. *Physical Review B* **1983**, *28*, 3427-3438.

- [25] Henderson, M. A.; Epling, W. S.; Perkins, C. L.; Peden, C. H. F.; Diebold, U. *Journal of Physical Chemistry B* **1999**, *103*, 5328-5337.
- [26] Diebold, U.; Lehman, J.; Mahmoud, T.; Kuhn, M.; Leonardelli, G.; Hebenstreit, W.; Schmid, M.; Varga, P. *Surface Science* **1998**, *411*, 137-153.
- [27] Linsebigler, A.; Lu, G. Q.; Yates, J. T. *Journal of Physical Chemistry* **1996**, *100*, 6631-6636.
- [28] Lu, G. Q.; Linsebigler, A.; Yates, J. T. *Journal of Physical Chemistry* **1994**, *98*, 11733-11738.
- [29] Ghicov, A.; Tsuchiya, H.; Macak, J. M.; Schmuki, P. *Electrochemistry Communications* **2005**, *7*, 505-509.
- [30] Zwillig, V.; Aucouturier, M.; Darque-Ceretti, E. *Electrochimica Acta* **1999**, *45*, 921-929.
- [31] Gong, D.; Grimes, C. A.; Varghese, O. K.; Hu, W. C.; Singh, R. S.; Chen, Z.; Dickey, E. C. *Journal of Materials Research* **2001**, *16*, 3331-3334.
- [32] Chanmanee, W.; Watcharenwong, A.; Chenthamarakshan, C. R.; Kajitvichyanukul, P.; de Tacconi, N. R.; Rajeshwar, K. *Electrochemistry Communications* **2007**, *9*, 2145-2149.
- [33] Kasuga, T.; Hiramatsu, M.; Hoson, A.; Sekino, T.; Niihara, K. *Langmuir* **1998**, *14*, 3160-3163.
- [34] Xu, J. W.; Ha, C. H.; Cao, B.; Zhang, W. F. *Electrochimica Acta* **2007**, *52*, 8044-8047.
- [35] Li, G.; Liu, Z. Q.; Yan, X.; Zhang, Z. *Chinese Journal of Catalysis* **2008**, *29*, 680-682.
- [36] Wang, W. Z.; Varghese, O. K.; Paulose, M.; Grimes, C. A.; Wang, Q. L.; Dickey, E. C. *Journal of Materials Research* **2004**, *19*, 417-422.

- [37] Macak, J. M.; Tsuchiya, H.; Ghicov, A.; Yasuda, K.; Hahn, R.; Bauer, S.; Schmuki, P. *Current Opinion in Solid State & Materials Science* **2007**, *11*, 3-18.
- [38] Yasuda, K.; Macak, J. M.; Berger, S.; Ghicov, A.; Schmuki, P. *Journal of the Electrochemical Society* **2007**, *154*, C472-C478.
- [39] Shin, Y.; Lee, S. *Nano Letters* **2008**, *8*, 3171-3173.
- [40] Yang, H. G.; Sun, C. H.; Qiao, S. Z.; Zou, J.; Liu, G.; Smith, S. C.; Cheng, H. M.; Lu, G. Q. *Nature* **2008**, *453*, 638-642.
- [41] Macak, J. M.; Tsuchiya, H.; Taveira, L.; Aldabergerova, S.; Schmuki, P. *Angewandte Chemie-International Edition* **2005**, *44*, 7463-7465.
- [42] Bauer, S.; Kleber, S.; Schmuki, P. *Electrochemistry Communications* **2006**, *8*, 1321-1325.
- [43] Mor, G. K.; Shankar, K.; Paulose, M.; Varghese, O. K.; Grimes, C. A. *Nano Lett.* **2005**, *5*, 191-195.
- [44] Macak, J. M.; Tsuchiya, H.; Schmuki, P. *Angewandte Chemie-International Edition* **2005**, *44*, 2100-2102.
- [45] Chen, C. C.; Chung, H. W.; Chen, C. H.; Lu, H. P.; Lan, C. M.; Chen, S. F.; Luo, L.; Hung, C. S.; Diao, E. W. G. *Journal of Physical Chemistry C* **2008**, *112*, 19151-19157.
- [46] Macak, J. M.; Tsuchiya, H.; Ghicov, A.; Schmuki, P. *Electrochemistry Communications* **2005**, *7*, 1133-1137.
- [47] Flores, I. C.; de Freitas, J. N.; Longo, C.; De Paoli, M.-A.; Winnischofer, H.; Nogueira, A. F. *Journal of Photochemistry and Photobiology A: Chemistry* **2007**, *189*, 153-160.

- [48] Hahn, R.; Stergioulus, T.; Macak, J. M.; Tsoukleris, D.; Kontos, A. G.; Albu, S. P.; Kim, D.; Ghicov, A.; Kunze, J.; Falaras, P.; Schmuki, P. *Physica Status Solidi-Rapid Research Letters* **2007**, *1*, 135-137.
- [49] Mor, G. K.; Varghese, O. K.; Paulose, M.; Shankar, K.; Grimes, C. A. *Solar Energy Materials and Solar Cells* **2006**, *90*, 2011-2075.
- [50] Aprile, C.; Corma, A.; Garcia, H. *Physical Chemistry Chemical Physics* **2008**, *10*, 769-783.
- [51] Park, J. H.; Kim, S.; Bard, A. J. *Nano Letters* **2006**, *6*, 24-28.
- [52] Henderson, M. A. *Surface Science Reports* **2002**, *46*, 5-308.
- [53] Allegretti, F.; O'Brien, S.; Polcik, M.; Sayago, D. I.; Woodruff, D. P. *Physical Review Letters* **2005**, *95*.
- [54] Belelli, P. G.; Ferullo, R. M.; Branda, M. M.; Castellani, N. J. *Applied Surface Science* **2007**, *254*, 32-35.
- [55] Casarin, M.; Maccato, C.; Vittadini, A. *Journal of Physical Chemistry B* **1998**, *102*, 10745-10752.
- [56] Selloni, A.; Vittadini, A.; Gratzel, M. *Surface Science* **1998**, *404*, 219-222.
- [57] Vittadini, A.; Selloni, A.; Rotzinger, F. P.; Gratzel, M. *Physical Review Letters* **1998**, *81*, 2954-2957.
- [58] Lindan, P. J. D.; Harrison, N. M.; Gillan, M. J. *Physical Review Letters* **1998**, *80*, 762-765.
- [59] Blomquist, J.; Walle, L. E.; Uvdal, P.; Borg, A.; Sandell, A. *Journal of Physical Chemistry C* **2008**, *112*, 16616-16621.
- [60] Onal, I.; Soyer, S.; Senkan, S. *Surface Science* **2006**, *600*, 2457-2469.

- [61] Shapovalov, V.; Stefanovich, E. V.; Truong, T. N. *Surface Science* **2002**, *498*, 103-108.
- [62] Wendt, S.; Schaub, R.; Matthiesen, J.; Vestergaard, E. K.; Wahlstrom, E.; Rasmussen, M. D.; Thostrup, P.; Molina, L. M.; Laegsgaard, E.; Stensgaard, I.; Hammer, B.; Besenbacher, F. *Surface Science* **2005**, *598*, 226-245.
- [63] Sato, S.; White, J. M. *Journal of Catalysis* **1981**, *69*, 128-139.
- [64] Bahnemann, D.; Henglein, A.; Lilie, J.; Spanhel, L. *Journal of Physical Chemistry* **1984**, *88*, 709-711.
- [65] Van Damme, H.; Hall, W. K. *Journal of the American Chemical Society* **1979**, *101*, 4373-4374.
- [66] Henderson, M. A. *Surface Science* **1994**, *319*, 315-328.
- [67] Smith, P. B.; Bernasek, S. L. *Surface Science* **1987**, *188*, 241-254.
- [68] Herman, G. S.; Dohnalek, Z.; Ruzycski, N.; Diebold, U. *Journal of Physical Chemistry B* **2003**, *107*, 2788-2795.
- [69] Bard, A. J. *Science* **1980**, *207*, 139-144.
- [70] Nozik, A. J. *Nature* **1975**, *257*, 383-386.
- [71] Tsai, S. C.; Kao, C. C.; Chung, Y. W. *Journal of Catalysis* **1983**, *79*, 451-461.
- [72] Imanishi, A.; Okamura, T.; Ohashi, N.; Nakamura, R.; Nakato, Y. *Journal of the American Chemical Society* **2007**, *129*, 11569-11578.
- [73] Liu, H.; Imanishi, A.; Nakato, Y. *Journal of Physical Chemistry C* **2007**, *111*, 8603-8610.

- [74] Nakamura, R.; Imanishi, A.; Murakoshi, K.; Nakato, Y. *Journal of the American Chemical Society* **2003**, *125*, 7443-7450.
- [75] Nakamura, R.; Nakato, Y. *Journal of the American Chemical Society* **2004**, *126*, 1290-1298.
- [76] Nakamura, R.; Okamura, T.; Ohashi, N.; Imanishi, A.; Nakato, Y. *Journal of the American Chemical Society* **2005**, *127*, 12975-12983.
- [77] Nakamura, R.; Tanaka, T.; Nakato, Y. *Journal of Physical Chemistry B* **2004**, *108*, 10617-10620.
- [78] Nowotny, J.; Bak, T.; Nowotny, M. K.; Sheppard, L. R. *Journal of Physical Chemistry B* **2006**, *110*, 18492-18495.
- [79] Cronmeyer, D. C. *Physical Review* **1959**, *113*, 1222-1226.
- [80] Ghosh, A. K.; Wakim, F. G.; Addiss, R. R. *Physical Review* **1969**, *184*, 979-988.
- [81] Nowotny, M. K.; Bak, T.; Nowotny, J. *Journal of Physical Chemistry B* **2006**, *110*, 16302-16308.
- [82] Nowotny, J.; Bak, T.; Burg, T. *Physica Status Solidi B-Basic Solid State Physics* **2007**, *244*, 2037-2054.
- [83] Nowotny, J.; Bak, T.; Burg, T. *Ionics* **2007**, *13*, 71-78.
- [84] Nowotny, J.; Bak, T.; Burg, T. *Ionics* **2007**, *13*, 79-82.
- [85] Nowotny, M. K.; Sheppard, L. R.; Bak, T.; Nowotny, J. *Journal of Physical Chemistry C* **2008**, *112*, 5275-5300.
- [86] Valdes, A.; Qu, Z. W.; Kroes, G. J.; Rossmeisl, J.; Norskov, J. K. *Journal of Physical Chemistry C* **2008**, *112*, 9872-9879.

- [87] Osterloh, F. E. *Chemistry of Materials* **2008**, *20*, 35-54.
- [88] Kudo, A.; Miseki, Y. *Chemical Society Reviews* **2009**, *38*, 253-278.
- [89] Kato, H.; Asakura, K.; Kudo, A. *Journal of the American Chemical Society* **2003**, *125*, 3082-3089.
- [90] Maeda, K.; Teramura, K.; Lu, D. L.; Takata, T.; Saito, N.; Inoue, Y.; Domen, K. *Journal of Physical Chemistry B* **2006**, *110*, 13753-13758.
- [91] Maeda, K.; Teramura, K.; Lu, D. L.; Takata, T.; Saito, N.; Inoue, Y.; Domen, K. *Nature* **2006**, *440*, 295-295.
- [92] Reber, J. F.; Meier, K. *Journal of Physical Chemistry* **1984**, *88*, 5903-5913.
- [93] Smotkin, E.; Bard, A. J.; Campion, A.; Fox, M. A.; Mallouk, T.; Webber, S. E.; White, J. M. *Journal Of Physical Chemistry* **1986**, *90*, 4604-4607.
- [94] Khan, S. U. M.; Al-Shahry, M.; Ingler, W. B. *Science* **2002**, *297*, 2243-2245.
- [95] Kitano, M.; Kikuchi, H.; Hosoda, T.; Takeuchi, M.; Matsuoka, M.; Eura, T.; Anpo, M.; Thomas, J. M. *Key Engineering Materials* **2006**, *317-318*, 823-826.
- [96] Kitano, M.; Takeuchi, M.; Matsuoka, M.; Thomas, J. A.; Anpo, M. *Catalysis Today* **2007**, *120*, 133-138.
- [97] Kitano, M.; Tsujimaru, K.; Anpo, M. *Applied Catalysis A-General* **2006**, *314*, 179-183.
- [98] Macak, J. M.; Gong, B. G.; Hueppe, M.; Schmuki, P. *Advanced Materials* **2007**, *19*, 3027-3031.

- [99] Ghicov, A.; Tsuchiya, H.; Hahn, R.; Macak, J. M.; Munoz, A. G.; Schmuki, P. *Electrochemistry Communications* **2006**, *8*, 528-532.
- [100] Xie, Y.; Zhou, L.; Huang, C.; Huang, H.; Lu, J. *Electrochimica Acta* **2008**, *53*, 3643-3649.
- [101] Ruan, C. M.; Paulose, M.; Varghese, O. K.; Grimes, C. A. *Solar Energy Materials and Solar Cells* **2006**, *90*, 1283-1295.
- [102] Cheng, X. F.; Leng, W. H.; Liu, D. P.; Xu, Y. M.; Zhang, J. Q.; Cao, C. N. *Journal of Physical Chemistry C* **2008**, *112*, 8725-8734.
- [103] deTacconi, N. R.; Chenthamarakshan, C. R.; Yogeeswaran, G.; Watcharenwong, A.; deZoysa, R. S.; Basit, N. A.; Rajeshwar, K. *Journal of Physical Chemistry B* **2006**, *110*, 25347-25355.
- [104] Mohapatra, S. K.; Raja, K. S.; Mahajan, V. K.; Misra, M. *Journal of Physical Chemistry C* **2008**, *112*, 11007-11012.
- [105] Mohapatra, S. K.; Misra, M.; Mahajan, V. K.; Raja, K. S. *Journal of Physical Chemistry C* **2007**, *111*, 8677-8685.
- [106] Mohapatra, S. K.; Misra, M.; Mahajan, V. K.; Raja, K. S. *Journal of Catalysis* **2007**, *246*, 362-369.
- [107] Fujishima, A.; Kohayakawa, K.; Honda, K. *Journal of the Electrochemical Society* **1975**, *122*, 1487-1489.
- [108] Schrauzer, G. N.; Guth, T. D. *Journal of the American Chemical Society* **1977**, *99*, 7189-7193.
- [109] Sato, S.; White, J. M. *Chemical Physics Letters* **1980**, *72*, 83-86.
- [110] Wagner, F. T.; Somorjai, G. A. *Journal of the American Chemical Society* **1980**, *102*, 5494-5502.

- [111] Abe, R.; Hara, K.; Sayama, K.; Domen, K.; Arakawa, H. *Journal Of Photochemistry And Photobiology A-Chemistry* **2000**, *137*, 63-69.
- [112] Arakawa, H.; Sayama, K. *Catalysis Surveys From Japan* **2000**, *4*, 75-80.
- [113] Yoshida, Y.; Matsuoka, M.; Moon, S. C.; Mametsuka, H.; Suzuki, E.; Anpo, M. *Research On Chemical Intermediates* **2000**, *26*, 567-574.
- [114] Zou, Z. G.; Ye, J. H.; Sayama, K.; Arakawa, H. *Nature* **2001**, *414*, 625-627.
- [115] Abe, R.; Sayama, K.; Domen, K.; Arakawa, H. *Chemical Physics Letters* **2001**, *344*, 339-344.
- [116] Abe, R.; Sayama, K.; Arakawa, H. *Chemical Physics Letters* **2003**, *371*, 360-364.
- [117] Gondal, M. A.; Hameed, A.; Yamani, Z. H.; Suwaiyan, A. *Chemical Physics Letters* **2004**, *385*, 111-115.
- [118] Lee, K.; Nam, W. S.; Han, G. Y. *International Journal of Hydrogen Energy* **2004**, *29*, 1343-1347.
- [119] Luo, H. M.; Takata, T.; Lee, Y. G.; Zhao, J. F.; Domen, K.; Yan, Y. S. *Chemistry Of Materials* **2004**, *16*, 846-849.
- [120] Iwase, A.; Kato, H.; Kudo, A. *Catalysis Letters* **2006**, *108*, 6-9.
- [121] Sakai, N.; Fujishima, A.; Watanabe, T.; Hashimoto, K. *Journal of the Electrochemical Society* **2001**, *148*, 395-398.

APPENDIX A

PLATINUM LOADING ON TITANIUM/TITANIUM DIOXIDE BY DIFFERENT MEANS

During the course of study, different means of loading platinum on titanium metal or oxide film on top was tried. This section reports the findings of these studies.

First type of Pt loading technique is reported also in the main text for the sample Pt/TNT-aq-1. This is the wet impregnation. Preparation of this sample is as follows from the very beginning: A titanium foil of 3x3 cm² size is anodized at 20 V against a Pt foil counter electrode in a solution of 1 M NH₄H₂PO₄ + 0.5 wt% NH₄F. Anodized foil is rinsed with DI water and air dried. 0.03 M Pt(NH₃)₄Cl₂ aqueous solution is used to wet both surfaces of the foil. Foil is placed horizontally on a glass boat and heated to 450 °C with a heating rate of 2 °C/min under air flow. Annealing takes 3 hours and sample is let cool naturally in the furnace.

Second and third techniques for Pt deposition are electrochemical techniques and are applied to non-oxidized titanium foils. In both techniques, first, natural oxide of titanium is removed by keeping the foil in 850 g/L H₂SO₄ (aqueous) at 80 °C for 20 minutes. Electrochemical deposition comes next.

Second technique utilizes a high voltage DC source. Titanium foil is made cathode under 3 V of potential difference with a stainless steel anode. Electrolyte is 10 g/L H₂PtCl₆ + 150 g/L NaNO₃ + 1-2 g/L NH₄OH. Current was passed for 10 minutes. Experimental conditions lead to ca. 50 mA/cm² current density. CV of the produced electrode in 1 N H₂SO₄ is given in Figure A-1.

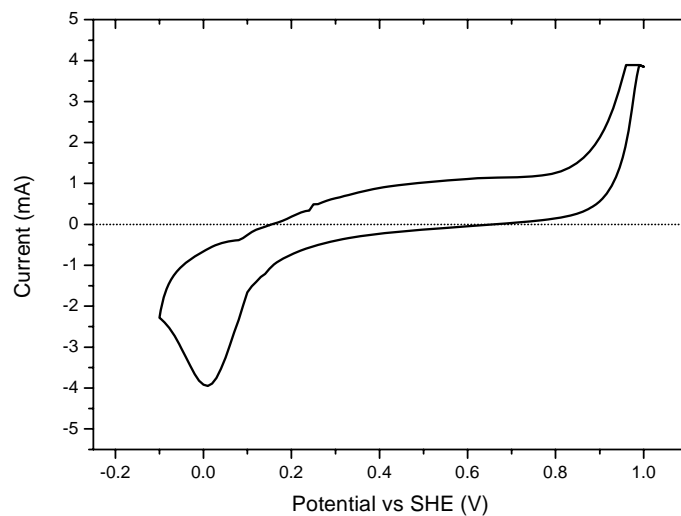


Figure A-1. CV of the Pt/Ti electrode, Pt deposited by high voltage DC source, taken in 1 N H_2SO_4 , with a sweep rate of 0.05 V/s

Third technique utilizes the potentiostat that is mentioned in the main text. Same materials and electrolyte was used. 16 cycles from +0.15 to -0.50 V (relative to SHE) was scanned at a rate of 0.01 V/s. The final CV of this deposition procedure is given in Figure A-2.

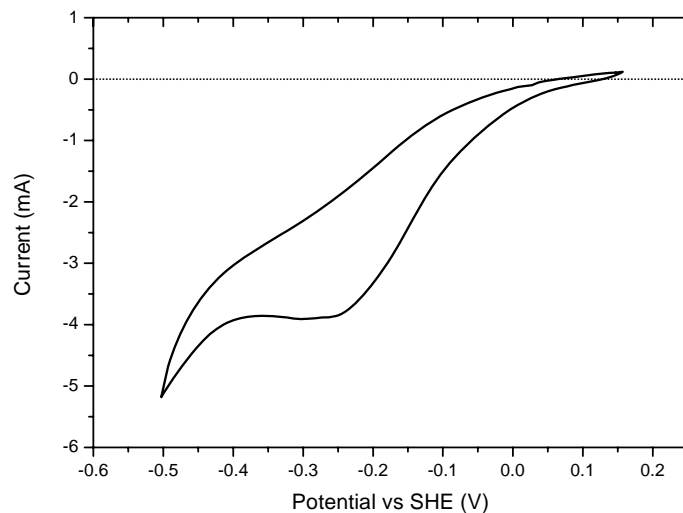


Figure A-2. Current-voltage curve of the final cycle of 16 Pt deposition cycles by using a potentiostat.

The cyclic voltammogram of the third prepared electrode, taken in 1 N H₂SO₄ is given in Figure A-3.

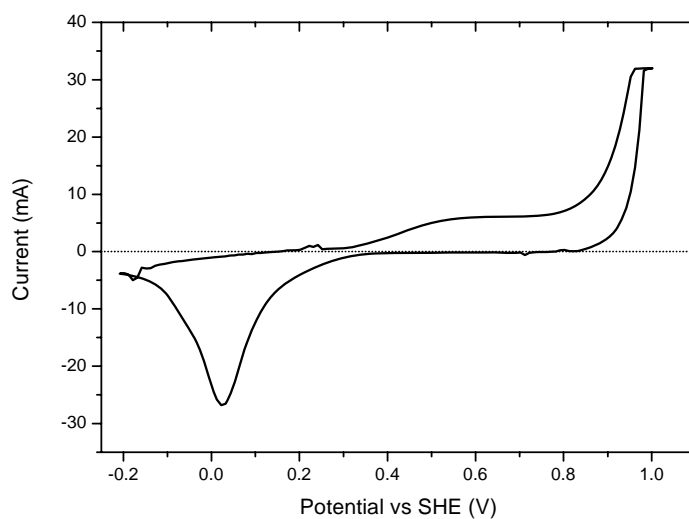


Figure A-3. CV of the Pt/Ti electrode, Pt deposited by potentiostat, taken in 1 N H₂SO₄, with a sweep rate of 0.05 V/s

SEM images of the formed Pt deposits on the surfaces are given in Figure A-4 at nearly the same magnification for better comparison.

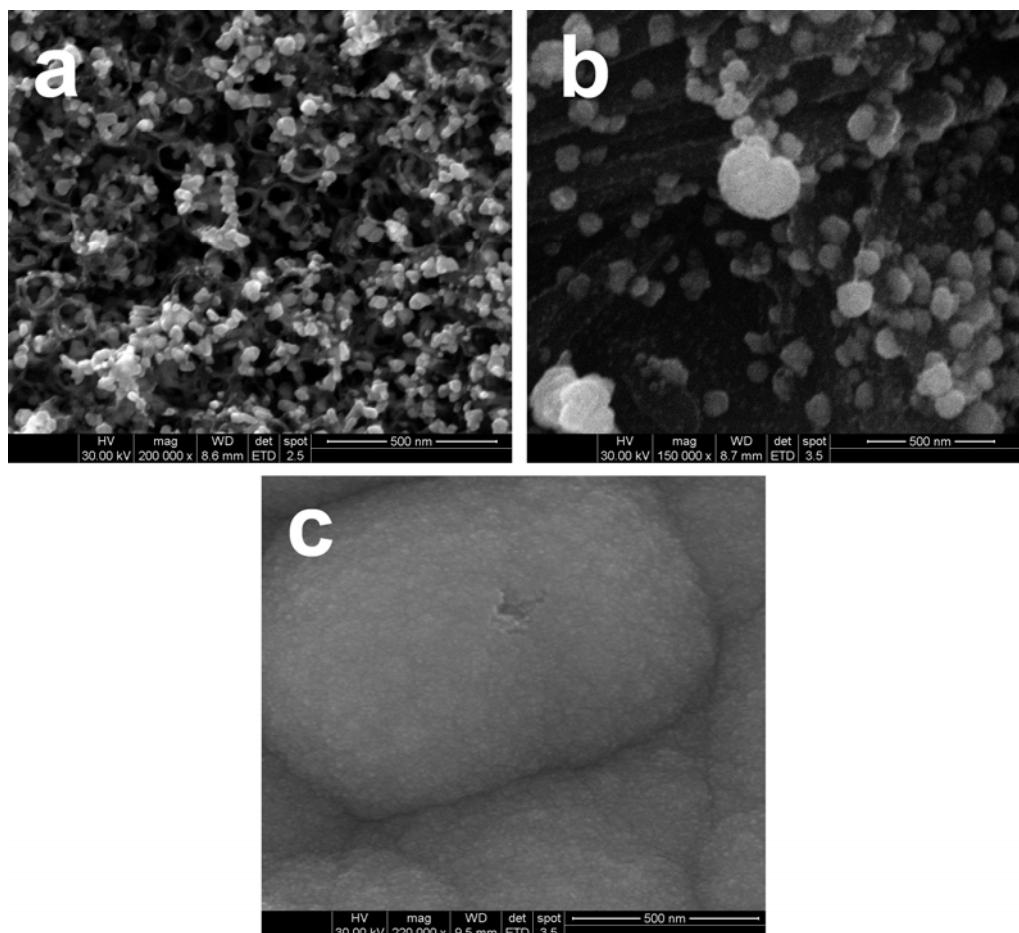


Figure A-4. SEM images of (a) Pt wet impregnated TNT film (b) Pt deposited on titanium metal via high voltage source (c) Pt deposited on titanium metal via potentiostat

APPENDIX B

INFORMATION ON PURE TITANIUM

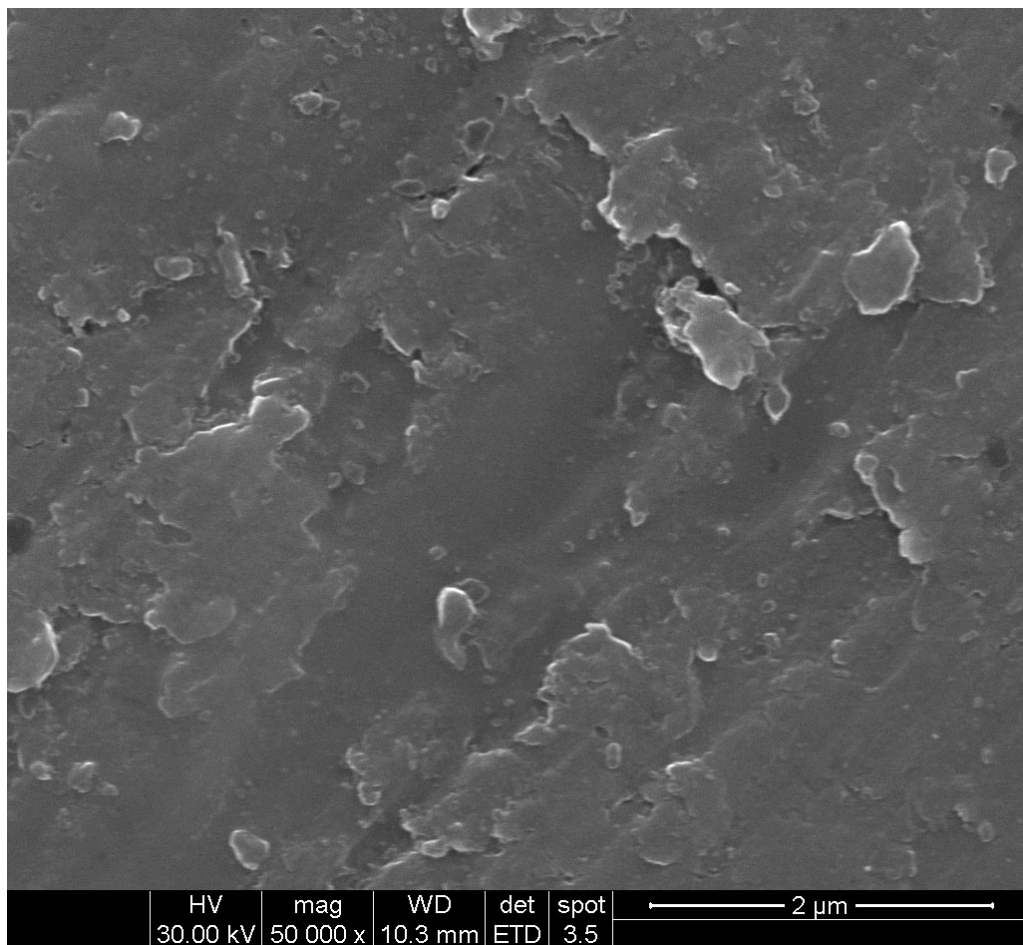


Figure B-1. SEM image of the surface of a pure titanium foil

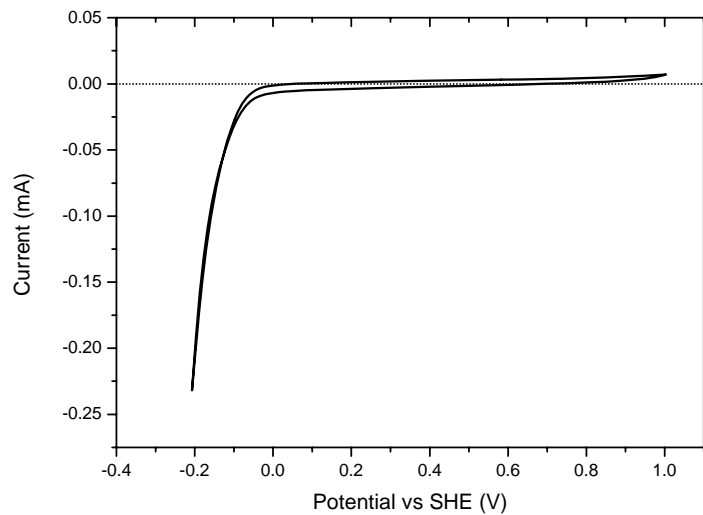


Figure B-2. CV of pure titanium foil ($\sim 1 \text{ cm}^2$) in 1 N H_2SO_4 taken in the dark with 0.05 V/s sweep rate

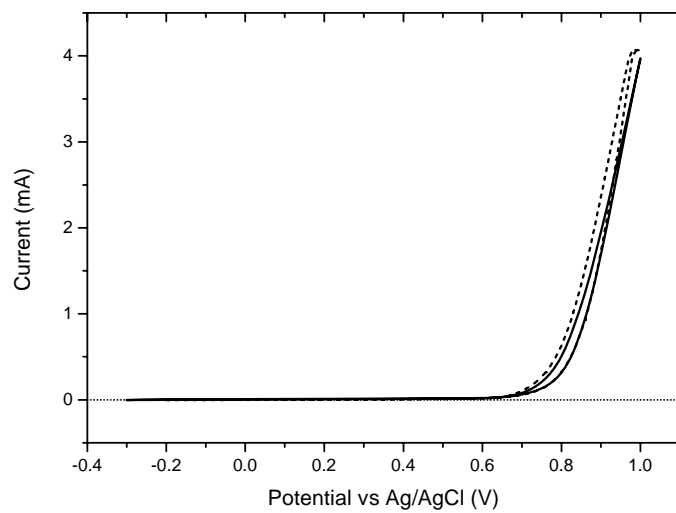


Figure B-3. CV of pure titanium foil ($\sim 8 \text{ cm}^2$) in 0.1 N KOH taken in the dark (solid line) and under UV illumination (dotted line) with 0.05 V/s sweep rate

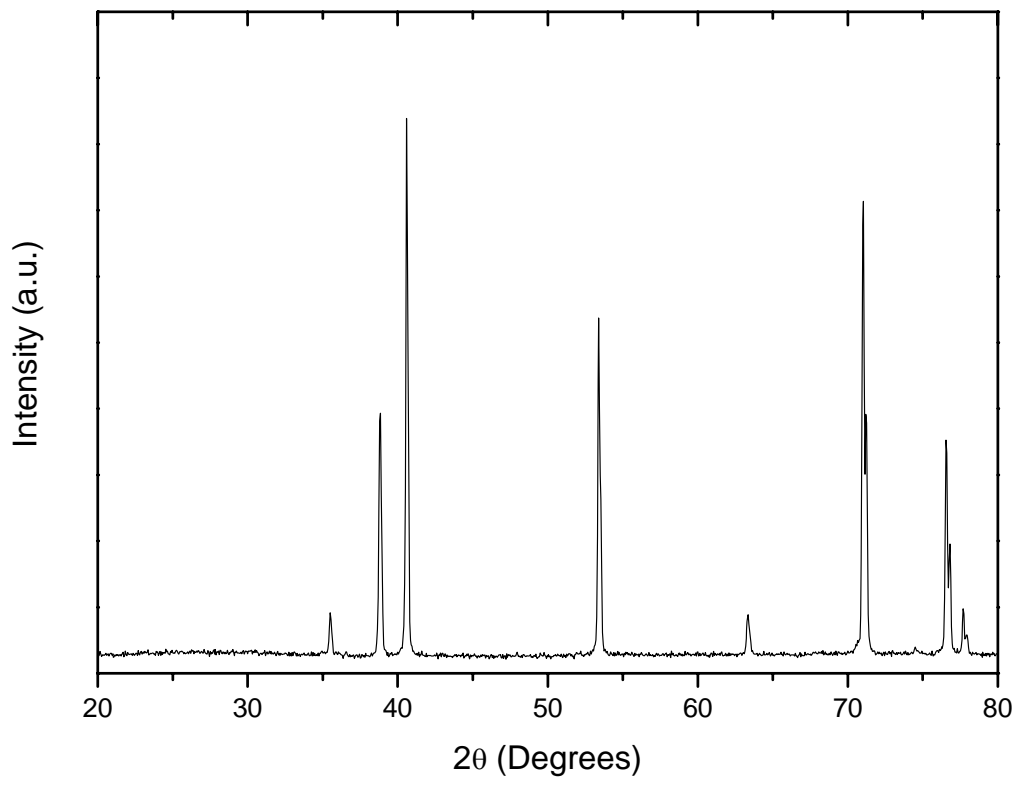


Figure B-4. X-ray diffractogram of pure titanium (foil)

APPENDIX C

CO OXIDATION IN THE GAS PHASE USING Pt/TNT

In order to investigate the catalytic activity of titania nanotubes, CO oxidation experiments were conducted in the gas phase. Scheme of the setup that was used in these experiments is given in Figure C-1. A photograph of the setup is also presented in Figure C-2.

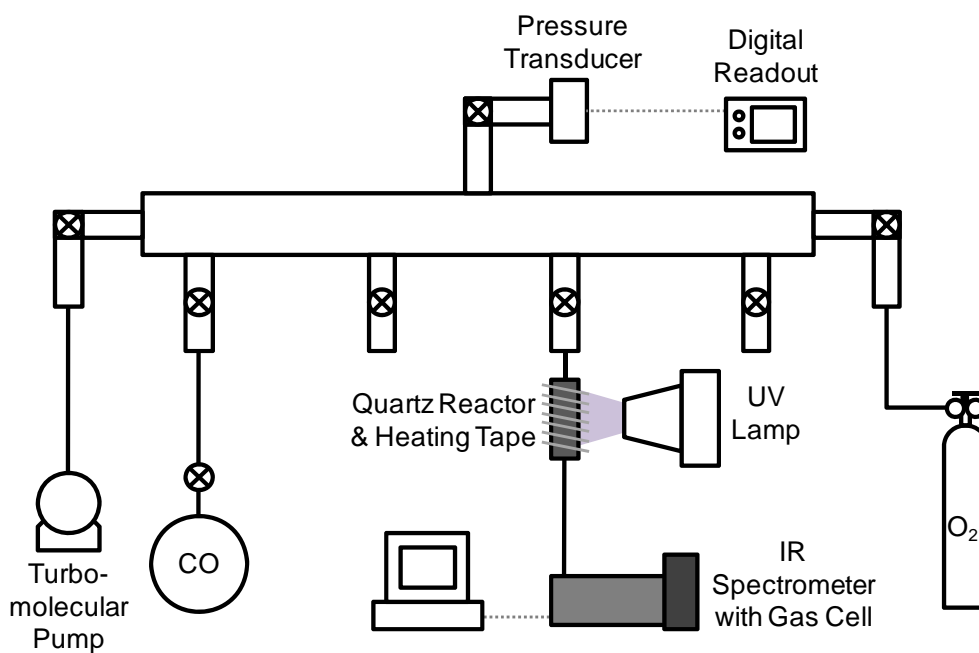


Figure C-1. Schematic illustration of the setup that was used to study CO oxidation over titania nanotubes in batch and semi-flow through conditions.

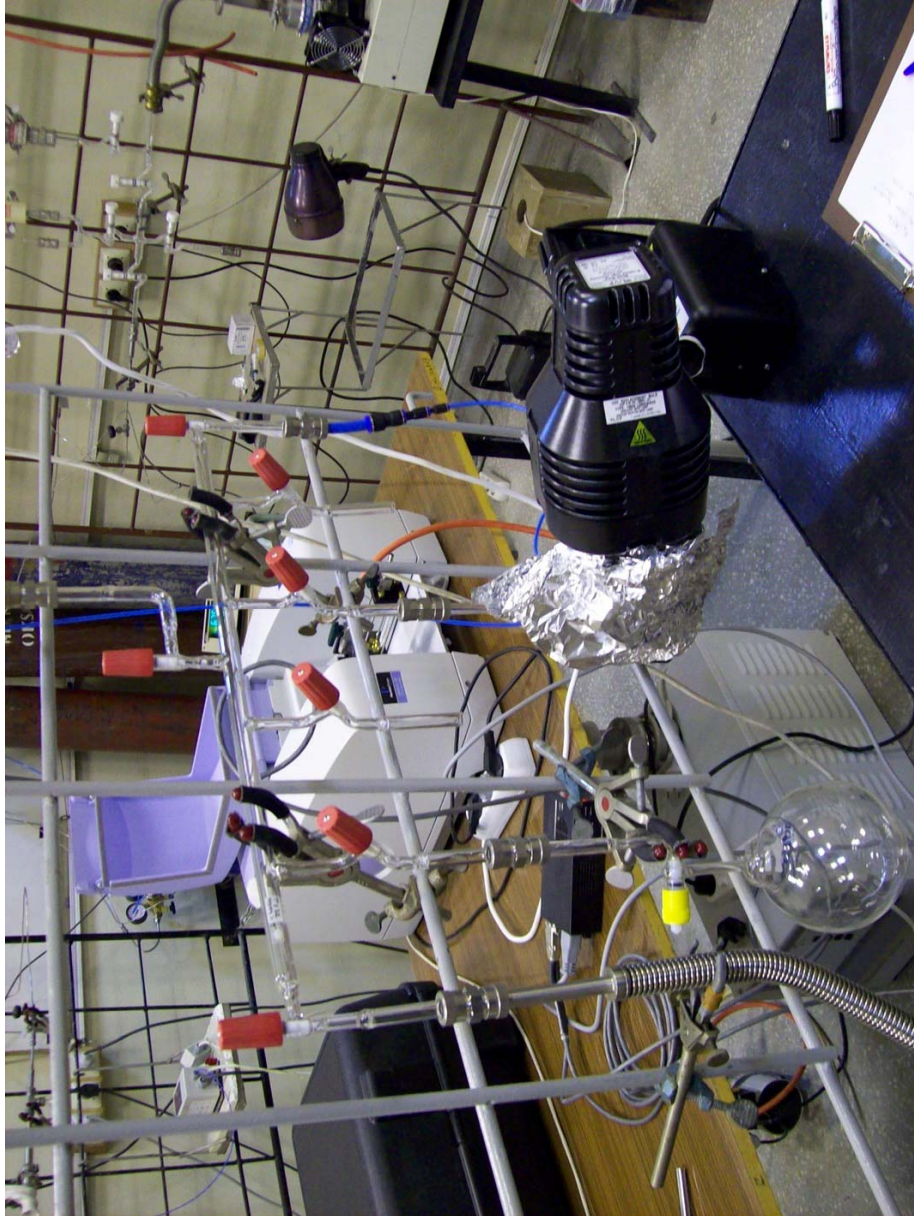


Figure C-2. Photograph of the setup that was used to study CO oxidation over titania nanotubes in batch and semi-flow through conditions.

Approximately 2 cm² of the two side platinized sample, Pt/TNT-aq-1, was cut by scissors and put inside the quartz reactor (total of ca. 4 cm² active area). Bottom of the reactor was plugged with glass wool. Temperature near the heating tape was set to 200 °C (temperature inside the reactor is expected to be less). Outside of the reactor was covered with aluminum foil for isolation.

All system was evacuated first and the manifold-reactor valve was shut. 3.0 torr CO was let inside the manifold first. Then O₂ was let in until pressure reached 19.0 torr and waited for ca. 5 minutes for gases to mix uniformly in the manifold. Manifold-reactor valve was opened slowly and reactant mixture was flown over the catalyst. When the pressure equilibrated, manifold-reactor valve was shut down again to minimize leaks into the system. The IR spectra taken during the course of time is presented in Figure C-3.

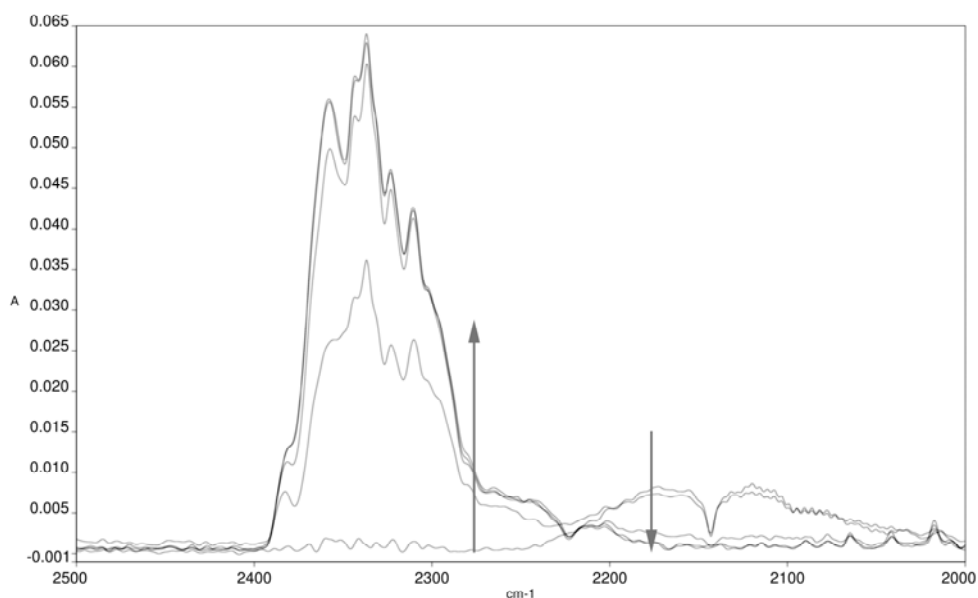


Figure C-3. IR spectra of gases during thermal CO oxidation test.

24 hours have passed between the first and last spectra in Figure C-3 and the arrows indicate the time direction. The peak that covers 2250-2400 cm^{-1} range belongs to CO_2 and the peak that covers 2000-2250 cm^{-1} range belongs to CO. This indicates the consumption of CO and production of CO_2 in 24 hours of time period. However due to the long diffusion distance (and small cross-section) between the reactor and the IR cell observed rate is limited by the diffusion of gases in the system.

Same procedure was followed for the photocatalytic reaction as well but this time, amount of catalyst was increased to twice its value in the thermal test (ca. 8 cm^2 total). Reactor was not heated but illuminated using the same UV light (365 nm).

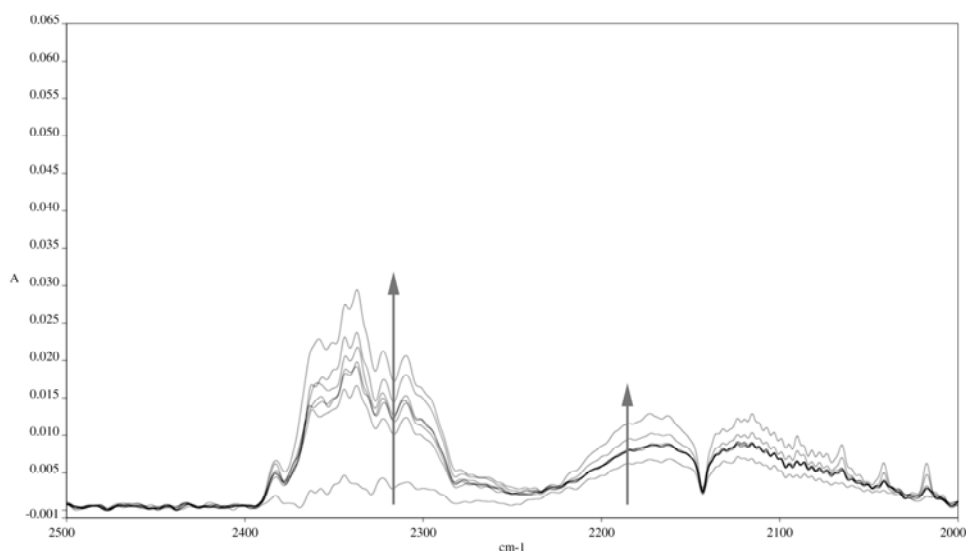


Figure C-4. IR spectra of gases during photocatalytic CO oxidation test.

Changes in the peak intensities of CO and CO_2 for 20 hours during the photocatalytic test are presented in Figure C-4. In this case both peaks show increase in intensity. This implies another the source of carbon since interconversion of these two molecules would not yield such spectra.

Therefore, this result may be ascribed to the burning of surface carbonaceous species (impurities) by the excess oxygen present in the medium. Both CO and CO₂ may be produced via this path.